ABSTRACT

FRACTIONATION AND SEGREGATION OF SUSPENDED PARTICLES USING ACOUSTIC AND FLOW FIELDS

by
Nazhat Aboobaker

The fractionation of particles by size or by density has many applications in a variety of technologies. Decontamination and separation of fine sediments is useful in treating sediments. The application of acoustic standing wave fields for the fractionation and segregation of suspended particles was studied.

The above technology was implemented at the bench scale by building a Plexiglas chamber. Two ultrasound transducers were fixed to opposite sides of the chamber to generate the acoustic standing wave field. The technology was evaluated using silica dioxide (SiO_2) (1-5 μm) and silicon carbide (SiC) (5-20 μm) particle suspensions in deionized water. Due to the acoustic force field, SiO_2 particles migrated towards the pressure nodes at half wavelength intervals within the channel at optimum frequency of 333 kHz and 40 W power.

The fractionation process was mathematically modeled, by deriving particle trajectories and concentration. The SiC particle's displacements due to an acoustic force were used to be compared with the mathematical model predictions. For input power level between 3.0 to 5.0 W, the experimental data were comparable to mathematical model predictions. Also, based on the experimental data it was possible to develop a relationship between input power and acoustic energy in the resonance chamber. The proposed technology will provide viable alternatives to the classical fractionation methods.

FRACTIONATION AND SEGREGATION OF SUSPENDED PARTICLES USING ACOUSTIC AND FLOW FIELDS

By
Nazhat Aboobaker

A Dissertation
Submitted to the Faculty of
New Jersey Institute of Technology
In Partial Fulfillment of the Requirements for the Degree of
Doctor of Philosophy in Civil Engineering

Department of Civil and Environmental Engineering

February 2001

APPROVAL PAGE

FRACTIONATION AND SEGREGATION OF SUSPENDED PARTICLES USING ACOUSTIC AND FLOW FIELDS

Nazhat Aboobaker

Dr. Jay Meegoda, Dissertation Advisor — Date
Professor of Civil and Environmental Engineering, NJIT

Dr. Denis Blackmore, Dissertation Advisor — Date
Professor of Mathematical Sciences, NJIT

Dr. John Schuring, Committee Member — Date
Chairman, Professor of Civil and Environmental Engineering, NJIT

Dr. Taha Marhaba, Committee Member — Date
Associate Professor of Civil and Environmental Engineering, NJIT

Dr. Kauser Jahan, Committee Member — Date
Associate Professor of Civil and Environmental Engineering, Rowan University, NJ

BIOGRAPHICAL SKETCH

Author: Nazhat Aboobaker

Degree: Doctor of Philosophy in Civil Engineering

Undergraduate and Graduate Education:

- Doctor of Philosophy in Civil Engineering,
  New Jersey Institute of Technology, Newark, NJ, 2001.

- Master of Science in Environmental Engineering,
  New Jersey Institute of Technology, Newark, NJ, 1996.

- Bachelor of Science in Civil Engineering,
  NED University, Karachi, Pakistan, 1989.

Major: Environmental Engineering

Presentations and Publications:

Aboobaker, N., Blackmore, D., Meegoda, J. N.,
"Analysis of Fractionation of Sediments caused by an Acoustic Field," Proceedings of International Conference on Computer Methods and Advances in Geomechanics, edited by Chandra S. Desai, Tribikram Kundu, Satya Harpalani, Dinshaw Contractor, and John Kemeny, Vol. 1, pp775-780, January 2001.

Aboobaker, N., Meegoda, J., N., Blackmore, D.,
"Fractionation and Segregation of Suspended Particles using Acoustic and Flow Fields," Proceedings Hazardous and Industrial Waste_32nd Mid_Atlantic Industrial and Hazardous Waste Conference, Technomic Publishing Company, INC. Lancaster, PA, pp. 659-669, 2000.

Meegoda, J. N., Veerawat, Perera, Ruvini, Aboobaker, Nazhat, and Zapata, Alejandra,
"Ultrasound to Decontaminate Dredged Sediments," Final report to the National Science Foundation submitted by the New Jersey Institute of Technology, Newark, pp119, July 2000.

Meegoda, J. N., Veerawat, Perera, Ruvini, Aboobaker, Nazhat, and Zapata, Alejandra,
"Ultrasound to Decontaminate Dredged Sediments," Proceedings of the 4th. International Symposium on Environmental Geotechnology and Global Sustainable Development, H. I. Inyang Editor, A.A. Balkema Publishers, Danvers, MA. , August 1998.

This dissertation is dedicated

To my Parents,

Husband and Kids

ACKNOWLEDGMENTS

I would like to express my deepest appreciation to Dr. Jay N. Meegoda and Dr. Denis Blackmore, who not only served as my research supervisors, providing valuable and countless resources, insight, and intuition, but also gave me support, encouragement, and reassurance. I greatly appreciate and thank Dr. Meegoda for nominating me for the presidential fellowship throughout my Ph.D program and supervising my project very closely. My deepest appreciation to Dr. Denis Blackmore for helping me in establishing the mathematical equation and his constant effort to achieve the best and simplest approach. Special thanks are given to Dr. John Schuring, for being an active committee member as well as for his advice, help and encouragement, including lending his computer, VCR and television for the experiments.

I also express my appreciation to Dr. Kauser Jahan, and Dr. Taha Marhaba for actively participating in my research as thesis committee members. I also appreciate the generous advice and electrical equipment that I received from Dr. Edip Niver, Electrical Engineering Department who virtually served as a committee member providing measurements, equipment training and introducing me to his student Mr. Farhad who helped me to overcome equipment compatibility problems. My special thanks to Dr. Ronald Kane for financial and academic support during my Ph.D. program. I would also like to thank Mr. Frank Johansson, mechanical technician, for building several iterations of the physical models for this research.

My thanks also to Dr. Edward Dreizin, Research Professor, for his advice on many aspects of the research, for providing information on the NASA Tracker computer

program, and lending his microscope for the research. I also would like to thank Dr. Boris Khoser and Mr. John Batton for providing the Fiber optics light source for the microscope and the radical scale, and for helping me in capturing digital video of the experiment using a high speed digital Kodak camera.

Thanks to Dr. Sunil Dhar from the Mathematical Sciences Department for helping me with statistical analysis of the experimental data. I also would like to thank Dr. Jonathan Luke for his help and suggestion to use different representative samples for this research. Thanks to Mr. Chandrakant Patel, Geoenvironmental Laboratory for allowing me to use the CCD camera, eyepieces and objective lens. Special thanks also to Mathematical Sciences Department for the use of their laboratory for numerical and statistical analysis and thanks to the Electrical Engineering Department for lending me electrical measuring devices for my research. I also like to thank the New Jersey Center for Multimedia Research of NJIT for letting me use their Adobe software in the laboratory.

This research was partially supported by NSF grant # CMS-9700318 entitled Ultrasounds to Decontaminate Dredged Sediments. I wish to acknowledge the interim program manager Dr. Richard Fragaszy for approving a budget transfer to purchase the power amplifier.

I would also like to thank National Science Foundation (NSF) for providing funds for me to attend a short course in Particle Technology at Clausthal University, Germany. I also like to thank Dr. Robert Pfeffer from chemical Engineering Department and Dr. George Klinzing from University of Pittsburgh, PA, for nominating and accepting me for this short course.

I also thank my beloved family, and friends who have been very supportive and have never lost faith in me. Finally, thanks to the people in the Civil and Environmental Engineering Department for their help throughout these long years.

TABLE OF CONTENTS

Chapter **Page**

1 INTRODUCTION 1

1.1 Management of Dredged Sediments from NY/NJ Harbors 1

1.1.1 Types and Categories of Dredged Sediments 2

1.1.2 Composition of Contaminated Dredged Sediments 4

1.1.3 Available Classical Methods for Segregation 5

1.2 Need for New Technology 6

1.2.1 Basic Definitions 7

1.2.1.1 Acoustic 7

1.2.1.2 Sound 7

1.2.1.3 Piezoelectric 7

1.2.1.4 Transducer 8

1.2.1.5 Standing Waves 8

1.2.1.6 Acoustic Radiation and Energy 9

1.2.1.7 Acoustic Pressure and Velocity Amplitudes 9

1.3 Research Objective 10

1.4 Overview 12

2 LITERATURE SEARCH 13

2.1 Introduction 13

2.2 Theory 14

2.2.1 Primary Axial Acoustic Radiation Force 15

2.2.2 Primary Transverse Acoustic Radiation Force and Secondary Acoustic Radiation Force 17

2.3 Application of Newton's Second Law to a Particle Suspended in Acoustic Field 18

TABLE OF CONTENTS
(Continued)

Chapter **Page**

2.4 Parameter Contributing to the Acoustic Fractionation and Segregation 25

2.4.1 Cavitation and Streaming 27

2.4.2 Effect of Temperature Change 29

2.4.3 Acoustic Energy Density (E_{ac}) and its Distribution the Resonator 31

2.4.4 Viscosity 35

2.5 Summary and Conclusions 37

3 MATHEMATICAL MODEL 39

3.1 Mathematical Analysis of Equilibrium of Particle in an Acoustic Field 40

3.1.1 Preliminary Analysis 41

3.2 Equation for Particles Trajectories 50

3.3 Concentration Equation 56

3.4 Summary and Conclusions 64

4 DESIGN OF PHYSICAL MODEL 65

4.1 Electrical Equipment 65

4.1.1 Transducer 65

4.1.2 Signal Generator 69

4.1.3 Power Amplifier 69

4.1.4 Oscilloscope 70

4.1.6 Electrical Equipment Connection 70

4.2 Acoustic Chamber 71

4.3 Representative Sample 74

4.3.1 Silicon Dioxide 74

4.3.2 Silicon Carbide 77

4.4 Observation Techniques (Microscope and Illumination Source) 79

4.5 Recording and Image Capturing 80

TABLE OF CONTENTS
(Continued)

Chapter **Page**

4.6 Image Analysis 81

4.7 Conclusions 83

5 EXPERIMENTAL OBSERVATION 90

5.1 Experimental Observations 90

5.2 Particle Column Formation with SiO_2 91

5.3 SiC Particles Sedimentation 96

5.4 SiC particle Trajectories in an Acoustic Field 101

5.5 Comparison between Experimental Data and Mathematical Model 107

5.5.1 Statistical Analysis 107

5.5.2 Data Optimization 118

5.5.3 Particle Trajectories from Experimental and Optimization Technique ... 122

5.6 Conclusions 133

6 CONCLUSIONS 134

6.1 Summary 134

6.2 Future Research 137

6.3 Implementation 139

APPENDIX A 141

APPENDIX B 160

REFERENCES 163

LIST OF TABLES

Table		Page
1.1	Types of Dredged Material Encountered I NY/NJ Ports	3
1.2	Review of Current Technologies	6
2.1	Velocity of Sound in Deionized Water as a Function of Temperature	31
2.2	Mean Oscillation Velocity Amplitude value	34
3.1	Properties of Particle and Suspending Fluid	40
3.2	Particles Displacement vs. Time	54
3.3	Concentration Ratio vs. Time	62
4.1	Piezoelectric Material Characteristics	66
4.2	Physical Properties of Suspended Particles and Host Fluid	77
5.1	A Single Particle Velocity by Experiment	99
5.2	Diameter of Particle by Stokes' Law	100
5.3	Different Power Ranges used in the Experiment	102
5.4	Possible Combinations of the Three Variables	119
5.5	Acoustic Energy Corresponding Power input after Smoothing	120

LIST OF FIGURES

Figure	Page
1.1 Standing Waves	9
1.2 Planes of Nodes and Antinodes	10
2.1 Acoustic Forces	15
2.2 Forces on a Particle in an Acoustic Field	20
2.3 Acoustic Force on the Particles	22
2.4 Mix Suspension of Particles	23
2.5 Multi_wavelength Width Chamber	24
2.6 Average Temperature Rise at Power Level of 180W/L	30
2.7 Piezoceramic Transducer Surface-Oscillation Velocity	33
2.8 Glass Reflector Surface-Oscillation Velocity	34
3.1 Phase Plane near $(2l\pi/\beta, 0)$	45
3.2 Phase Plane near $((2l+1)\pi/\beta, 0)$	46
3.3 Phase Portrait of Equation (3.5)	46
3.4 Displacement vs. Time	55
3.5 Concentration vs. Displacement	63
4.1 Resonance Frequency	68
4.2 Block Diagram of Electrical Connection	71
4.3 Acoustic Chamber	73
4.4 Particle Size Analysis (AEE) for SiO_2	75
4.5 Hydrometer Analysis for SiO_2	76
4.6 Particle Size Analysis (AEE) for SiC	78
4.7 Microscope and Light Source	80
4.8 CCD Camera Connections for Recording and Capturing	80
4.9 Photograph of the Radical Scale Vertical Direction	82
4.10 Photograph of the Radical Scale Horizontal Direction	82
4.11 Photograph of the Transducer with Electric Connections	84

LIST OF FIGURES
(Continued)

Figure **Page**

4.12 Photograph of the Transducers from the Front 84

4.13 Photograph of the Microscope, Adopter and the CCD Camera 85

4.14 Photograph of the CCD Camera 85

4.15 Photograph of the Connections between Microscope and CCD Camera 86

4.16 Photograph of the Microscope Lens in front of an Acoustic Chamber 86

4.17 Photograph of the Fiber Optics Light Source 87

4.18 Photograph of the Signal Generator 87

4.19 Photograph of the Power Amplifier 88

4.20 Photograph of Oscilloscope 88

4.21 Photograph of the Experimental Setup 89

4.21 Photograph of the Experimental Setup 89

5.1 Formulation of Particle Columns 92

5.2 Positions of Four Nodes in the Chamber 93

5.3 Chamber is full of Bubbles 95

5.4 Photograph of the Particles in an Acoustic Chamber before Energy 98

5.5 Photograph of the Particles during Sedimentation at 0.3 seconds Intervals 99

5.6 Photograph of the Displacement of SiC Particles in an Acoustic Field 103

5.7 Experimental Data at 1W 104

5.8 Experimental Data at 2W 105

5.9 Experimental Data at 3W 106

5.10 Different Smoother, Sample 1 111

5.11 Different Smoother, Sample 2 112

5.12 Different Smoother, Sample 3 113

5.13 Experimental Data at 1 W after using Super Smoother 115

5.14 Experimental Data at 2 W after using Super Smoother 116

LIST OF FIGURES
(Continued)

Figure **Page**

5.15 Experimental Data at 3 W after using Super Smoother 117

5.16 Relation between input Power and Acoustic Energy 121

5.17 Particle Displacement vs. Time at Power 0.5 W 123

5.18 Particle Displacement vs. Time at Power 1.0 W 124

5.19 Particle Displacement vs. Time at Power 1.5 W 125

5.20 Particle Displacement vs. Time at Power 2.0 W 126

5.21 Particle Displacement vs. Time at Power 2.5 W 127

5.22 Particle Displacement vs. Time at Power 3.0 W 128

5.23 Particle Displacement vs. Time at Power 3.5 W 129

5.24 Particle Displacement vs. Time at Power 4.0 W 130

5.25 Particle Displacement vs. Time at Power 4.5 W 131

5.26 Particle Displacement vs. Time at Power 5.0 W 132

6.1 Implementation of the Technology.....139

CHAPTER 1

INTRODUCTION

The fractionation of particles by size or other physical properties such as density has many applications in a variety of technologies including material processing, polymer recycling, food processing, and the fuel industry. The use of monodisperse particles has advantages for diagnostic and treatment purposes in fields of life sciences. More effective separation of cells, bacteria, or yeast is desired in biotechnology. Fractionation of particles can be used in engineering applications such as decontamination of dredged sediments. The dredged sediments of harbors are composed of fine and coarse particles. Decontamination and separation of fine sediments is useful in treating sediments, leaving contaminated water to be treated separately, and cleaned sediments to be reused as construction soil or returned to the sea. Thus, separating the sediments from the contaminants and recycling the clean sediments back to the harbor may reduce the volume of the contaminated solid waste to be treated or disposed. Since the research described in this thesis is ultimately to be used in decontamination of dredged sediments, it is necessary to describe the current management of the dredged sediments.

1.1 Management of Dredged Sediments from NY/NJ Harbors

To ensure safe, navigable waters, rivers and waterways must be dredged. Dredging in the US requires long-term alternatives for treatment as more than 230 million cubic meters of dredged material per year need to be disposed of. In many locations, containment facilities are almost full. Sites for additional capacity are scarce and expensive

to construct. Dredged material research has been ongoing for a number of years. However, the disposal techniques have concentrated on sea disposal, artificial islands or disposal into lagoons for either containment or for long-term land reclamation.

Recently, the Ocean Dumping Act prevented ocean dumping and encouraged inland disposal of contaminated dredged sediments from ports such as New York/ New Jersey and Boston. This is due to high levels of contaminants such as metals, Dioxins, PAHs, and PCBs in dredged sediments. The difficulty in finding suitable inland sites for contaminated dredged sediments has resulted in partial stoppage of dredging activities at some ports making them less competitive. The resulting economic impact to the regions surrounding these ports has been severe.

1.1.1 Types and Categories of Dredged Sediments

It is estimated that dredging of NY/NJ ports will generate more than seven million tons of residues per year. Table 1.1 shows the types of dredged material encountered in NY/NJ ports. Table 1.1 also shows that dredging of NY/NJ ports annually produce 1.6 million tons of Category III dredged sediments with toxicity and bioaccumulation; these need a permanent inland home.

The analysis of NY/NJ metropolitan area Category III dredged sediments supplied by the Brookhavan National Lab, NY, produced the following results:

Water Content: 225%

Loss on Ignition: 14%

Clay Content: 27%

Silt Content: 45%

pH: 8.0

TOC: 7.5%

Pesticides: ~ 400 mg/kg

PCB (total): ~4,000 mg/kg

Dioxins: ~5,000 mg/kg

Furans: ~15,000 mg/kg

PAHs: ~100,000 mg/kg

Chromium: ~370 mg/kg

Lead: ~600 mg/kg

TCLP Chromium: ~0.03 mg/kg

Table 1.1 Types of Dredged Material Encountered in NY/NJ Ports

	Description	Disposal	Amount in million tons
Category I	Sediments that do not cause unacceptable toxicity or bio-accumulation	Sediments can be ocean disposed	2.3
Category II	Material that shows some evidence of toxicity or bio-accumulation	Sediments may be disposed in the ocean with capping	3.1
Category III	Material that fails to meet federal criteria for toxicity or bio-accumulation	Sediments not permitted for ocean disposal	1.6

There are two problems associated with cost effective disposal of dredged sediments from NY/NJ harbors: de-watering and de-contamination. Due to the high water content (typically 200 - 500%) of dredged sediments, most of the economical treatment methods such as thermal desorption are not cost effective in remediating dredged sediments. It appears that the most politically appealing treatment technology

is Solidification/Stabilization. Solidification/Stabilization is associated with increasing volume. Also, if implemented, there is a need to locate +1.6 million-tons/year disposal volume for the solidified/stabilized product.

1.1.2 Composition of Contaminated Dredged Sediments

Contaminated dredged sediments are composed of contaminants, water, coarse particles, fine particles, and suspended particles. The contaminants (heavy metals and organics) are usually attached to the clay and silt fractions. Meegoda, et al. (1995), showed that ultrasound energy can remove organic compounds and metals from dredged sediments. Application of ultrasound energy to soil slurry such as dredged sediments causes acoustic cavitation, and the formation, growth and implosive collapse of bubbles in a liquid. Shock waves from cavitation in liquid-solid slurries produce high-velocity inter-particle collisions, the impact of which is sufficient to desorb contaminants from soils. The separation of coarse particles from fines using ultrasound with vacuum pressure was studied and modeled by Meegoda, et al., 1998. However, this researcher found that separation and treatment of ultra fine particles such as clay poses a major problem. Therefore, there is a need exist to develop a new technology to separate clay size particles if the above technology is to be commercialized.

Appendix A presents the element composition and pictures of the dredged sediments from New York harbor, using an Environmental Scanning Electron Microscope (ESEM) and the Energy Dispersive X-Ray instrument in the Geoenvironmental laboratory. The main elements found in most of the analyzed area are oxygen and silica. This confirms the high concentration of silt and clay as observed by

the Brookhavan National Lab, about 45% and 27% respectively. These analyses by ESEM also revealed the presence of irregular shaped dredged sediments. The sediments dredged from the NY/NJ harbors are a complex mixture of soil and contaminant and the cleaning process proposed here should be able to segregate and fractionate and eventually recycle the clean soil back into the ocean.

1.1.3 Available Classical Methods for Segregation

Varieties of methods are available for the separation of particles. They include: physical methods involving filters, screens, or sieves, application of gravitational or centrifugal fields, and application of electrical or magnetic fields. Filters are used for particle size of less than 0.75 mm. The filters are inexpensive and simple to use, but they need high-pressure drops and may cause fouling of filter material. Screens are used for particle sizes greater than 0.75 mm, and are simple to use and inexpensive. However, they may have problems due to clogging and they usually require long processing times. Gravitational or centrifugal fields are routinely used for fractionation of particles based on size and/or density differences. When particles have higher density when compared with a suspending fluid, it causes the separation of particles from the fluid as they settle at the bottom. Higher gravitational forces, or centrifugal forces, expedite the settlement of the particles. This method can only treat small quantities and may be subject to mechanical failures. Separation methods were applied using electric or magnetic fields for size separation, for particles having surface charges or particles exhibiting magnetic properties. These particles are either naturally charged, or charges may be induced by adding chemical compounds. Thus, the cost of adding and subsequently removing of

facilitating chemicals and the high power consumption are some of the drawbacks of this technology. A brief review of the current technologies for particle separation is given in Table 1.2 along with some of the advantages and disadvantages of each method.

Table 1.2 Review of Current Technologies

Methods	Example	Mechanics	Advantages	Disadvantages
Physical Methods	Filters	Particle size <0.75 mm	Inexpensive	High pressure drops. Filter clogging. Fouling of filter material.
	Screens	Particle size >0.75 mm	Easy	Long time processing.
Size/density differences	Sedimentation	Settlement of particles at the bottom with higher density than fluid	Inexpensive	Long holdup time. Not possible when density of particle and fluid are same.
	Centrifuge	Centrifugal force to settle the particles	Faster than sedimentation	Mechanical failure. Small quantities.
Electric and Magnetic field	Electric charge Magnetic properties	Electrical or magnetic attraction or repulsion between the particles and suspended fluid	Fast (depending on chemical reactions) Easy	Requires high electric or magnetic fields. Induced or natural charges. High power consumption.

1.2 Need for New Technology

Ultra-fine particles, and particles with neutral buoyancy, or a uniform electromagnetically charged surface pose difficulties with fractionation. Existing methods require excessive time, prohibitive pressure drops, or extremely high electric or magnetic fields. Also, in the case of particles having very narrow ranges of sizes and densities, none of the above

methods can be used. Based on the above discussion there is a need for cost effective technology for fine soil particles. Therefore, it is proposed to develop a new technology to fractionate the suspended particles and at the same time to segregate them. In this new technology, particles are discriminated, based on density and compressibility differences rather than on particle size. The technology used in this research is that of an acoustic field, and is called "Fractionation and Segregation of Suspended Particles using Acoustic and Flow Fields".

1.2.1 Basic Definitions

In order to understand this technology, brief introductions of various terms used in this proposed technology are given below.

1.2.1.1 Acoustic. The science that deals with production, control, transmission, reception, and effects of sound is called Acoustics.

1.2.1.2 Sound. Sound is generated by pressure variation in a medium. Sound waves can be produced in a medium when there is continuous expansion and contraction of the medium by a mechanical excitation of a sound source.

1.2.1.3 Piezoelectric. A common sound source is vibrating piezoelectric crystals. Piezo is derived from a Greek word, "to press", thus, piezoelectric means pressure electric. A plate cut from piezoelectric crystal with an applied electrical signal, serves as a device for converting electrical energy to mechanical energy.

1.2.1.4 Transducer. A sound source usually made of piezoelectric crystals for generating sound waves is called a transducer. When an electrical signal with a given frequency is sent to the transducer, electrical energy is converted to mechanical energy. This mechanical energy causes the medium to vibrate; expanding when the electrical voltage is positive and contracting when the electric voltage is negative. The expansion and contraction of the transducer causes compression and contraction of the medium, producing acoustic sound waves in the medium. If the frequency of vibration is higher than 18,000 cycles per second, it is not audible and is called ultrasound.

1.2.1.5 Standing waves. When the travelling waves meet a perpendicular boundary, they are reflected back to the source. These reflected waves carry some amount of energy. If waves are continuously sent out and reflected back, the two waves reach a state of equilibrium, when the distance between the source and the reflector is a multiple of a half-wavelength, $n\lambda/2$, where n is an integer number and λ is the sound wavelength. This type of wave field is called an acoustic standing wave field. Thus, the necessary and sufficient condition for the formation of a standing wave is that the distance between the source and the reflecting source (L) is $L=n\lambda/2$. The standing wave with n=1 is called the fundamental or first harmonic. The wave for n=2 is the second harmonic, the wave for n=3 is the third harmonic and so forth. This is shown in Figure 1.1 with corresponding wavelength λ and the distance between the two boundaries $L=n\lambda/2$.

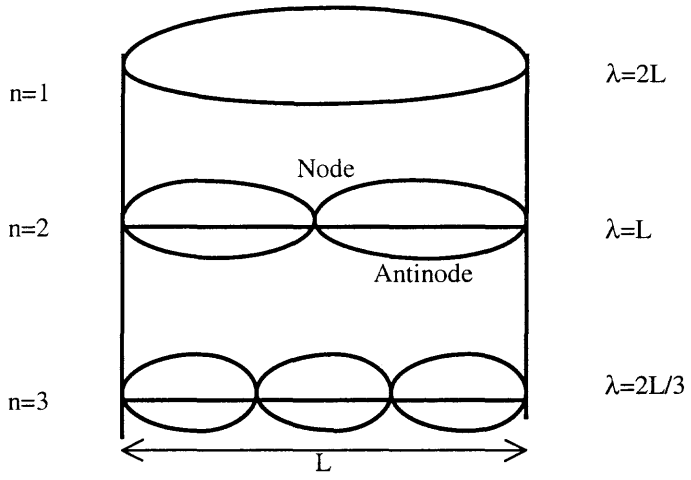

Figure 1.1 Standing Waves

1.2.1.6 Acoustic Radiation and Energy. The total energy in a sound wave is always the summation of the Kinetic and Potential energy. The waves of energy, which travel at the speed of sound in an acoustic field, are the acoustic radiation. Under a stable situation in a standing wave, the amount of energy at various points in the path of travel for a standing wave may differ and points of maximum and minimum energy occur. If the frequency is changed, the wavelength changes cause a shift in the position of maximum and minimum energy. The force exerted by an acoustic standing wave field on the medium is called the acoustic radiation force.

1.2.1.7 Acoustic Pressure and Velocity Amplitudes in an Acoustic Field. A plane standing-wave field arises from the superposition of two waves of equal wavelength and amplitude traveling in opposite directions. Equal wavelengths are necessary for reflection of the waves, and equal amplitudes are required to have constant pressure values at any time along the wave-guide. Figure 1.2 shows the formation of stationary planes of

maximum velocity or zero pressure (antinode planes) and zero velocity or maximum pressure (node planes) in the medium. The node planes lie at half wavelength intervals, with the antinode planes lying equidistant between them. The pressure nodes coincide with the velocity antinodes and vice versa.

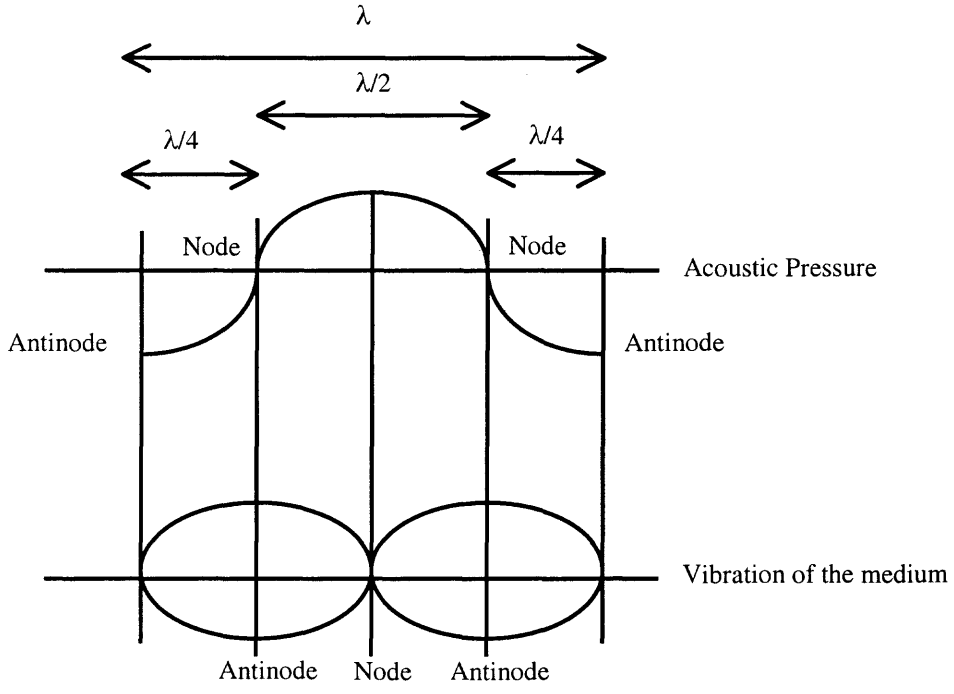

Figure 1.2 Planes of Nodes and Antinodes

1.3 Research Objective

The primary objective of this research is to fractionate suspended particles based on acoustic contrast, which is a function of particle and fluid densities and compressibilities. Acoustic forces generated by acoustic pressure can drive particles to locations of zero acoustic pressure within the acoustic standing wave field. The magnitude of acoustic forces acting on a particle in a medium depends on the acoustic contrast. For particles

with little or no density contrast, the proposed technique is able to discriminate them on the basis of their compressibility. Particles with different size, density, or compressibility respond at different rates to the imposed acoustic wave field. The ultimate separation between the fluid and the particles is achieved by either removing the fluid while the particles are held stationary by applying force or pressure which can act on the particles only, or by transporting the particles through the fluid while keeping the fluid stationary by applying a special type of acoustic force on the particles.

The application of an acoustic field to the fractionation of sediments in suspension will be studied in this research. The acoustic fractionation method proposed in this research will provide an alternative to the classical fractionation methods for sediments. Only a few separation or purification methods exist for the discrimination of particulate materials based on their compressibilities. Conventional methods rely upon differences in particles size (sieve or filtration), electrical charge (electrophoresis), density (centrifugation or sedimentation), interfacial properties (floatation), or thermodynamic properties (selective solubility). However, particles that have traits such as small size, neutral buoyancy, or uniform electromagnetic characteristics pose difficult fractionation problems. As stated before, the existing methods usually require excessive time, prohibitive pressure drops, or extremely high electric or magnetic fields.

Some of the advantages of using this technology of acoustic field separation are to increase the resolution of the separation of the sediments, high production rates by continuous acoustic treatment, and low energy requirement. Unique separation of neutral buoyant particles and particles exhibiting compressibility differences can be achieved. The proposed research attempts to fractionate particles from a bulk suspension in a

relatively long and narrow rectangular separation chamber using an acoustic field and then harvest the particles at the other end of the chamber using a laminar flow field.

1.4 Overview

This research focuses on investigating a technology spanning many different subject areas. The basic theory of the process of segregation and fractionation is provided in Chapter 2. Chapter 3 provides a detailed mathematical derivation and a mechanistic explanation of this technology. In addition, computational difficulties faced in solving governing equations are also discussed in this chapter.

Detailed experimental setup, equipment and model design are described in Chapter 4 along with pictures of the actual experimental setup in the laboratory. The design of physical model was the most challenging aspect of this research. An iterative approach for the design was taken. The steps that were used during iterations are also discussed along with an explanation for their needs.

In Chapter 5, the results from the experiments and comparison between the theoretical predictions and the experimental results are discussed. The last chapter, Chapter 6, provides a summary of the technology along with conclusions based upon the research and suggestions for future investigation.

CHAPTER 2

LITERATURE SEARCH

2.1 Introduction

The aggregation of micron size particles when exposed to an acoustic standing wave field was first observed more than a century ago by Kundt and Lehmann (1874). The real applications and implementations of this theory were not practiced or used until recent years. The search for narrative solutions of particle-liquid separation problems has produced a renewed interest in systems that make use of the acoustic forces on particles suspended in a standing wave field. During the last decade, there has been a growing interest in the manipulation of particles, droplets or bubbles suspended in liquid or gases by forces associated with a resonant acoustic field. The response of particles subjected to various combinations of acoustic forces with hydrodynamic, gravitational or diffusion forces have been experimentally studied by many researchers.

When a particle suspended in a host medium in the presence of an acoustic field, it will experience force associated with the field. It was noted by Kundt (1874) that the acoustic pressure in a medium having waves propagating in one direction, is normal to the waves and is numerically equal to the energy per unit volume. He also observed the effect of acoustic forces through measurements of the motion of dust particles in resonant tubes. King (1934) was the first to present a detailed theoretical formulation of acoustic forces for a rigid sphere in a plane standing or progressive wave field in an ideal fluid. He calculated the radiation forces by summing the effect of acoustic pressures acting on each surface element of the rigid sphere. Yosioka and Kawasima (1955) extended this method

to include the effects on compressible spheres. King's theory was verified experimentally for liquid (Klein, 1938) and gaseous (Rudnick, 1977) media. King's (1934) approach was later extended by Embleton (1956) to the case of a rigid sphere in a progressive spherical or cylindrical wave field. Gor'kov (1962) derived a simple method to determine the forces acting on a particle in an arbitrary acoustic field using a different approach than that proposed by King (1934). He showed that his expression was equivalent to King's expression for a plane standing wave. Nyborg (1967) also derived simple expressions for the acoustic force by extending the methods of King and Embleton. In the case of standing waves, Nyborg's expression reduced to that of Gor'kov. The book "High Intensity Ultrasonic Sound Fields" by Rosenberg (1971) gives several additional references and it is an excellent review of high intensity sound fields.

A complete literature search for this topic was performed. This included literature on detailed descriptions of particles suspended in acoustic wave fields, the parameters that contribute to the phenomena, and results from selected research projects. These are discussed in this chapter based on the applicability to the proposed research.

2.2 Theory

King (1934), was the first person to propose the theoretical basis for the force acting on a spherical particle suspended in a standing acoustic wave field. This analysis was restricted to a rigid particle with a radius much smaller than the wavelength of sound, for a standing wave field created by oppositely travelling, single frequency, sinusoidal waves. Later, Yosioka and Kawasima (1955) extended the above analysis to include compressible particles. When particles are suspended in an acoustic field,

the medium exerts hydrodynamic forces on them. In an acoustic field, forces exerted on particles in the medium are proportional to the local velocities of the fluid and when averaged they become zero. In an acoustic standing wave field, the averaged forces acting on a particle are not zero and play an important part as they arise from second order effects (Gor'kov, 1962).

Figure 2.1 shows forces acting on a particle in an acoustic field. These forces are:

1. Primary Axial Acoustic Radiation Force (F_{PARF})
2. Primary Transverse Acoustic Radiation Force (F_{PTRF}), and
3. Secondary Acoustic Radiation Force (F_S)

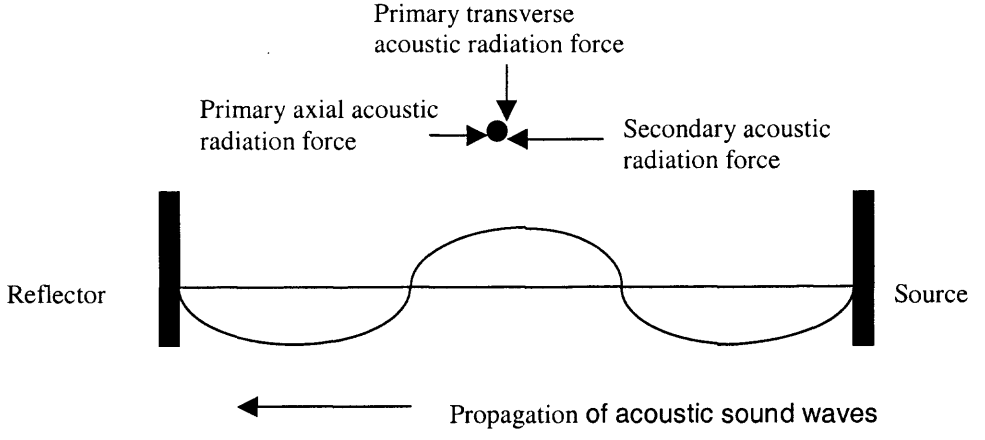

Figure 2.1 Acoustic Forces

2.2.1 Primary Axial Acoustic Radiation Force

Immediately after the application of an acoustic field, particles experience a time-averaged primary axial acoustic force, F_{ac} (F_{PARF}), which is generated by the interaction between particles and the wave field. The primary axial radiation force drives dispersed particles toward the velocity antinodes of the resonance field, so that the average distance

between the particles will decrease considerably. The magnitude of the force depends on the compressibility and density difference between the particle and the medium. The primary acoustic force was derived by Yosioka and Kawasima (1955) and expressed as:

$$F_{ac} = V_0 E_{ac} K G \sin(2Kx) \vec{k} \tag{2.1}$$

The acoustic energy density, E_{ac}, is a measure of the energy residing in a wave field, and is equal to the sum of the time-averaged potential and kinetic energy densities. V_o is the volume of one particle, $K= 2\pi/\lambda$ is the wave number of the acoustic radiation, λ is the sound wavelength, x is the axial distance from a pressure node, and $\vec{k}$ is the unit vector in the axial direction. The axial primary radiation force varies sinusoidally with axial position and is proportional to the acoustic energy density. This force acts in the direction parallel to the propagation of waves.

The response of any solid suspended in a fluid to a resonant acoustic field depends on the acoustic contrast factor, G. For any solid particle suspended in fluid with size $r << \lambda$, the acoustic contrast factor is given by Yosioka and Kawasima (1955):

$$G = \frac{\left(\beta_f - \beta_p\right)}{\beta_f} + \frac{3\left(\rho_p - \rho_f\right)}{\left(\rho_f + 2\rho_p\right)} \tag{2.2}$$

Where, β_f and β_p are the compressibility of the fluid and particle respectively, and ρ_f and ρ_p are the densities of fluid and particle respectively. If G is positive, the particles move towards the pressure nodes and if G is negative, the particles move towards the pressure antinodes.

2.2.2 Primary Transverse Acoustic Radiation Force and Secondary Acoustic Radiation Force

The Primary transverse force acts normal to the wave propagation. An expression for the transverse force on a single particle in an acoustic field with uniform energy distribution was derived by Whitworth et al. (1991), and expressed as:

$$F_{PTRF} = V_O \nabla E_{ac} \left(\frac{3(\rho_P - \rho_f)}{\rho_f + 2\rho_P} \cos^2(Kx) - \frac{\beta_f - \beta_P}{\beta_f} \sin^2(Kx) \right) \tag{2.3}$$

The sound field reflected from a particle generates a time-averaged secondary radiation force, known as Bjerkiness Force, on adjacent particles if they are in the same vicinity (Wiser et al., 1984). For the case of two particles aligned parallel to the node planes, the secondary force acting in the direction of the centerline is expressed as (Weiser et al., 1984):

$$F_S = -\frac{E_{ac} V_O^2}{\pi L^2} \left[\frac{3 (\frac{\rho_p}{\rho f} - 1)^2 \sin^2(Kz)}{2 L^2} + k (1 - \frac{\beta_p}{\beta_f})^2 \cos^2(Kz) \right] \tag{2.4}$$

Where "L" is the center-to-center inter-particle distance and z is the transverse distance from a pressure node. Both primary and secondary radiation forces are proportional to the particle volume, and their magnitudes increase with the size of the particle. Of the three forces, the primary axial radiation force generally has the

greatest magnitude. The magnitude of the transverse primary force is about 100-fold weaker than the axial force (Steven M. et al., 1997). The secondary radiation force is approximately six orders of magnitude lower than the primary axial radiation force. For a very diluted suspension, there are no secondary radiation forces.

The response of the suspended micron-sized particles to a combination of acoustic, hydrodynamic, gravitational and diffusion forces has been experimentally studied by Haar and Wyard (1978). Suspended particles respond to a resonant acoustic field if there is an acoustic contrast between the particles and their suspending fluid. Acoustic forces are sensitive to the size of the particles as well as to the density and compressibility of both the solid and the suspending fluid. Acoustic forces on particles are typically several orders of magnitude larger than their weight; thus, fast fractionation is possible. In order to evaluate the particle fractionation effects of acoustic waves, the acoustic forces described above have to be added to the other dynamic forces on a particle to determine its motion. Also, it must be noted that the acoustic particle separation technology proposed here uses lower power and higher frequency than required; this may cause cavitation and particle disruption.

2.3 Application of Newton's Second Law to a Particle Suspended in an Acoustic Field

What follows is a derivation of particle (dynamic) equilibrium in an acoustic force field is generated inside a rectangular narrow channel of upward fluid flow, where the two walls of the channel are made with a piezoelectric transducer and rigid reflecting surface, as shown in Figure 2.2. Assume that the spacing between the transducer and the reflecting

surface is λ /2. When the transducer is energized at the proper frequency to maintain a resonant acoustic field, there will be a pressure node located on the mid-plane of the chamber, and pressure antinodes located on the chamber walls. The acoustic force on a suspended particle results from the particle-fluid interaction that arises when the particle and suspending fluid have different acoustic properties (density and compressibility). This force is maximum when the particle is at the pressure node at the quarter wavelength, mid-plane of the chamber width.

For a dilute suspension, the secondary radiation forces, the body forces and the hydrodynamic interactions are neglected. Using Newton's Second Law, the following equations describe the (dynamic) equilibrium of the particle suspended in an acoustic field:

The time rate of change of particle momentum is equal to:

$$(\rho_p V_0 + 0.5\rho_f V_0)\ \overrightarrow{dv/dt} = \overrightarrow{F_{PARF}} + \overrightarrow{F_{PTRF}} + V_0(\rho_p - \rho_f)\,g + \overrightarrow{F_D} \qquad (2.5)$$

or

$$\overrightarrow{m_v a} = \overrightarrow{F_{PARF}} + \overrightarrow{F_{PTRF}} + V_0(\rho_p - \rho_f)\,g + \overrightarrow{F_D} \qquad (2.6)$$

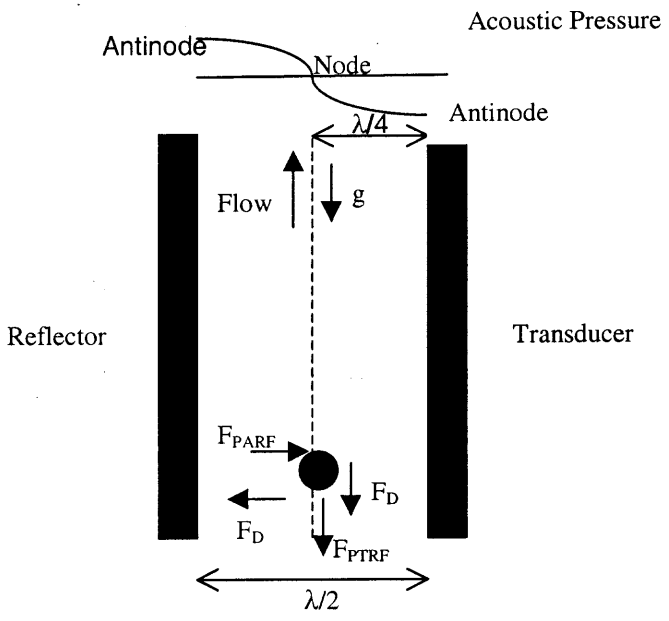

Figure 2.2 Forces on a Particle in an Acoustic Field

Where v is the particle velocity, g is the gravitational acceleration and the arrow on the force term is the vector direction. The mass in the momentum term is the "virtual mass" of the particle, m_v, that is the sum of the true particle mass and a fluid mass that behaves effectively as if it was entrained with the particle. The particle's velocity (v) in the fluid due to the primary radiation force is very small, which yields a Reynolds numbers less than 0.01 (Woodside, 1997), then the drag force is given by Stokes' Law as shown below:

$$\vec{F_D} = -6\pi\mu r\vec{v} \tag{2.7}$$

Here, μ is the viscosity of the fluid and r is the radius of the particle in the suspension. The summation of the forces in the direction of the acoustic wave propagation gives:

$$\vec{m_v a_h} = \vec{F_{PARF}} + \vec{F_D} \tag{2.8}$$

or

$$\vec{F_{PARF}} = \vec{m_v a_h} + \vec{6\pi\mu r v} \tag{2.9}$$

The summation of the forces normal to the wave propagation gives:

$$\vec{m_v a_v} = \vec{F_{PTRF}} + V_0 (\rho_p - \rho_f) \vec{g} + \vec{F_D} \tag{2.10}$$

or

$$\vec{F_{PTRF}} = \vec{m_v a_v} - V_0 (\rho_p - \rho_f) \vec{g} + 6\pi\mu r \vec{v} \tag{2.11}$$

Where, a_h and a_v are the acceleration along and normal to the direction of the wave propagation.

As stated before, the value of the transverse force is very small and thus can be ignored. Thus, the acoustic force, F_{ac} without the vector notation, on a particle in an acoustic field is due to the primary axial radiation force, F_{PARF}, is defined below and shown in Figure 2.3.

$$F_{ac} = F_{PARF} = m_v a_h + 6\pi\mu r v = V_0 E_{ac} K G \sin(2Kx) \tag{2.12}$$

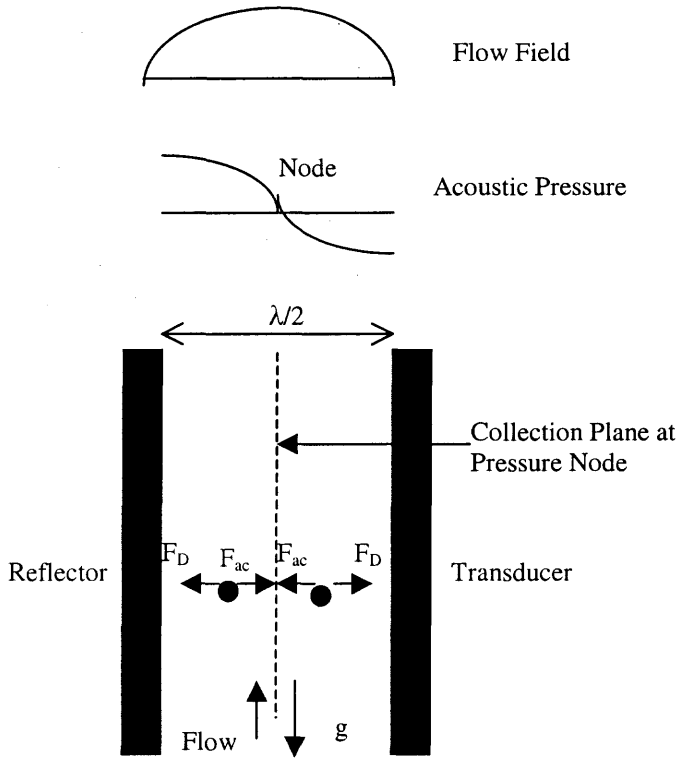

Figure 2.3 Acoustic Force on the Particles

The hydrodynamic drag on the particles as they move across the channel in response to the acoustic field, is proportional to the radius of the particle, r. Since the acoustic force is proportional to r^3, the speed of response of the particles is a function of r^2. Therefore, larger particles will be driven to the node faster than smaller particles. In a mix suspension of particles, the speed of response will depend on the Gr^2 combination as shown in Figure 2.4. Ultimately, all particles will be driven to the pressure node.

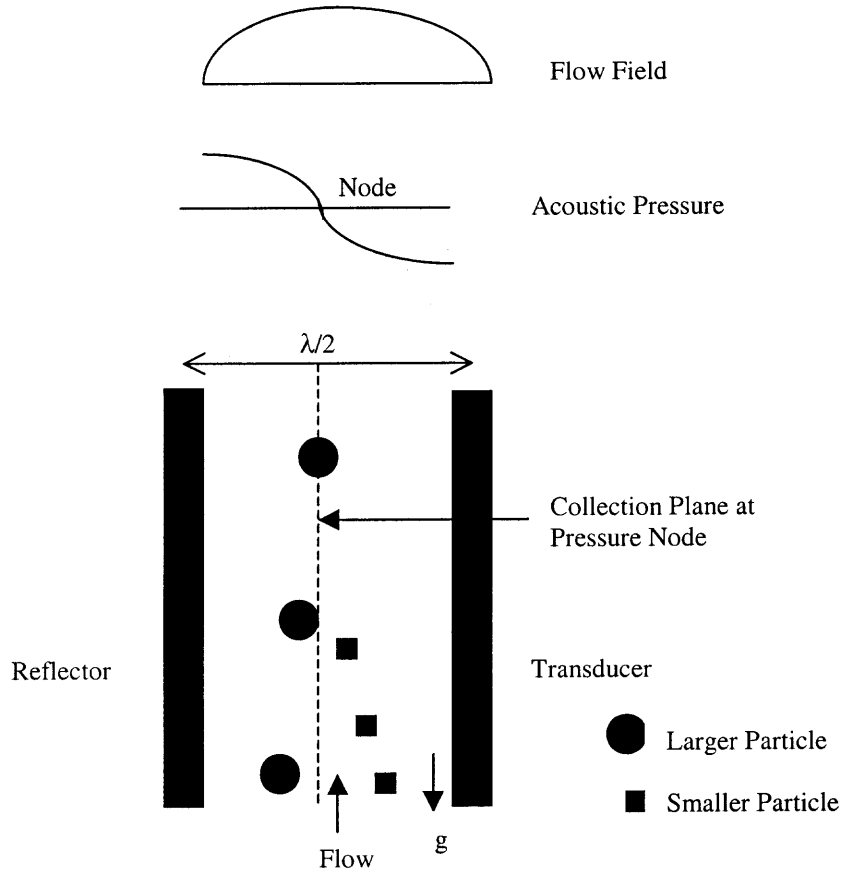

Figure 2.4 Mix Suspension of Particles

Figure 2.5, shows a chamber width greater than a half wavelength. For this chamber, there will be a multiple of collection planes depending upon the frequency of the sound waves and the width of the channel. The collection planes are equidistant at half wavelength intervals.

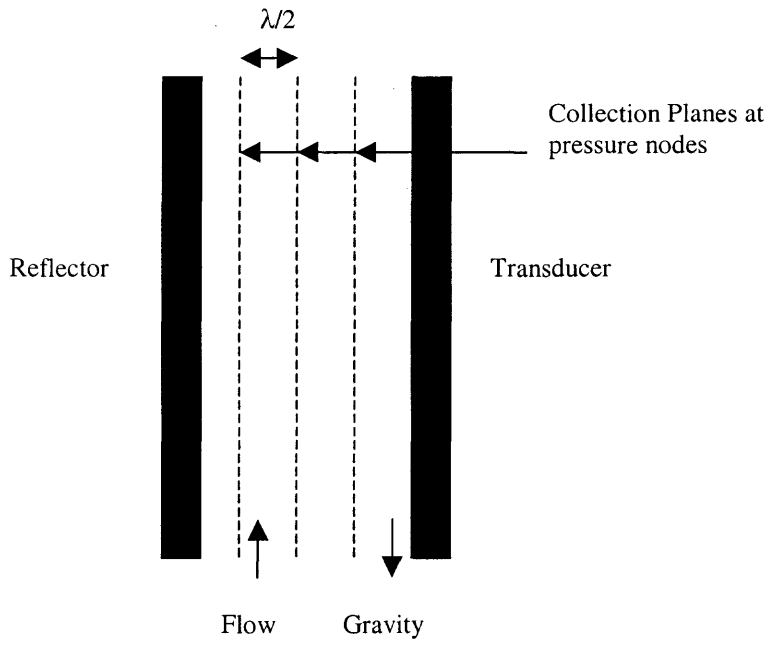

Figure 2.5 Multi-wavelength Width Chamber

Separation of particles from the host media using acoustic standing wave fields has been studied and used in many practical applications. In medical science it has been used for separation of blood composition for treatment and diagnosis. Standing wave fields have been used to determine the acoustic properties of red blood cells, to accelerate imunoprecipitation and to enhance the sedimentation of mammalian cells (Weiser et al., 1984). Weiser observed that after particles in a standing wave have moved to form bands at half-wavelength spacing, the particles within these bands often redistribute to form multiple columns in the direction of wave propagation. The redistribution of the particles within the bands is due to the primary transverse acoustic force (discussed in the previous section) which arises when the particles are at slightly different positions in the primary acoustic field. This acoustic force causes the particles to move relative to each other.

2.4 Parameters Contributing to the Acoustic Fractionation and Segregation Technology

The parameters that affect the proposed technology for the separation of fine suspended particles in an acoustic field can be divided into two groups. The parameters in the first group were obtained from the assumptions or conditions on which the acoustic force equation was developed by Kings (1934). Those in the second group were obtained based on the different parameters of the Equation (2.12).

In order to determine the contributing parameters in the first group, one needs to re-examine Equation (2.12):

$$F_{ac} = F_{PARF} = m_v a_h + 6\pi\mu rv = V_0 E_{ac} KG\sin(2Kx) \qquad (2.12)$$

The acoustic force was derived by assuming the following conditions:

1. The sound is a sinusoidal wave of a single frequency.
2. The stationary waves are composed of plane progressive waves with the same amplitude travelling in opposite directions.
3. The particle size is significantly smaller than the wavelength of the sound wave.
4. The suspension is so dilute that there is no impact on the motion of the other particles in the vicinity.
5. The sound field is not disturbed by either ultrasonic cavitation or suspended particles, and hence the energy density remains constant in the entire field.
6. There is no change in temperature due to the irradiation of sound.

In order to use the acoustic force acting (Equation 2.12) on suspended particles (King, 1934), it is essential that the above six conditions are satisfied. The first two

conditions are necessary for the formation of standing waves in the resonator. The distance between the transducer and the reflector has to be a multiple of a half wavelength ($n\lambda/2$, where n is an integer). Progressive waves are formed when distance differs from the above. Deviations can occur in the wave-guide when there is a change of sound speed, frequency, or energy. The Equation (2.12) can be used as long as particles are very small compared to the sound wavelength. In this research the size of the particles tested are a small fraction of the wavelength. The above does not imply that for large size particles lower frequency can be used. There is a limiting frequency value depending on the treatment time and temperature. When the fourth condition is maintained, one can ignore the transverse and secondary forces. Conditions 5 and 6 are the most critical conditions and difficult to control. Cavitation and temperature increase will occur during the tests and will be studied carefully.

From Equation (2.12), the most important parameters are the acoustic energy (E_{ac}), contrast factor (G), and viscosity of the fluid (μ). The contrast factor is a function of particle and fluid density and compressibility as described in Equation (2.2). The proposed separation technology can work as long as the contrast factor is not zero. If the G value is positive then the particles move towards the pressure nodes and for negative G value, the movement is towards the pressure antinodes. Thus the technology must be applied within the limitation of a non-zero contrast factor.

Therefore, the most significant parameters that contribute to the efficiency of the proposed technology are cavitation, temperature, acoustic energy, and viscosity of the fluid, and hence, a detailed examination of prior researches is given below.

2.4.1 Cavitation and Streaming

Acoustic cavitation refers to the generation of bubbles by sound fields in liquids containing dissolved gases. The motion of such bubbles is called streaming. Acoustic cavitation concentrates energy by transforming the relatively low energy density of a sound field into the high energy density characteristic of the neighborhood and interior of a collapsing bubble. As a result, the development of cavitation at high sound pressures interferes with the orderly concentration of particle in a standing wave field. Hence, there should not be cavitation or streaming during the application of the proposed technology in order to obtain high segregation efficiencies. The rate of particle movement to a fixed nodal or antinode column position is directly proportional to the applied standing-wave pressure amplitude. By increasing sound pressure, one would expect to reduce the time to form concentrated columns. However, the application of high pressure to an air-saturated liquid suspension would also enhance the probability of occurrence of cavitation and enhance acoustic streaming within the chamber.

In cases when it is difficult to control the cavitation, the behavior of the particles in the presence of cavitation was studied by Gould et al. (1991). Gould and his collaborators worked on the maximum acoustic pressure for which the particles suspended in an acoustic field could tolerate cavitation without disturbance. In their study, the transducer was driven at a frequency of about 1.02 MHz. The chamber was filled with either water-saturated gases or with degassed water. Water saturated with gas had 100% dissolved oxygen and did not contain visible bubbles before treatment. The first sign of acoustic cavitations in water occurred at about eight times the minimum pressure, P_{min}, required to cause a detectable weak striation of 9 micron polystyrene

particles. The particle separation also persisted at the higher sound pressure levels where low noise levels (indication of cavitation) were detected and bubbles were observed. The vertical particle columns continued to form until strong continuous noise levels were observed at a sound pressure of 27 times the pressure P_{min}.

A strong noise signal is usually associated with transient cavitations in which the active bubbles expands to at least twice its initial size and then collapses violently often disintegrating into many smaller bubbles. Cavitation bubbles grow from nuclei or from micro bubbles in sonicated water. Bubbles in a sound field are like inhomogeneities in liquid due to micro spheres, and are subjected to radiation forces both due to the standing wave field and pressure force produced by the vibrations of the bubbles themselves. For gaseous bubbles in a standing-wave field, bubbles move either towards maximum or minimum pressure depending on the size of the bubbles. Bubbles smaller than particle sizes are attracted to zones near pressure maxima. Once a bubble grows larger than the particle size, it will no longer be driven toward a pressure maxima but will move close to pressure nodal regions (Gouldd et al., 1991). Nomura et al. (1998) made similar observations.

With respect to cavitations, high levels of cavitations are disruptive to the proposed technology. However, aggregated particles can tolerate some bubble activity and cavitations including the presence of low noise levels. This tolerance may be due to the separation of regions of particle clumping and regions of bubble aggregation in a standing wave field. The results above emphasized that cavitation and streaming are the two main limitations to the use of high transducer forces. Streaming can be controlled to some degree by careful choice of chamber geometry and sound field design.

That is, by having parallel transducers to allow perfect reflection of sound waves for the standing field. Use of degassed water for the control of cavitation is another alternative.

In this research, the contribution due to cavitation and streaming is minimized by the careful design of the chamber and application of vacuum pressure at the outlet at the top of the chamber.

2.4.2 Effect of Temperature Change

Most of the prior research reported in the literature was conducted with deionized water at 25°C. The deionized water was used to prevent the flow of current inside the resonator. If the temperature of the suspension is not kept constant, the speed of the sound is not constant during the experiment. When the acoustic field is used for particle separation, the rise in temperature affects the wavelength required for a standing wave field due to change of the sound speed in the liquid.

McSkimin (1964) studied the velocity of sound in deionized water for the temperature range of 20° to 75° C at a frequency near 60 MHz, shown in Table 2.1. According to his study, the mean velocity obtained at 25° C is 1496.65±0.010 m/sec and for 74.00° C is 1555.10±0.10 m/s (maximum value for the range measured). The temperature increase in the chamber is directly related to acoustic treatment time. Pui et al. (1995) showed that the average rate of temperature increase inside the chamber is 1.2°C/min. According to Pui, this heating resulted from attenuation of the acoustic energy in the transducer, reflector, and particle suspension. Temperature differences in the chamber induced convection currents, which disrupted particle aggregation. Free convection currents move some columns of particles to join with other columns.

Figure 2.6 shows the average temperature rise with respect to acoustic treatment time (Pui et al., 1995).

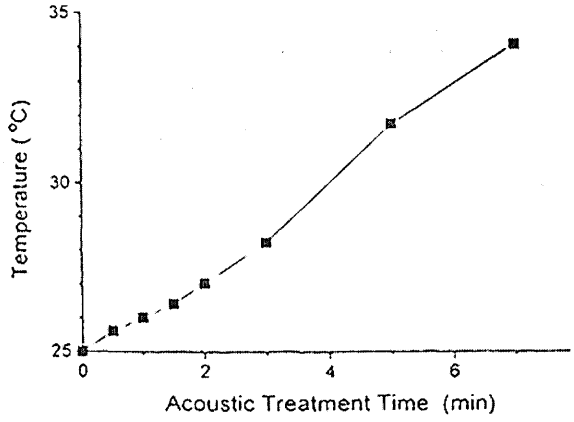

Figure 2.6 Averaged Temperature Rise at Power Level of 180W/L (Pui, et al., 1995)

Since the temperature and hence speed of sound cannot be controlled, some means of frequency control or distance adjustment is required from a high efficiency driving source to limit the power input in the resonator to accommodate the increase in temperature. However, if the frequency is changed the transducer may not function at optimum conditions, hence it is recommended to adjust the distance between the transducer and reflector. Another alternative is to adjust the treatment time to avoid substantial rise in temperature. Table 2.1 will be used as a guide for predicting the velocity of sound during the experiments, while the temperature will be checked by using a thermocouple inserted just above the upper end of the acoustic field.

Table 2.1 Velocity of Sound in De_ionized Water as a Function of Temperature (McSkimin, 1964).

Temp. ^{O}C	Velocity m/sec	Temp. ^{O}C	Velocity m/sec
23.41	1492.27	72.45	1555.05
23.79	1493.33	72.94	1555.07
24.20	1494.48	73.38	1555.08
24.63	1495.58	73.59	1555.09
25.02	1496.65	73.99	1555.09
25.41	1497.70	74.19	1555.11
25.83	1498.77	74.58	1555.10
28.00	1504.29	74.99	1555.08
29.00	1506.72	75.38	1555.06
29.93	1509.01	75.82	1555.06
30.06	1509.34	76.09	1555.01
31.00	1511.33	76.36	1555.00
34.99	1519.81	76.96	1554.94
40.00	1528.83	77.45	1554.88
45.00	1536.36	77.99	1554.80
49.97	1542.53	78.51	1554.70
54.96	1547.32	78.94	1555.62
59.98	1550.94	-	-
64.98	1553.39	-	-
71.64	1554.97	-	-

2.4.3 Acoustic Energy Density (E_{ac}) and its Distribution in the Resonator

The axial primary radiation force (PRF) is the force that acts on a particle when subjected to a standing wave field. This force pushes the particle towards the pressure node. The transverse PRF aggregates the particle within the nodal planes and retains them in the field against the dragging force. These two forces, primary axial and primary transverse acoustic forces, are functions of acoustic energy density (E_{ac}). The acoustic energy density, E_{ac}, is a measure of the energy residing in a wave field. Ultrasonic force measurements by Woodside et al. (1997) showed that the E_{ac} in the ultrasonic field was highly nonuniform. Optimization and scale-up of ultrasonic fields must be improved and

that can be done only by improving knowledge of the ultrasonic force distribution and having a better understanding of the mechanisms involved in generating uniform acoustic energy.

In systems operated with non-resonant standing waves, a common technique for E_{ac} estimation is to equilibrate the gravitational force with the PRF on particles with known acoustic properties (Weiser et al., 1984). For these systems, the E_{ac} is proportional to the driving voltage. For a systems with a resonant standing wave (as in the case of the present research), this method is not accurate because it will disturb the sound field in the medium. A very slight change in frequency (on either side) from the driving frequency required for a resonance, strongly influences the E_{ac} in the system. At the resonance frequency, the admittance which is the inverse of the impedance of the system reaches a maximum while the current and the power density, P, of the system reach a peak for a constant driving voltage. The degree of resonance in an oscillatory system can be characterized by a unitless quality factor, Q (French, 1971), and is defined as:

$$Q = \frac{E_{ac}\,\omega}{P} \tag{2.13}$$

Here Q refers to the ratio of volume of the chamber divided by its area and boundary layer thickness, and ω is the angular frequency ($\omega=2\pi f$). Resonators driven at a resonance frequency with a high Q require a lower power input to generate a given E_{ac}. This minimizes temperature gradients and convective flows due to inhomogeneous heating of the resonator.

Woodside et al., (1998) related the acoustic energy density of the transducer, reflector and resonator to their respective distributions of velocity amplitude according to the following equation: $E_{ac}= 1/4\rho v_0^2$, where ρ is the density of the material and v_0 is the velocity amplitude of transducer, or liquid at the interface. The transducer surface-velocity amplitude distribution of the resonator is shown in Figure 2.7. According to Woodside's observation, the measured amplitudes were highest near the center of the Piezoceramic transducer and fell toward zero at the edges. Local displacement amplitude maxima on the surface appeared as dark spots relative to the background and formed a grid like pattern. The oscillation amplitude map of a portion of the reflector surface is shown in Figure 2.8. The amplitude was again found to be highest near the center of the resonator and a grid like pattern of localized amplitude maxima was visible.

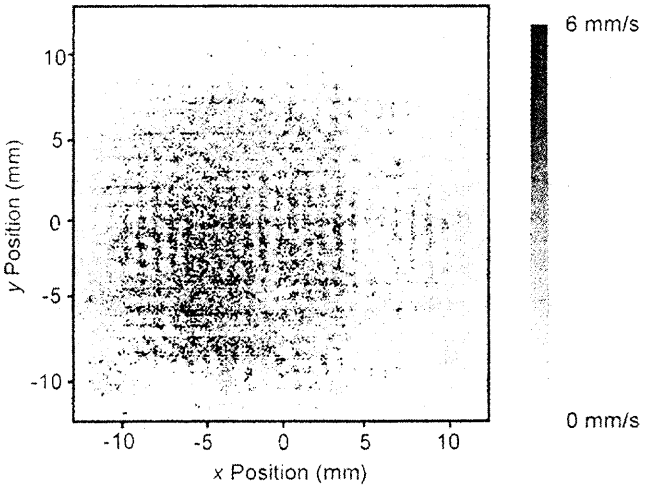

Figure 2.7 Piezoceramic Transducer Surface-Oscillation Velocity

(Woodside et al., 1998)

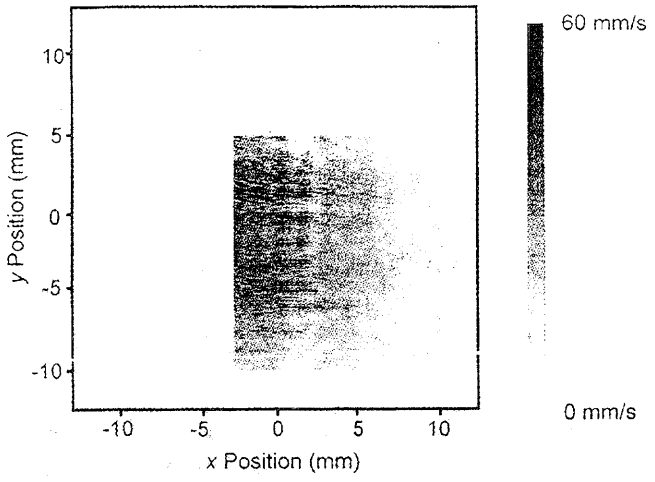

Figure 2.8 Glass Reflector Surface-Oscillation Velocity (Woodside et al., 1998)

The liquid vibration amplitude followed the same trend as the reflector amplitude, with maximum at the center and tending to zero near the surface boundaries.

Groschl (1997) predicted the acoustic energy densities and velocity amplitude in the transducer, reflector and the fluid of an ultrasonic resonator. Table 2.2 shows the comparison between the velocity amplitude predicted by Woodside (1998) and Groschl, (1997), at frequency of 2.251 MHz, power of 0.5W/L, and quality factor Q of 5000. In both cases the transducer velocity amplitude is the lowest, the reflector is second highest and liquid velocity amplitude is the highest.

Table 2.2 Mean Oscillation Velocity Amplitude values Obtained from Groschl (1997) and Woodside (1998)

Layer	Velocity (mm/sec) (Groschl, 1997)	Velocity (mm/sec) (Woodside,1998)
Transducer	14	7.8
Liquid	170	190
Reflector	25	93

From the above table, it can be concluded that the reflector and transducer behave as stationary boundary conditions, resulting in a fluid with a high amplitude near the center and zero amplitude near the walls (transducer and reflector). Also from the above table, it can be concluded that there is non uniform energy distribution in the liquid and the application for the treatment of the dredged sediments can be achieved successfully in the maximum energy field nearly at the center of the system.

The quality factor of the resonator can be measured using a computer controlled admittance measurement as explained by Woodside et al., (1997). By knowing the quality factor and power input into the system, it is possible to find the energy in the fluid using Equation (2.13). The higher the Q value, the lower the power input required for generating the required energy for acoustic separation. If the Q value is low, energy losses into the medium, transducer and reflector will cause increase in the temperature of the fluid. The temperature inside the fluid must be maintained constant for the generation of the acoustic force given by Equation 2.12. Thus, it is possible to decrease the acoustic energy required for treatment by controlling the degree of resonance in the system (Q value) through proper design of resonator volume, area of the resonator and thickness of boundary layer. Groschl, 1997, reported experimental values of Q between 5000 and 10000. In this research, a Q value of 5000 will be assumed.

2.4.4 Viscosity

The influence of fluid viscosity on the acoustic radiation pressure was first investigated by Westervelt (1951). He found that the radiation force exerted by the progressive wave on a rigid immobile sphere is greater than that given by King's theory. The fluid viscosity

effect arises due to losses within the boundary layer of the object and is significant for small spheres and at low frequencies (Danilov, 1994).

Viscosity of the suspended fluid can have a considerable influence on the primary radiation force (PRF). The ideal fluid approximation provides a good estimate of the PRF in cases where the particle radius is much smaller than the wavelength and much greater than the viscous boundary layer thickness. The radiation force in the viscous medium can be several orders of magnitude higher than in the non-viscous case (Equation 2.12). On the other hand, this effect of viscosity decreases rapidly with increase in frequency. When dealing with low viscosity fluids like water, the impact of viscosity on the technology is minimal. One other problem due to the increase of the radiation force in a high viscosity fluid is the development of acoustic streaming that leads to an additional drag force. This drag force causes an increase in the amplitude of the scattered field affecting the primary radiation force. The secondary radiation force between particles is influenced by viscosity in the same qualitative way as the primary force. Thus, the influence of viscosity can be explained as a change in the phase and amplitude relations between the primary and scattered fields.

When dealing with suspended particles in a low viscosity liquid (as is the case in this research), the effect of viscosity on the technology can be controlled by appropriate resonance frequency and solution concentration. But for viscous solutions, additional care should be taken so as to minimize the effects of streaming and scattered fields depending on the type of medium.

2.5 Summary and Conclusions

Segregation and fractionation of suspended particles using acoustic standing wave fields require a high degree of control of different parameters governing the technology. Based on the above discussion and a study of experimental observations of several researchers, the following can be concluded and will be employed or considered during the implementation of the proposed technology:

1. The particles to be separated have to be smaller than the wavelength of sound. The original equation of acoustic force on the particle derived by King (1934) was based on the fact that the particles are much smaller than the wavelength of the sound.
2. Only sinusoidal waves will be used to produce sonic oscillation in the system, as required by Equation (2.1).
3. To produce a stationary field in the system a reflector is required which reflects the waves with the same amplitude in opposite directions. This can be achieved by requiring that the distance between the transducer and the reflector be an integral multiple of a half wavelength.
4. The secondary interaction force between particles is influenced by concentration. Taking a dilute suspension will reduce the secondary radiation forces. This is due to the fact of dilute concentration and also because of the short residence time of the suspension in the acoustic field (few seconds) during treatment.
5. Acoustic particle separation technology uses lower power and higher frequency than is usually associated with cavitation and particle disruption. Cavitation and steaming factors should be avoided in the field. Cavitation occurs when small air bubbles are trapped in the liquid and can be controlled by using degassed water.

Acoustic streaming can be controlled to some extend by proper design of the chamber, that is, there should be no irregular surfaces and the walls of transducers should be parallel to each other to avoid energy dissipation and losses. The formation of air bubbles and noise will be used as indicators to predict cavitation. Small cavitation may be tolerated by the system causing the separation of regions of particle clumping and regions of bubble concentration in a standing wave field. A moderate frequency in the kilohertz range is considered optimal and will be used in this research.

6. A large acoustic chamber will be built to have a large volume of liquid where the temperature effect will be neglected due to the dissipation of heat through a larger area. The standard working temperature for the experiment will be around 25°C, where the speed of sound is approximately 1497 m/s. Significant temperature fluctuation is unfavorable for the proposed technology. Table 2.1 will be used as a guide for dealing with changes in sound velocity due to changes of temperature.

Design of an ideal acoustic separation chamber can be achieved if all the above-discussed points are considered simultaneously. It is an integrated design where mismatching any parameter may lead to unsuccessful acoustic treatment technology.

The design of the experimental chamber and experimental results using the above considerations will be further discussed in Chapter 4 and Chapter 5, respectively. But before doing that there is a need to understand the mechanics behind the process. This is discussed in Chapter 3. In the next chapter all the steps and assumption used for the derivation of particle trajectories and the concentration equation are also discussed in detail.

CHAPTER 3

A MATHEMATICAL MODEL

When particles of size smaller than the sound wavelength are suspended in an acoustic standing wave field, a number of forces act on them. One such force is the primary acoustic force, which is in the direction of the propagation of the waves. The (dynamic) equilibrium of the particles under the different forces was described by Equation (2.12):

$$(\rho_p V_0 + 0.5\rho_f V_0)\frac{dv}{dt} + 6\pi\mu r\frac{dx}{dt} - 4\pi r^3 KE_{ac} G\sin(2Kx) = 0 \qquad (2.12)$$

In this chapter the particle trajectories in an acoustic wave field are determined. Table 3.1 gives the properties of particles and fluid that are assumed for the derivation of equations of particle trajectories and concentrations when suspended in a host medium.

Simplifying the Equation (2.12) with values in Table 3.1 yields:

$$\frac{dv}{dt} + 1.42\times10^6\frac{dx}{dt} - 10^8\sin(2.78\times10^{-3}x) = 0 \qquad (3.1)$$

In the next section, detailed derivations of rather accurate approximations of the particle trajectories and concentration are provided. But before that, a study of the behavior of the solutions is discussed with an explanation of the available solution techniques. Solutions of Equation (3.1) will be used as a basis for concluding some results during the derivation.

Table 3.1 Properties of Particles and Suspending Medium

Description	Solid (Silica Fume)	Medium (DI Water)
Density (ρ) (Kg/micron^3)	2.649E-15	1.0E-15
Particle Size, Diameter (micrometer)	2	-
Contrast Factor (G) between particle and medium	1.724	1.724
Frequency of Sound in medium (f) (kHz)	-	333
Viscosity of medium (μ) (N-sec/micron^2)	-	9.98 E-16
Acoustic Energy in medium (J/m^3)	-	133
Speed of sound (m/sec)	3750	1500
Power in medium W/m^3	-	56000
Quality Factor (Q) of chamber	-	5000

3.1 Mathematical Analysis of Equilibrium of Particle in an Acoustic Field

For simplicity, the above Equation (3.1) is replaced by an equivalent equation with constants representing the numerical values of the parameter. The particle velocity and the acceleration terms are replaced by their respective derivatives, that is, $dx/dt=x'$, and $dv/dt= x''$. Rewriting Equation (3.1) in different form:

$$x'' + c\,x' - k\sin\beta x = 0 \tag{3.2}$$

Where, c= 1.42E6, k=E8, and β=2.78E-3 are constants representing the physical parameters of Equation (3.1). This equation will be constantly used during the mathematical derivation. The notation ($'$) indicates the derivative of the function, d/dt,

and x is the position of the migrating particle in the x-direction between a transducer and a reflector separated by one half wavelength (= $\lambda/2$) of the resonant sound at the given frequency. The parameters c, k, and β are all positive constants having the following orders of magnitude:

$c = O(10^6), k = O(10^8), \beta = O(10^{-3})$

Note that Equation (3.2) has the form somewhat like a damped nonlinear spring (or pendulum) equation. Several publications cited in the literature assumed instantaneous viscous relaxation where the inertial term dv/dt was neglected. This type of singular perturbation approximation; namely:

$$c\,x' - k \sin \beta x = 0 \tag{3.3}$$

has been used to approximate the solution for Equation (3.2). It will be shown in this chapter that although this approximation produces results that are qualitatively correct, quantitative errors are incurred that can be significant for some applications.

3.1.1 Preliminary Analysis

There is no closed form solution for Equation (3.2), so one has to rely on qualitative and approximate analysis techniques that will be discussed in this section. Useful information on the nature of the solutions of Equation (3.2) can be obtained by recasting it as a 2-dimensional system and performing a careful phase plane analysis. To do this, first set $x' = v$ and then rewrite (3.2) as the following system in the x, v-plane:

$$x' = v \tag{3.4}$$

$$v' = k \sin\beta x - cv <=> (x', v') = F(x, v) \tag{3.5}$$

Equation (3.5) in matrix form, with f_1 and f_2 as function of x' and v' respectively is:

$$\begin{bmatrix} x' \\ v' \end{bmatrix} = F = \begin{bmatrix} f_1 \\ f_2 \end{bmatrix} = \begin{bmatrix} v \\ k \sin \beta x - cv \end{bmatrix} \tag{3.6}$$

The fixed (critical or stationary) points of Equation (3.5) are those points in the x, v-plane satisfying function $F(x, v) = 0 \Leftrightarrow v = 0, k \sin\beta x - cv = 0$:

$$k \sin \beta x - c \times 0 = 0 \tag{3.7}$$

$$\sin \beta x = 0 \quad when\ x = \frac{m\pi}{\beta}$$

Hence, these points are $(m\pi/\beta, 0)$, where m is an integer.

To find the local behavior of the solutions Equation (3.6) near the fixed points, the derivative of F, F', is computed at these fixed points:

$$F' = \begin{bmatrix} \frac{\partial f_1}{\partial x} & \frac{\partial f_1}{\partial v} \\ \frac{\partial f_2}{\partial x} & \frac{\partial f_2}{\partial v} \end{bmatrix} = \begin{bmatrix} 0 & 1 \\ \beta k \cos \beta x & -c \end{bmatrix} \tag{3.8}$$

Consequently, when $x = \frac{m\pi}{\beta}$, and when m is even:

$$F'\left(\frac{m\pi}{\beta}, 0\right) = \begin{bmatrix} 0 & 1 \\ \beta k & -c \end{bmatrix} \tag{3.9}$$

And when m is odd:

$$F'(\frac{m\pi}{\beta}, 0) = \begin{bmatrix} 0 & 1 \\ -\beta k & -c \end{bmatrix} \tag{3.10}$$

To compute the spectral properties of Equations (3.9) and (3.10), one needs to calculate the eigenvalues of the derivative matrices. The eigenvalues (μ) of Equation (3.9) are the roots of the equation:

$$\begin{vmatrix} 0-\mu & 1 \\ -\beta k & -c-\mu \end{vmatrix} = 0 \tag{3.11}$$

$$\mu^2 + c\,\mu - \beta\, k = 0; \tag{3.12}$$

$$\mu = \frac{-c \pm \sqrt{c^2 + 4\beta k}}{2} \tag{3.13}$$

Hence, there is one negative eigenvalue (μ_-^e) and one positive eigenvalue (μ_+^e) given, respectively, by:

$$\mu_-^e = -\frac{c}{2}\left(1 + \sqrt{1 + \frac{4\beta k}{c^2}}\right) \cong -c \tag{3.14}$$

$$\mu_+^e = \frac{c}{2}\left(\sqrt{1 + \frac{4\beta k}{c^2}} - 1\right) \cong \frac{\beta k}{c} \tag{3.15}$$

where the approximate formulas followed from Equation (3.2). The eigenspaces (E) associated to these eigenvalues are calculated as follows:

$$E(\mu_-^e) : \begin{bmatrix} \mu_-^e & -1 \\ -\beta k & \mu_-^e + c \end{bmatrix} \begin{bmatrix} \xi \\ \eta \end{bmatrix} = \begin{bmatrix} 0 \\ 0 \end{bmatrix} \Rightarrow \begin{bmatrix} \xi \\ \eta \end{bmatrix} = const \begin{bmatrix} 1 \\ \mu_-^e \end{bmatrix} \tag{3.16}$$

$$E(\mu_+^e) : \begin{bmatrix} \mu_+^e & -1 \\ -\beta k & \mu_+^e + c \end{bmatrix} \begin{bmatrix} \xi \\ \eta \end{bmatrix} = \begin{bmatrix} 0 \\ 0 \end{bmatrix} \Rightarrow \begin{bmatrix} \xi \\ \eta \end{bmatrix} = const \begin{bmatrix} 1 \\ \mu_+^e \end{bmatrix} \tag{3.17}$$

Similarly, the eigenvalues of Equation (3.10) are the roots of the equation:

$$\mu^2 + c\mu + \beta k = 0 \Rightarrow \mu = \frac{-c \pm \sqrt{c^2 - 4\beta k}}{2} \tag{3.18}$$

Both of these roots are negative. One of these $\mu^0_{\equiv}$ has a large magnitude and the other μ^0_- has small absolute value; these are given as:

$$\mu_{\equiv}^0 = -\frac{c}{2}\left(1 + \sqrt{1 - \frac{4\beta k}{c^2}}\right) \cong -c, \tag{3.19}$$

$$\mu_-^0 = -\frac{c}{2}\left(1 - \sqrt{1 - \frac{4\beta k}{c^2}}\right) \cong -\frac{\beta k}{c}, \tag{3.20}$$

The corresponding eignespaces (E) are:

$$E(\mu_{=}^{0}) : \begin{bmatrix} \mu_{=}^{0} & -1 \\ \beta k & \mu_{=}^{0}+c \end{bmatrix} \begin{bmatrix} \xi \\ \eta \end{bmatrix} = \begin{bmatrix} 0 \\ 0 \end{bmatrix} \Rightarrow \begin{bmatrix} \xi \\ \eta \end{bmatrix} = const \begin{bmatrix} 1 \\ \mu_{=}^{0} \end{bmatrix} \qquad (3.21)$$

$$E(\mu_{-}^{0}) : \begin{bmatrix} \mu_{-}^{0} & -1 \\ \beta k & \mu_{-}^{0}+c \end{bmatrix} \begin{bmatrix} \xi \\ \eta \end{bmatrix} = \begin{bmatrix} 0 \\ 0 \end{bmatrix} \Rightarrow \begin{bmatrix} \xi \\ \eta \end{bmatrix} = const \begin{bmatrix} 1 \\ \mu_{-}^{0} \end{bmatrix} \qquad (3.22)$$

It is concluded that the fixed points of the form (2 $l\pi/\beta$, 0) are all saddle points having local phase plane behavior that looks like Figure 3.1. Where l is any interger ≥ 0. Note that the angle θ between eigenvector (w^u) and x axis is $\theta = Tan^{-1}(\mu^e_-)$.

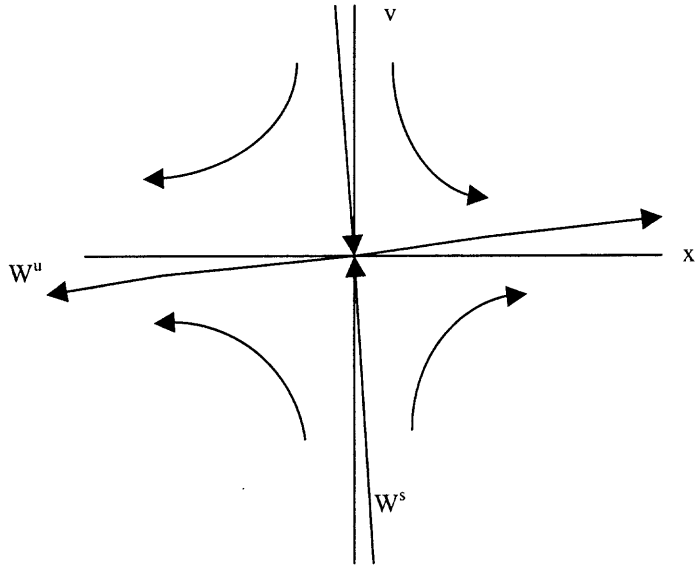

Figure 3.1 Phase Plane near (2 $l\pi/\beta$, 0)

On the other hand, the fixed points of the form ((2l+1)π/β, 0) are all sinks with local phase plane behavior shown below in Figure 3.2:

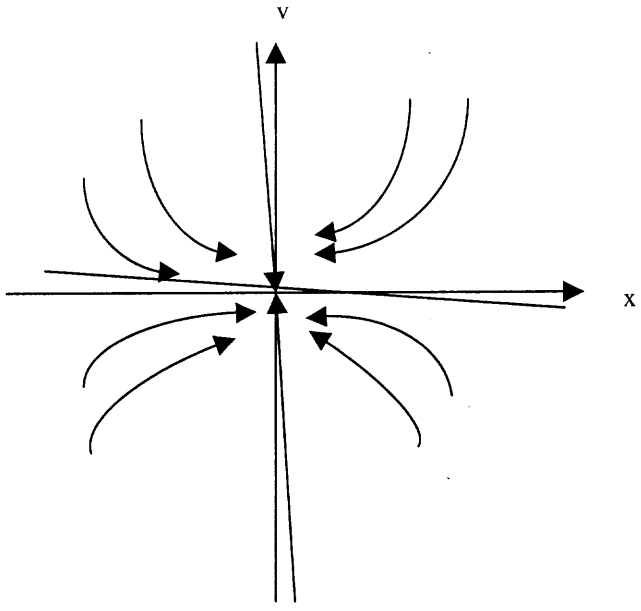

Figure 3.2 Phase Plane near $((2l+1)\pi/\beta, 0)$

Figure 3.3 shows the entire phase plane of Equation (3.5) obtained by collecting the above results:

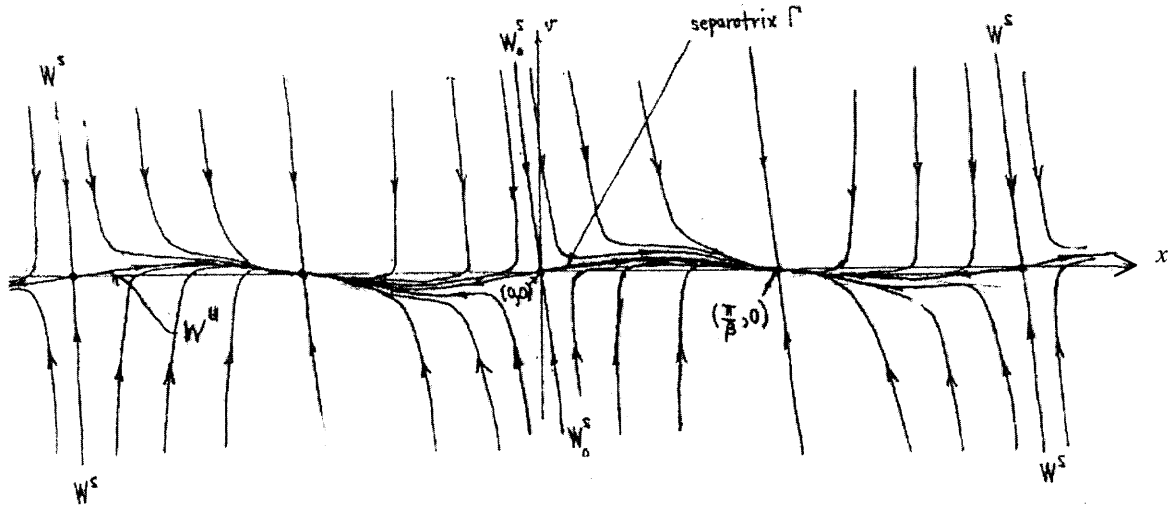

Figure 3.3 Phase Portrait of Equation (3.5)

Useful information on the solutions of Equation (3.2) (and equivalently (3.5)) can be extracted from the above analysis. The relevant portion of the phase plane for our research is the region R={(x, v): 0≤x≤8π/β}. Clearly any trajectory θ_t $(x_o, v_o) = (x(t), v(t))$ starting at $(x_0, v_0) \in R$, except for points on the stable manifold, has the property:

$$(x(t), v(t)) \rightarrow \left(\frac{\pi}{\beta}, 0\right) \quad as\ t \rightarrow \infty \tag{3.23}$$

Moreover,

$$\frac{dv}{dx} = \frac{x''}{x'} \rightarrow -\frac{\beta k}{c} \quad as \quad t \rightarrow \infty \quad \left(or\ x \rightarrow \frac{\pi}{\beta}\right) \tag{3.24}$$

In fact, all of these trajectories converge very rapidly to the separatrix ⌜ (which is just the portion of the unstable manifold for the origin, W^u_0, that is contained in R). This separatrix appears to be quite close to the graph of $v = k/c \sin\beta x$, and so one can infer the following result that shall be proved in the sequel:

$$(x(t), v(t)) \rightarrow \left(x, \frac{k}{c}\sin\beta x\right) \quad as\ t \rightarrow \infty \left(or\ x \rightarrow \frac{\pi}{\beta}\right) \tag{3.25}$$

One can also see from the above analysis that the often used singular perturbation approximation Equation (3.3) is not really adequate to represent the solutions of Equation (3.2) (⇔ (3.5)) since it is just a single curve in the phase plane region R beginning at origin, O= (0,0) and terminating at (π/β, 0); albeit a curve to which (almost) all of the

solutions (trajectories, orbits) of Equation (3.2) converge to rather rapidly as $t \rightarrow \infty$ ($x \rightarrow \pi/\beta$).

Since Equation (3.2) ($\Leftrightarrow$(3.5)) apparently has no closed form solution, it is natural to try to compute numerical approximate solutions using a standard ODE solver such as the Runge-Kutta method. However, an attempt to apply the Runge-Kutta method to Equation (3.2) directly leads to rather surprising results that are completely unsatisfactory. To explain what happens, first note that the system form of Equation (3.2), namely (3.5), is such that there is an enormous discrepancy between the magnitude of the derivative of the first component f_1: = v and the corresponding magnitudes of the second component f_2 : = $k\sin\beta x - cv$; in fact, the ratios of the second set of magnitudes to the first is at least O (10^6). Such systems of differential equations are called stiff. In the presence of such enormous magnitudes, one might expect to encounter some problems with conventional ordinary differential equation (ODE) solvers. More specifically, in order to obtain good accuracy using the Runge-Kutta method one should take a time step of size (h), no more than about h= 0.1 in order to benefit from the global approximation error of $O(h^4)$ of the Runge-Kutta method. If one uses this increment, it is found that there is a little movement in the trajectory after several hundred steps, so if one starts in R near $x = 0$, very little progress is made in moving across R to the point (π/β, 0) even after hundreds of steps. Furthermore, if one continues this for thousands of steps, round-off errors accumulate to the point where the approximate numerical solution starts behaving in ways that are not consistent with the properties of the solution that are deduced from the above analysis.

In conclusion, the properties of the solutions of Equation (3.2) ($\Leftrightarrow$ (3.5)) discussed above actually reveal the source of the problems encountered using numerical methods. Suppose the trajectory starts at a point (x_0, v_0) in R near origin = (0, 0). Then this trajectory converges to the separatrix Γ very rapidly, in fact, the distance between θ_t (x_0, v_0) and Γ decreases with time as e^{-ct} . Once θ_t is very close to Γ (which is $R \cap W^u_0 \cup \{(\pi/\beta, 0)\}$), it moves towards R near $(\pi/\beta, 0)$ as $e^{\beta k t/c}$. Hence, the time required to get very close to $(\pi/\beta, 0)$ is roughly $e^{\beta k t/c} = \pi/\beta \Rightarrow t = c/\beta k \log(\pi/\beta)$, thus it follows from the orders of magnitude of the constants (c, k, β) that the time required is roughly O (10^2). So with a time step of about h=0.1, the number of steps required to come close to seeing the asymptotic nature of the solution as $t \to \infty$ is O (10^3). Using this many steps is not only computationally expensive; it also makes the contamination of the approximate numerical data by round off errors almost inevitable. Moreover, one can see from the intrinsic nature of the solutions described above that the basic problems with numerical solutions cannot be ameliorated through the use of standard rescaling techniques. One infers from all of this that were shall need to employ other methods to determine useful approximate trajectories of Equation (3.2) that stretch all the way from an initial point (x_0, v_0) to a very small neighborhood of the sink $(\pi/\beta, 0)$ and that these methods must be of an asymptotic nature for $t \to \infty$.

3.2 Equation for Particle Trajectories

The equation of motion of fine particles in a fluid with an acoustic sound field is given from Equation (3.2):

$$x'' + c\,x' - k\sin\beta x = 0 \tag{3.26}$$

$(x(0) = x_0 , x'(0) = v(x_0))$

In the literature, the inertia term x'' is neglected because it is small and the following singular perturbation solution is used:

$$x' = v \cong v_s = k/c \sin \beta x \tag{3.27}$$

Using Equation (3.27) forces the initial velocity to be $k/c \sin \beta x_0$ (it is usually assumed =0) and leads to errors in the solution that for very small time t, can be as large as $\cong k/c$. The solution obtained by using the approximation Equation (3.27), that is solving the initial value problem:

$$x' = k/c \sin\beta x,\ x(0) = x_0 \tag{3.28}$$

can easily be obtained from Equation (3.27):

$$v_s = \frac{k}{c}\sin \beta x_s \tag{3.29}$$

By separation of variables:

$$t = \frac{c}{k\beta}\left[\log \frac{\tan\frac{\beta x}{2}}{\tan\frac{\beta x_0}{2}}\right] \tag{3.30}$$

$$x = x_s(t) = \frac{2}{\beta}\tan^{-1}\left[\left(\tan\frac{\beta x_0}{2}\right)e^{\frac{\beta k t}{c}}\right] \tag{3.31}$$

$$v_s = v_s(t) = \frac{k}{c}\sin \beta x_s(t) \tag{3.32}$$

To obtain a more accurate approximation than the singular perturbation solution, let the assumed solution of Equation (3.26) be of the form:

$$x = u + x_s \tag{3.33}$$

Substituting Equation (3.33) in Equation (3.26), one obtains:

$$u'' + c\,u' - k\beta\,u - [k\sin\beta(u+x_s) - k\beta u - k\sin\beta x_s - x_s''] = 0 \tag{3.34}$$

If one assumes that u is small, it follows from Equation (3.31) that the terms in [ ] above are small, therefore it is reasonable to approximate u by the solution to the initial value problem:

$$u'' + cu' - k\beta u = 0 \qquad (u(0) = 0\ ,\ u'(0) = -k/c\ \sin\beta x_0) \tag{3.35}$$

Here it is assumed that $x'(0)= v(0)= 0$ in Equation (3.26). The solution of Equation (3.35) can be readily found by elementary means to be:

$$u(t) = \frac{k}{c}\frac{\sin \beta x_0}{r_1 - r_2}(e^{-r_1 t} - e^{-r_2 t}) \tag{3.36}$$

$$u'(t) = -\frac{k}{c}\frac{\sin \beta x_0}{r_1 - r_2}(r_1 e^{-r_1 t} - r_2 e^{-r_2 t}) \tag{3.37}$$

where,

$$r_1 = \frac{c + \sqrt{c^2 - 4\beta k}}{2} \cong c \tag{3.38}$$

$$r_2 = \frac{c - \sqrt{c^2 - 4\beta k}}{2} \cong \frac{\beta k}{c} \tag{3.39}$$

and $r_1 >>> r_2$. It is therefore plausible that the following approximate solutions $\phi(t)$ are quite accurate for all t:

$$x(t) \cong \phi(t) := \frac{k}{c}\frac{\sin \beta x_0}{r_1 - r_2}(e^{-r_1 t} - e^{-r_2 t}) + \frac{2}{\beta}\tan^{-1}\left[\left(\tan\frac{\beta x_0}{2}\right)e^{\frac{\beta k t}{c}}\right] \tag{3.40}$$

$$x'(t) \cong \phi'(t) = -\frac{k}{c}\frac{\sin \beta x_0}{r_1 - r_2}(r_1 e^{-r_1 t} - r_2 e^{-r_2 t}) + \frac{k}{c}\sin \beta x(t) \tag{3.41}$$

In fact, it can be proved rigorously that

$$|x(t)-\phi(t)|,\quad |x'(t)-\phi'(t)| \le \frac{3k}{c^2} e^{-\frac{r_2}{2}t} \quad for\ all\ t \ge 0 \tag{3.42}$$

and hence,

$$|x(t)-\phi(t)|,\quad |x'(t)-\phi'(t)| \to 0\ as\ t \to \infty \quad (like\ \frac{e^{-r_2 t}}{r_1}) \tag{3.43}$$

Note also then that:

$$x(t) \to x_s(t) \quad and \quad x'(t) \to x_s'(t) \quad as\ t \to \infty (like\ \frac{e^{-r_2 t}}{r_1}) \tag{3.44}$$

Therefore, particle trajectories can be calculated using Equation (3.40).

Equation (3.40) with the values of constants (c, k, β) are used to compute particle trajectories in the acoustic medium. Table 3.2 shows the computer values. In Table 3.2, the vertical columns represent the time in seconds for the sound field treatment. The values in horizontal rows represent the position of particles at corresponding times. The distances are in micrometers and for convenience taken at λ/16 of wavelength intervals from the first pressure antinode at the face of the transducer. The value 1126.126 micrometers in the table represents the first pressure node to which the particles are supposed to move. As can be seen from Table 3.2 and the corresponding graph in Figure 3.4, all the particles move toward the pressure node (1126.126 micrometer). Particles with 2 micrometer diameter take about 20 seconds to reach the node. Figure 3.3 shows where the sinks (pressure nodes) repeat at every 2π/β distance. Thus the behavior of the particle movement shown in Figure 3.4 using the trajectory equation represents the actual behavior of the system.

Table 3.2 Particles Disaplacement vs. Time

Time (sec)	Distance 140.76577 micron (Antinode)	Distance 281.53153 micron	Distance 422.2973 micron	Distance 563.06306 micron	Distance 703.82883 micron	Distance 844.59459 micron	Distance 985.36036 micron	Distance 1126.1261 micron (Node)
0.0000	140.76577	281.53153	422.2973	563.06306	703.82883	844.59459	985.36036	1126.1261
0.5000	150.52474	299.42478	445.41174	587.75732	726.35743	861.66483	994.55287	1126.126
1.0000	160.91743	318.16457	469.04579	612.33625	748.21531	877.88785	1003.1731	1126.126
2.0000	183.73089	358.11946	517.49163	660.6976	789.69661	907.83998	1018.8199	1126.126
3.0000	209.45263	401.15955	566.79234	707.31209	827.94778	934.59804	1032.5377	1126.126
4.0000	238.30361	446.86073	616.02817	751.49241	862.82076	958.36907	1044.5465	1126.126
5.0000	270.45461	494.60782	664.28532	792.73599	894.31378	979.39328	1055.0473	1126.126
10.0000	479.04889	734.43028	867.81924	949.46665	1006.8978	1051.9594	1090.6366	1126.126
15.0000	720.1450	913.9279	992.3700	1036.3458	1066.1323	1089.0742	1108.5821	1126.1260
20.0000	1009.2580	1091.5266	1098.1025	1111.0000	1111.0005	1111.0500	1111.5420	1126.1260

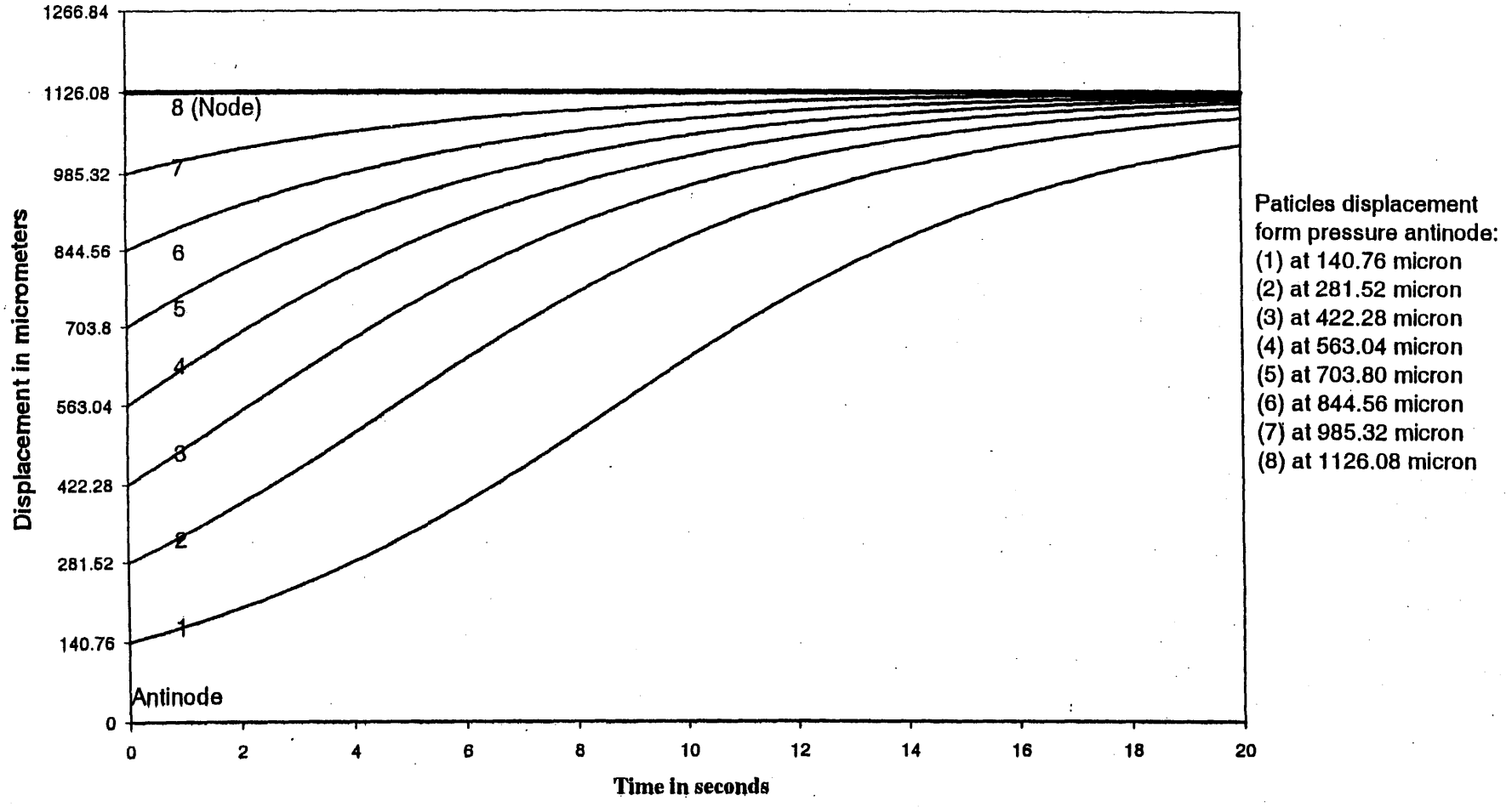

Figure 3.4 Displacement vs. Time

3.3 Concentration Equation

The approximate solution of Equation (3.40), obtained earlier will be used to obtain an approximate value of the particle concentrations. Since the particles are neither created nor disappear during the irradiation of sound, the equation of conservation of particles must hold:

$$\frac{\partial n}{\partial t}+\frac{\partial}{\partial x}(nv)=0, \quad n(x,0)=n_0 \quad (const.) \tag{3.45}$$

In order to use this equation, one must find an expression for the velocity field $v=v(x,t)$ as a function of just x and t. Now if the singular perturbation approximation $v\cong v_s=k/c \sin\beta x_s$ is used, one can simply substitute $v(x,t)=v_s(x,t)=v_s(x)=k/c \sin\beta x_s$ in Equation (3.45), with x_s a function of t and x_0, and get the result in the literature. A more accurate solution is obtained by employing the approximate formula of Equation (3.40):

$$\phi=\frac{k}{c}\frac{\sin\beta x_0}{r_1-r_2}(e^{-r_1 t}-e^{-r_2 t})+x_s(t,x_0) \tag{3.46}$$

for the solution of Equation (3.26) subject to the initial conditions $x(0)=x_0$, $\dot{x}(0)=0$. In order to do this; one must find the velocity of the particle that is at a distance x from the pressure antinode at time $t>0$, so that one can find the approximation for v as a function of x and t.

To use the approximation Equation (3.46) for the determination of the particle concentration, one must extract from it an approximation for $v(x,t)$ to be substituted into Equation (3.45), hence one must first solve:

$$x = \frac{k}{c}\frac{\sin \beta x_0}{r_1 - r_2}(e^{-r_1 t} - e^{-r_2 t}) + \frac{2}{\beta}\tan^{-1}\left[\left(\tan\frac{\beta x_0}{2}\right)e^{\frac{\beta k t}{c}}\right] \qquad (3.47)$$

Let the solution of the above equation for x_0 in terms of x and t be denoted by $x_0 = \Psi_*(x,t)$. This can not be done in closed form, but the following can readily be shown, by solving Equation (3.31) for x_0, to yield a good approximate solution for all $0<x<\pi/\beta$, $t>0$:

$$x_0 = \psi(x,t) \cong \psi_*(x,t) = \frac{2}{\beta}\tan^{-1}\left[\left(\tan\frac{\beta x}{2}\right)e^{-\frac{\beta k t}{c}}\right] \qquad (3.48)$$

From the above equation one can obtain a good approximation for the velocity field to be used in Equation (3.45) by replacing x_0 with ψ_* in Equation (3.41):

$$v(x,t) \cong v_*(x,t) = -\frac{k}{c}\frac{\sin \beta\psi_*}{r_1 - r_2}(r_1 e^{-r_1 t} - r_2 e^{-r_2 t}) + \frac{k}{c}\sin \beta x \qquad (3.49)$$

Where v_* is the velocity at a given x and t. Plugging the value of Ψ_* from Equation (3.48) into Equation (3.49), using the fact that $r_1 >> r_2$, yields the approximation:

$$v(x,t) \cong -\frac{k}{c}e^{-r_1 t}\sin\beta\left(\frac{2}{\beta}\tan^{-1}\left[\tan\left(\frac{\beta x}{2}\right)e^{\frac{-\beta k t}{c}}\right]\right) + \frac{k}{c}\sin \beta x \qquad (3.50)$$

As $e^{-\beta k t/c} \cong 1$ for all except very large t, Equation (3.50) yields an even simpler approximation $\hat{v}$ for v:

$$v(x,t) \cong \hat{v}(x,t) = -\frac{k}{c} e^{-\eta t} \sin \beta x + \frac{k}{c} \sin \beta x \tag{3.51}$$

Hence,

$$v(x,t) \cong \hat{v}(x,t) = \frac{k}{c}\left(1 - e^{-\eta t}\right) \sin \beta x \tag{3.52}$$

Observe that $\hat{v}$ converges very rapidly to $v_s(x)=k/c\sin\beta x$ with increasing t. Substituting $\hat{v}$ for v in Equation (3.45), one obtains:

$$\frac{\partial n}{\partial t} + \hat{v}(x,t)\frac{\partial n}{\partial x} = -\frac{\partial \hat{v}}{\partial x} n = -\frac{\beta k}{c} n(1 - e^{-\eta t}) \cos \beta x \tag{3.53}$$

which must be solved subject to the initial condition (Cauchy problem):

$$n(x,0)=n_0 \text{ (a positive constant)} \tag{3.54}$$

The method of characteristics can be used for Equation (3.53). For s as a parameter for the characteristic curves $x=x(s)$, $t=t(s)$, and $n=n(s)$, the standard characteristic equations for Equation (3.53) are:

$$(1)n_t + (v)n_x = (\text{constant})\, n \tag{3.55}$$

$$\frac{dt}{ds} = 1, \quad t = 0 \ @ \ s = 0 \tag{3.56}$$

$$\frac{dx}{ds} = \hat{v} = \frac{k}{c}\left(1 - e^{-r_1 t}\right)\sin \beta x \qquad x = \xi \ @ \ s = 0 \tag{3.57}$$

$$\frac{dn}{ds} = -\frac{\beta k}{c}(1 - e^{-r_1 t})\cos \beta x n \quad n = n_0 \ @ \ s = 0 \tag{3.58}$$

Clearly, Equation (3.56) implies that t=s. Hence, one has to solve the system of equations:

$$\frac{dx}{dt} = \frac{k}{c}\left(1 - e^{-r_1 t}\right)\sin \beta x \tag{3.59}$$

$$\frac{dn}{dt} = -\frac{\beta k}{c}\left(1 - e^{-r_1 t}\right)\cos \beta x n, \qquad x(0) = \xi, \quad n(0) = n \tag{3.60}$$

One starts with Equation (3.57) in order to find an approximate solution for ξ as a function of x and t. Setting s=t in Equation (3.57) yields:

$$\frac{dx}{dt} = \frac{k}{c}\left(1 - e^{-r_1 t}\right)\sin \beta x \tag{3.61}$$

Hence:

$$\left(1 - e^{-r_1 t}\right)dt = \frac{c}{k}\frac{dx}{\sin \beta x} \tag{3.62}$$

Integrating Equation (3.62) with limits on t from 0 to t and on x from ξ to x, one obtains:

$$t + \frac{1}{r_1}\left(e^{-r_1 t} - 1\right) = \frac{c}{\beta k}\log\left[\frac{\tan\frac{\beta x}{2}}{\tan\frac{\beta \xi}{2}}\right] \tag{3.63}$$

After exponentiating and some manipulation, one can readily obtain the following solution of Equation (3.63) for ξ as a function of x and t.

$$\xi \equiv \frac{2}{\beta}\tan^{-1}\left[e^{-\frac{\beta k}{c}\left[t+\frac{1}{r_1}\left(e^{-r_1 t}-1\right)\right]}\tan\frac{\beta x}{2}\right] \tag{3.64}$$

Now to solve for n, Equation (3.58) is divided by Equation (3.57), yielding:

$$\frac{dn}{dx} = -\frac{\beta\cos\beta x}{\sin\beta x}n \tag{3.65}$$

$$\frac{dn}{n} = -\beta\cot\beta x dx \tag{3.66}$$

Integrating with $n=n_0$ when $x=\xi$, one obtains:

$$\log\left(\frac{n}{n_0}\right) = -\log\left(\frac{\sin\beta x}{\sin\beta\xi}\right) \tag{3.67}$$

$$\frac{n}{n_0} = \frac{\sin\beta\xi}{\sin\beta x} \tag{3.68}$$

Therefore, the following approximation formula for the concentration is applicable for any time t:

$$\frac{n}{n_0} \cong \frac{\sin\left\{2\tan^{-1}\left[e^{-\frac{\beta k}{c}\left(t+\frac{1}{r_1}\left(e^{-r_1 t}-1\right)\right)}\tan\frac{\beta x}{2}\right]\right\}}{\sin \beta x} \tag{3.69}$$

Observe that this is very close to the formula:

$$\frac{n}{n_0} \cong \frac{\sin\left\{2\tan^{-1}\left[e^{-\frac{\beta k t}{c}}\tan\frac{\beta x}{2}\right]\right\}}{\sin \beta x} \tag{3.70}$$

obtained using the singular perturbation approximation, except for certain x and t values. For $x \cong \pi/2\beta$ *and* $t \ll 1$, the difference between Equation (3.69) and the above (3.70) formula can be O (1), depending on the values of β, k and c. It is worth noting in closing that it can be shown by a long and tedious-but straightforward computation that the error in using Equation (3.69) is $\leq 2\beta k/c$, for all $0 \leq x \leq \pi/\beta$, $t \geq 0$.

The ratio of the initial concentration (n_0) to final concentration (n) at that time (t), is taken as 1 when time=0. Using Equation (3.69) for particle concentrations with increasing t values is given in Table 3.3. The graphs in Figure 3.5 represent the concentration at 2, 5, and 10 seconds; note how the concentrations are highest at the sink π/β (Figure 3.3). Thus one sees that the approximate concentration closely follows the behavior of the actual system.

Table 3.3 Concentration Ratio vs. Time

Time (sec)	Distance 140.7658 micron	Distance 281.5315 micron	Distance 422.2973 micron	Distance 563.0631 micron	Distance 703.8288 micron	Distance 844.5946 micron	Distance 985.3604 micron	Distance 1126.126 micron (node)
0.0000	1.0000	1.0000	1.0000	1.0000	1.0000	1.0000	1.0000	1.0000
0.1000	0.9830	0.9870	0.9930	1.0000	1.0100	1.0100	1.0200	1.0200
0.5000	0.9180	0.9350	0.9620	0.9960	1.0300	1.0600	1.0900	1.1000
1.0000	0.8410	0.8710	0.9190	0.9830	1.0600	1.1300	1.1800	1.2000
2.0000	0.7050	0.7490	0.8240	0.9350	1.0800	1.2500	1.3900	1.4500
3.0000	0.5900	0.6370	0.7240	0.8640	1.0700	1.3400	1.6100	1.7400
4.0000	0.4920	0.5390	0.6270	0.7780	1.0200	1.4000	1.8500	2.0900
5.0000	0.4110	0.4530	0.5370	0.6860	0.9500	1.4100	2.0900	2.5200
10.0000	0.1640	0.1840	0.2260	0.3080	0.4840	0.9390	2.5300	6.3300
15.0000	0.0653	0.0735	0.0906	0.1250	0.2010	0.4180	1.4900	15.9000
20.0000	0.0259	0.0292	0.0361	0.0498	0.0806	0.1690	0.6410	40.0000

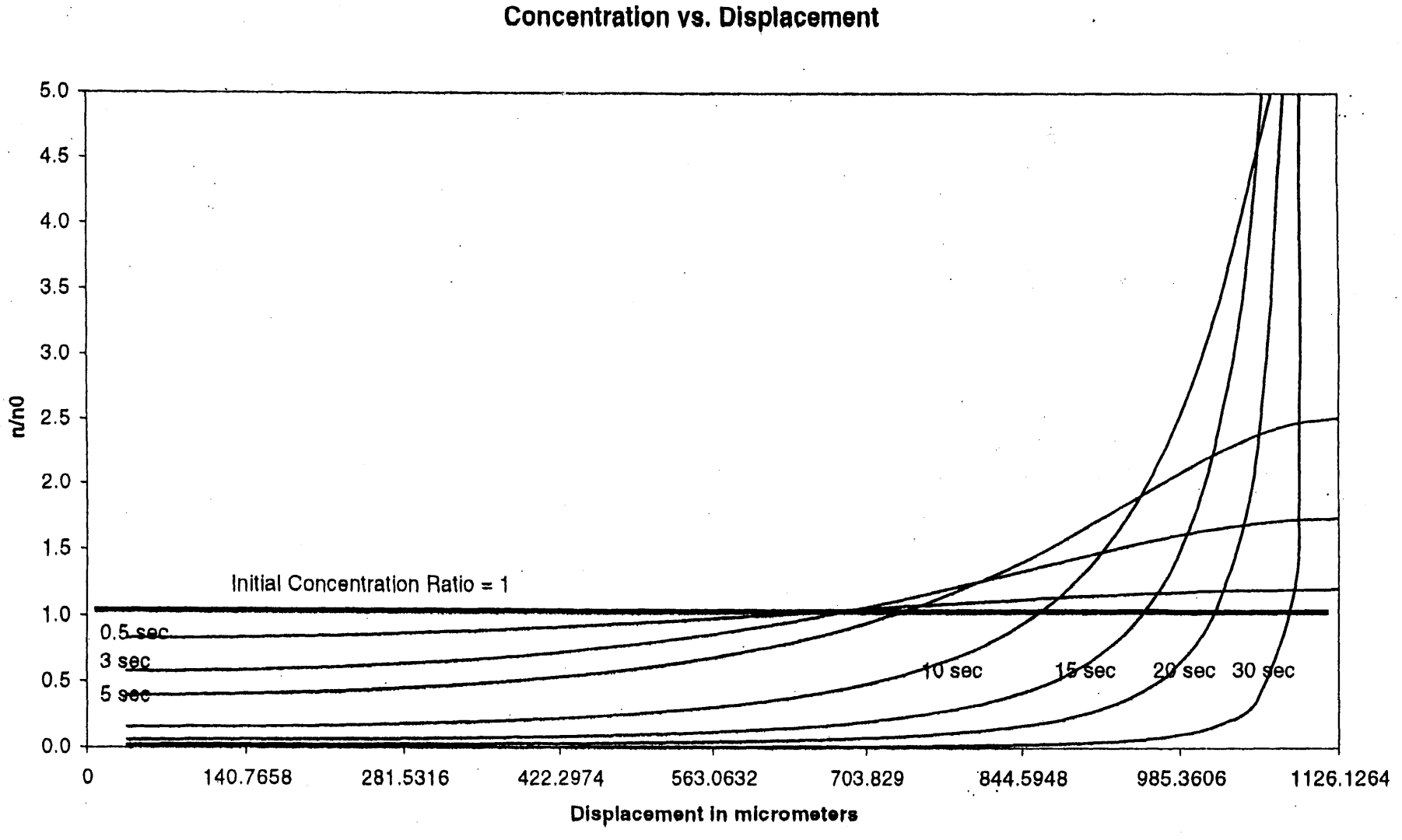

Figure 3.5 Concentration vs Displacement

3.4 Summary and Conclusions

In this chapter accurate approximate solutions to the particle trajectory equation and concentration equation were derived. These approximate solutions will be used to compare the experimental observations with expected theoretical values. There is no closed form solution for the particle trajectory Equation (3.2), and an attempt to apply the Runge-Kutta method directly led to rather surprising results that were completely unsatisfactory. The only possible approach was to use an approximate solution. If the experimental results can be compared to Figures 3.4 and 3.5, then it can be stated that the mathematical model derived in this thesis has solutions that are in good agreement with the actual behavior of the system and can be used for any type of medium or particle.

In the next chapter, the design of the physical (experimental) model is discussed in detail. The formulas for the derived equations, Equation (3.40) and Equation (3.69), of particle trajectories and concentrations will be used in Chapter 5 to compare the mathematical model with the physical model.

CHAPTER 4

DESIGN OF PHYSICAL MODEL

In Chapter 2, literature search, several parameters were identified as important in the designing of the physical model. To implement the proposed technology of particle separation, these parameters were considered in the design to obtain an optimal working physical model. In this chapter, details of the experimental design are discussed. This includes the electrical equipment required to produce the acoustic standing wave field, iterative acoustic chamber design, selection of representative particles, electrical equipment connections, and image capturing techniques.

4.1 Electrical Equipment

To implement the technology, the above physical model was built and electrical equipment was acquired to provide resonance in the chamber. The electrical equipment, which was used in this research, includes: 2 transducers, an electrical signal generator, power amplifier, and oscilloscope. The function of each unit and their connections are given below.

4.1.1 Transducer

An acoustic standing field is necessary to implement this technology. Using a piezoelectric transducer that converts electrical to mechanical energy can generate this standing acoustic field. Piezoelectric transducers are made of lead zirconate titanate, quartz, Rochelle salt, or barium titanate. Lead zirconate titanate (PZT) is a much stronger

piezoactive material, with higher energy conversion efficiency than commonly used piezoelectric crystals. It is mechanically very strong, as it can be used underwater and under high temperature situations. Hence lead zirconate titanate was used as the transducer material in this research. There are many transducers manufacturing companies such as American Piezo Ceramics Inc., SonoSep Biotech Inc., and PSI System Inc. (Canada) that can fabricate PZT transducers. The transducer used in this research was purchased from American Piezo Ceramics Inc. Table 4.1 gives some important properties of the transducer, of size 76.2 x 38.1 x 6.25 mm (Catalog number APC 880) with a fundamental resonance frequency of 320 kHz.

Table 4.1 Piezoelectric Materials Characteristics (Lead Zirconate Titanate, PZT)

Properties	Unit	Symbol	APC 880
Dissipation Factor	%	Tanδ	0.35
Piezoelectric Coefficient	10^{-12} m/V	d_{33}	215
Young's Modulus	10^{10} N/m^2	Y^E_{33}	7.2
Frequency Constants	Hz-m or m/s	N_L N_T	1725 2110
Elastic Compliance	10^{-12} m^2/N	s^E_{33}	15.0
Density	g/cc	ρ	7.6
Maximum Power	W	P	130
Impedance	Ohms	Z	15
Resonance Frequency	kHz	f	320

In the above table, the dissipation factor corresponds to imperfect energy conversion loss for nonideal materials under sinusoidal steady conditions. The piezoelectric coefficient is the strain in a free crystal for a given applied electrical field. The subscript 33 represents the rectangular axes, where the first number (3) symbolizes for 33 as x and z axis and the second number (3) corresponds to 33 as y and z axis,

in crystal terminology. Young's Modulus is the ratio of stress to strain, which is the property of the material for a constant electric field. Frequency constants consist of N_L, which is the product of the resonance frequency and length of the transducer, and N_T, which is the product of the resonance frequency and thickness of the transducer. Elastic compliance is the partial derivative of strain with respect to stress under a constant electrical field.

In order to produce a stationary or standing waves in the resonator, a reflector was attached to the chamber in front of the transducer to reflect the waves without any loss of energy. The reflector can be made of glass or of the same material as the transducer material. In this research, two transducers were used, one as a transmitter to supply energy into the liquid for resonance in the chamber and the other one as a reflector to reflect the waves in order to generate a standing wave field.

The transducer, which was received from the manufacturer, was in the form of a rectangular plate with no electrical connections. Therefore, an 80 x 40 x 0.45 mm copper plate was attached to the surface of the transducers using a conductive adhesive, Silver Epoxy from AI Technology Inc. This was used as a ground connection for the transducer. The signal was delivered to the transducer by soldering positive end of supply to a tiny hole provided in the transducer on the other flat face of the transducer.

Anritsu Synthesizer/Level Generator/tester MG443B was used to determine the resonance frequency of the transducer. This value (resonance frequency) corresponds to the maximum performance of the transducer that can be achieved, without being affected by the high input power. Figure 4.1 shows the frequency response of the transducer.

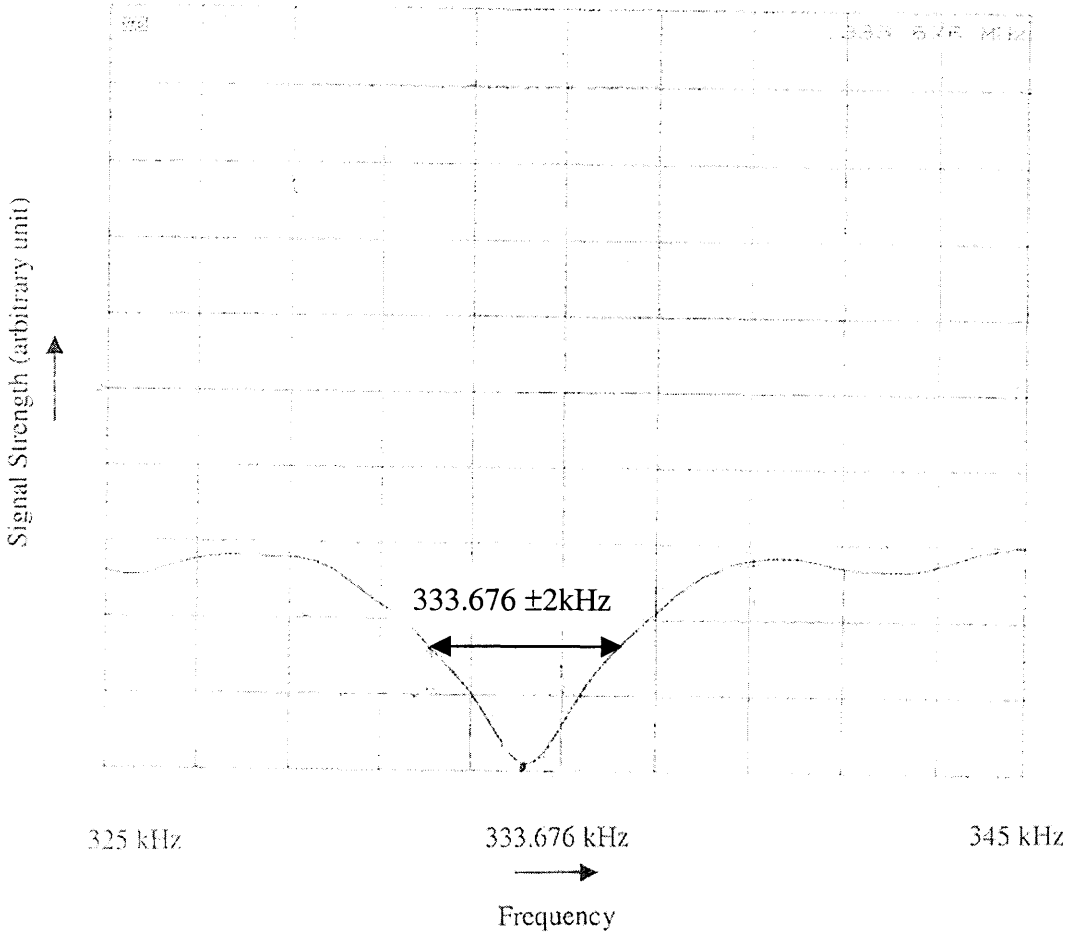

Figure 4.1 Resonance Frequency of the Transducers

It had a resonance frequency of 333.676 kHz with a very narrow bandwidth. Each horizontal division in Figure 4.1 corresponds to 3.33 kHz. Based on the curve, The resonance frequency can be used between 333.676 ± 2 kHz. Any frequency beyond this limit will result in inadequate performance of the transducer as shown in Figure 4.1.

4.1.2 Signal Generator

Input sinusoidal waves supplied to the transducer are generated by a sinusoidal signal generator. Synthesizer/level generator MG 443B by Anritsu was used in this research. This generator has a digital display for selected frequency and output power in decibel (dB). A dB value represents the natural logarithm of the electrical power (1dB =10 (log Power/mW)). The maximum frequency of this unit is in the range of megahertz and the maximum output power is 16 dB (40 mW).

This generator is capable of delivering input signal in units of Hz and ± 1.0 dB. This precise control of frequency and power input is required to control the input frequency. As was discussed earlier, if the frequency is other than the resonance frequency, the transducer will not operate at its maximum performance. The proper control of frequency is also required to control the standing waves in the medium, as the wavelength changes with change in the chamber temperature.

4.1.3 Power Amplifier

According to the literature review and mathematical calculations, electrical power greater than 1W will be needed to create an acoustic energy field in the medium. The maximum output power of the signal generator is 16 dB (40mW) and the maximum power that the

transducer can handle is 130W. To amplify the power input into the transducer, ENI 1040L, power amplifier was purchased. The maximum power output from this is 500 watts for an input signal with frequency range from 10 kHz to 500 kHz. This high power amplifier was purchased to excite several transducers simultaneously.

4.1.4 Oscilloscope

An oscilloscope was used to obtain resonance frequency. Under resonance the reflector will consume the least amount of energy and the oscilloscope displays the minimum voltage of the measured signal. A Textronix T912 10 MHz oscilloscope was used for this purpose and the resonance frequency was found to be 334.5 kHz, a value close to the 333.676 kHz obtained by Anritsu Synthesizer/level generator/tester MG 443B. The MG 443B was calibrated before testing and this value will be used as the resonance frequency.

4.1.5 Electric Equipment Connections

The different electrical units, which were used in this research and discussed earlier, were connected using BNC coaxial cables. The block diagram of these units and the connection is given in Figure 4.2.

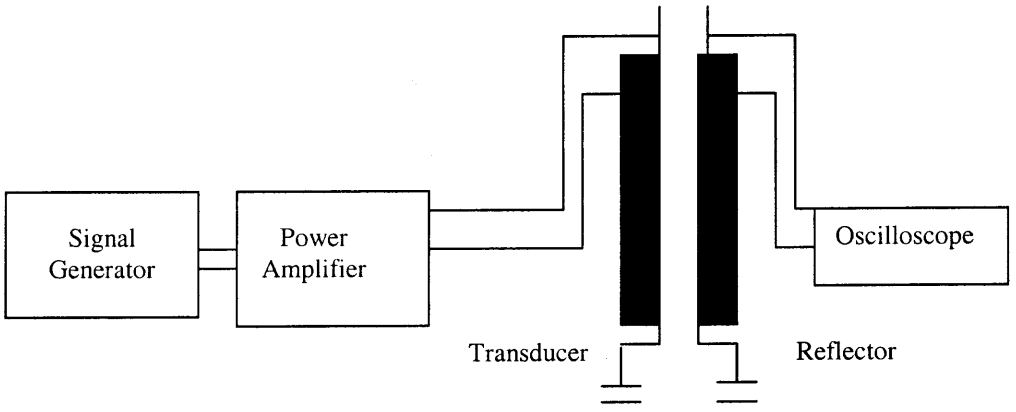

Figure 4.2 Block Diagram of Electrical Connections

4.2 Acoustic Chamber

The chamber was built with clear plexiglas to make it transparent. Assuming the velocity of sound as 1497.5 m/sec and a resonance frequency of 333.676 kHz, the wavelength is calculated as 4.45 mm. A chamber of two wavelengths was a good start to accommodate 4 pressure nodes (at half wavelength intervals) for the collection of particles during acoustic treatment. A plexiglas of 6.25 mm thickness was purchased from McMaster Supply Company. The overall dimensions of the chamber were 8.9 mm wide, 926.2 mm high, and 60 mm in depth. The depth was restricted by the dimension of the transducer and the height was selected to provide laminar flow of the liquid when running experiments under a continuous flow condition.

The chamber was built by first cutting four panels of two different dimensions and cutting windows into two of the frames, in which the transducers were fixed. The back electrode faces of the transducers were exposed to air. These assemblies were placed parallel to each other with a narrow gap of 8.9 mm to form the chamber. One transducer was used to deliver the signal and the other as a reflector (receiver) connected to the oscilloscope. The top portion of the chamber was connected to vacuum by a short

rubber tube, while the bottom was connected to a glass tube to pump water with suspended particles. Figure 4.3 shows a sketch of the chamber used in this research. The chamber was placed vertically, so the acoustic forces acted horizontally and the particles could flow vertically under the force of gravity. The reason for a vertical chamber was that the equation of acoustic force acting on the particle suspended in the field was derived with no gravitational force acting in the direction of wave propagation.

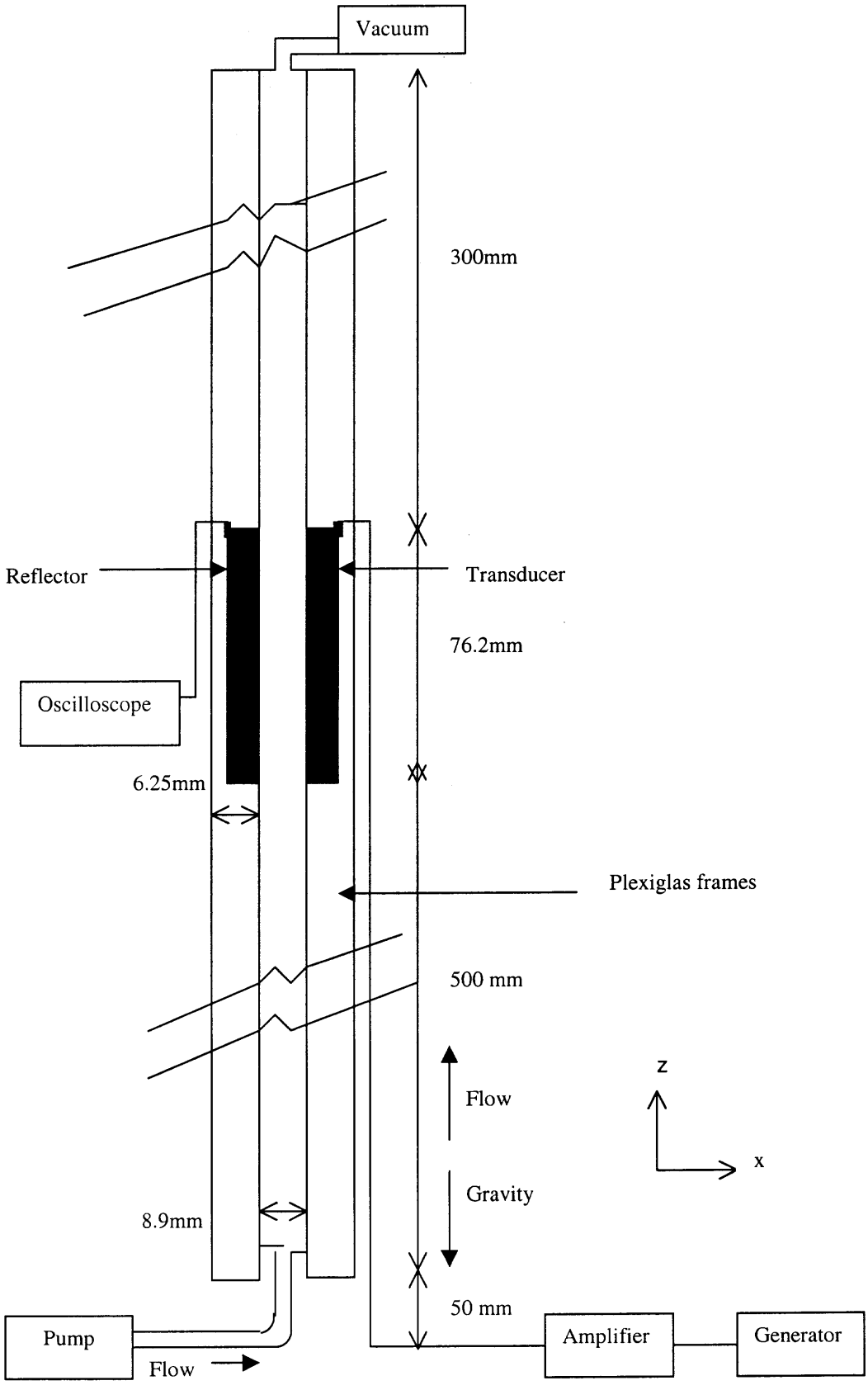

Figure 4.3 Acoustic Chamber

4.3 Representative Samples

It is intended to apply the research to segregate dredged sediments. The dredged sediments are composed of particles of different sizes ranging from submicron to millimeter. The morphology of sediments was analyzed using an Environmental Scanning Electron Microscope (Appendix A). The main composition of the sediment was silica and oxygen forming silicon dioxide or silica. Hence, silica fume was used as a representative sample for this research. The two types of silica were used during the research; these are silicon dioxide (SiO_2) and silicon carbide (SiC).

4.3.1 Silicon Dioxide

Silica fume (SiO_2) was purchased from Atlantic Equipment Engineering (AEE) (S1-601 with 99.9% purity), with size range of 1 to 5 micrometers. The reason for trying small particles of uniform size was as the particles get bigger and heavier they settle fast. Also for the larger sizes, the particle residence time is a fraction of a second.

Figure 4.4 shows the particle size analysis for AEE silica fume using a Malvern Instruments Inc., Master size X Ver. 1.2b, particle analyzer. Hydrometer analysis was also performed using ASTM D 421. Results of this analysis are shown in Figure 4.5. In both analysis methods, the mean particle diameter of silica fume was found to be 1.65 micrometers. Table 4.2 shows the properties of the suspended particles and fluid used for the calculation of the acoustic contrast factor.

Polydisperse model

Residual = 12.583 %
d (0.5) = 1.77 µm
D [4, 3] = 1.83 µm
Sauter Mean (D[3,2]) = 1.65 µm
Specific Surface Area = 3.6378 sq. m. / gm

Volume Result

Concentration = 0.000 %
d (0.1) = 1.33 µm
Span = 0.69

Focus = 300 mm.

Obscuration = 4.36 %
d (0.9) = 2.55 µm

Mode = 1.68 µm
Density = 1.00 gm. / c.c.

Size (Lo) µm	Result In %	Size (Hi) µm	Result Below %	Size (Lo) µm	Result In %	Size (Hi) µm	Result Below %
0.50	9.11	1.32	9.11	25.46	0.00	31.01	100.00
1.32	25.61	1.60	34.72	31.01	0.00	37.79	100.00
1.60	29.48	1.95	64.20	37.79	0.00	46.03	100.00
1.95	21.56	2.38	85.75	46.03	0.00	56.09	100.00
2.38	10.40	2.90	96.15	56.09	0.00	68.33	100.00
2.90	3.22	3.53	99.38	68.33	0.00	83.26	100.00
3.53	0.57	4.30	99.95	83.26	0.00	101.44	100.00
4.30	0.05	5.24	100.00	101.44	0.00	123.59	100.00
5.24	0.00	6.39	100.00	123.59	0.00	150.57	100.00
6.39	0.00	7.78	100.00	150.57	0.00	183.44	100.00
7.78	0.00	9.48	100.00	183.44	0.00	223.51	100.00
9.48	0.00	11.55	100.00	223.51	0.00	272.31	100.00
11.55	0.00	14.08	100.00	272.31	0.00	331.77	100.00
14.08	0.00	17.15	100.00	331.77	0.00	404.21	100.00
17.15	0.00	20.90	100.00	404.21	0.00	492.47	100.00
20.90	0.00	25.46	100.00	492.47	0.00	600.00	100.00

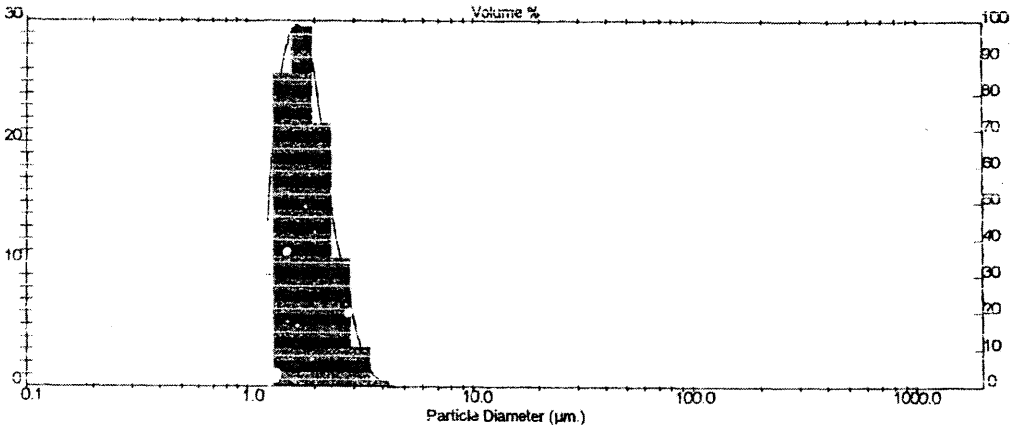

Malvern Instruments Inc.
Southborough, MA

Figure 4.4 Particle Size Analysis for SiO_2 (AEE)

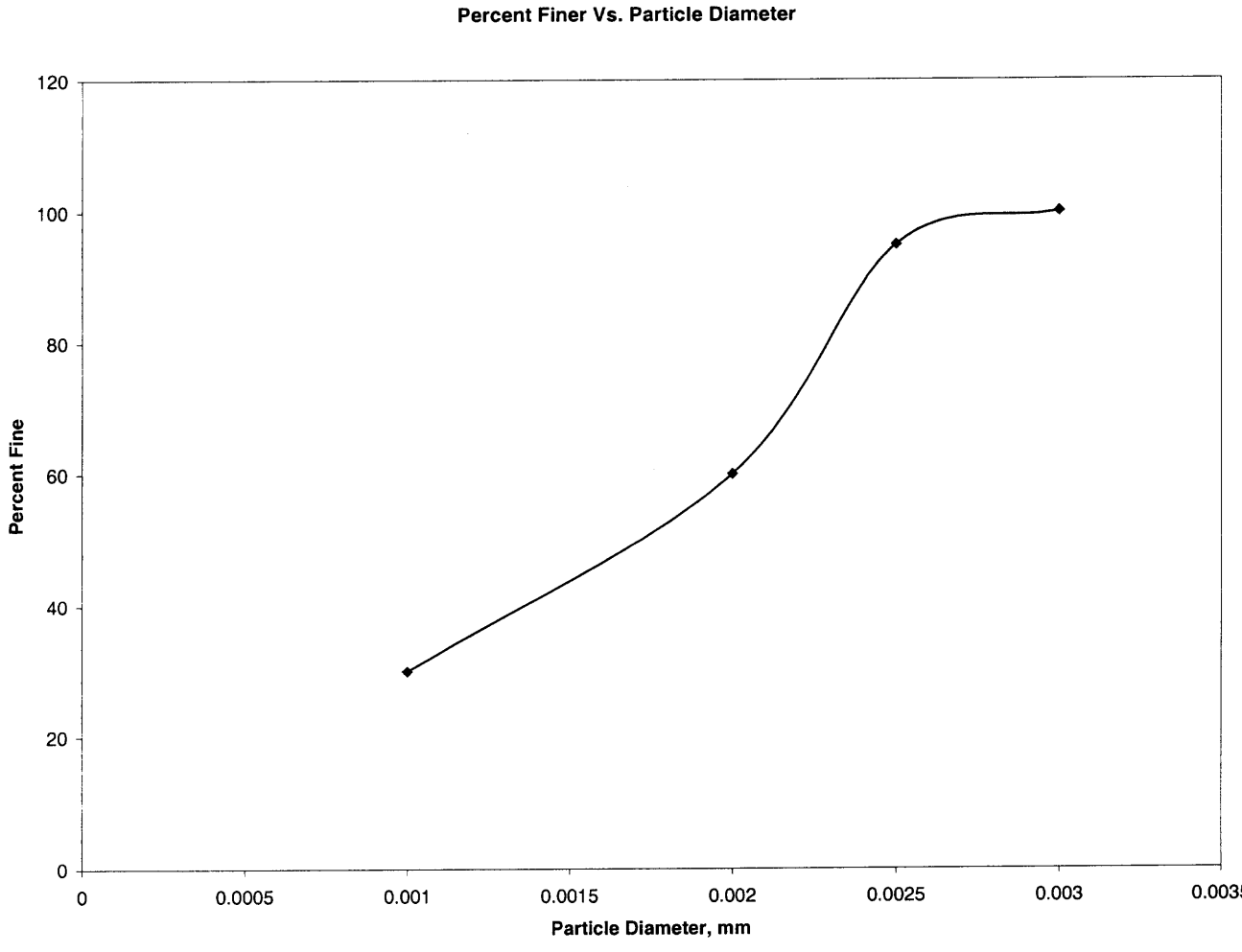

Figure 4.5 Hydrometer Analysis for SiO_2

Table 4.2 Physical Properties of Suspended Particles (SiO_2) and Host Fluid at 25 °C and 1 atm. (www.crystran.co.uk/qutzdata.htm)

	Specific Gravity	Compressibility (m^2/N)	Bulk Modulus (N/m^2)	Speed of Sound (m/s)
Solid (SiO_2)	2.649	2.75E-11	3.64E10	3750
Fluid (de-ionized water)	1.0	4.48E-10	0.223E10	1497

4.3.2 Silicon Carbide

Silicon Carbide (SiC), C=29.97% and Si= 70.03%, was also purchased from Atlantic Equipment Engineering. The size of the sample ranges between 5 and 20 micrometers with a specific gravity of 3.217. The purpose of using this sample was that in some experiments it was not possible to track the particle movement because of the very small size (5 micrometers) and also it was not possible to use greater magnification because of the thickness of the chamber which restricts the depth of focus. Figure 4.6 shows the particle size analysis for AEE silica fume using a Malvern Instruments Inc., Master size X Ver. 1.2b, particle analyzer

Both silica fumes were mixed with deionized water. To obtain a dilute suspension, the soil was mixed with deionized water at a ratio of 0.01-0.02 % by weight so that the only the primary axial force was assumed acting on the particles in the acoustic field.

Sample File Name: SIC1 , Record: 1 Source: Analysed
Measured on: Fri, Jan 04, 1980 10:33AM Last saved on: Fri, Jan 04, 1980 10:45AM

Presentation: 2OHD
Polydisperse model Volume Result Focus = 300 mm

Residual = 2.044 % Concentration = 0.008 % Obscuration = 7.78 %
d (0.5) = 7.92 µm d (0.1) = 4.62 µm d (0.9) = 12.62 µm
D [4, 3] = 8.36 µm Span = 1.01 Mode = 8.22 µm
Sauter Mean (D[3,2]) = 7.22 µm Density = 1.00 gm. / c.c.
Specific Surface Area = 0.8314 sq. m. / gm

Size (Lo) µm	Result In %	Size (Hi) µm	Result Below %	Size (Lo) µm	Result In %	Size (Hi) µm	Result Below %
0.50	0.00	1.32	0.00	25.46	0.00	31.01	100.00
1.32	0.00	1.60	0.00	31.01	0.00	37.79	100.00
1.60	0.00	1.95	0.00	37.79	0.00	46.03	100.00
1.95	0.00	2.38	0.00	46.03	0.00	56.09	100.00
2.38	0.02	2.90	0.02	56.09	0.00	68.33	100.00
2.90	2.43	3.53	2.45	68.33	0.00	83.26	100.00
3.53	4.89	4.30	7.35	83.26	0.00	101.44	100.00
4.30	8.72	5.24	16.06	101.44	0.00	123.59	100.00
5.24	13.77	6.39	29.83	123.59	0.00	150.57	100.00
6.39	18.44	7.78	48.27	150.57	0.00	183.44	100.00
7.78	19.69	9.48	67.96	183.44	0.00	223.51	100.00
9.48	16.72	11.55	84.68	223.51	0.00	272.31	100.00
11.55	10.01	14.08	94.69	272.31	0.00	331.77	100.00
14.08	4.23	17.15	98.92	331.77	0.00	404.21	100.00
17.15	1.05	20.90	99.97	404.21	0.00	492.47	100.00
20.90	0.03	25.46	100.00	492.47	0.00	600.00	100.00

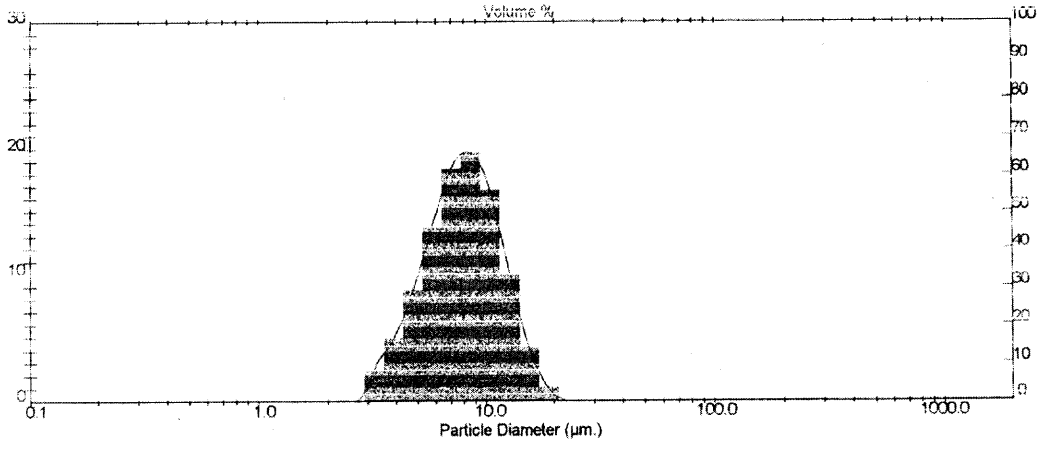

Malvern Instruments Inc. MasterSizer X Ver. 1.2b
Southborough, MA Serial No.

Figure 4.6 Particle Size Analysis for SiC (AEE)

4.4 Observation Techniques (Microscope and Illumination Source)

Particles of size 1 to 5 micrometers cannot be seen by the naked eye and some type of magnification was required. A microscope was used for magnification of the images. Most of the microscopes that are available on the market are of the type where the sample to be observed is placed on glass slide horizontally between the microscope lens and a light source. In this research, it was not possible to take the sample to the microscope for observation since the behavior of the particle movement is only observed during the application of the sound field. Another difficulty encountered for an ordinary microscope was that all the microscopes are fixed in such a way that the lens and eyepieces are lined up in a vertical position. The acoustic chamber in this research is placed vertically upward.

A microscope body was attached to a stand and it was placed in front of the chamber. Particles were observed by using 10X lens and a 10X eyepieces. To illuminate the particles in the chamber for observation, a Stocker and Yale Fiber optic light, model number 20, with 150 W intensity was placed behind the chamber. Figure 4.7 shows the arrangement for the microscope with a regular lamp source. To minimize vibration of the microscope and light source, rubber pads were attached to the bottom of the chamber.

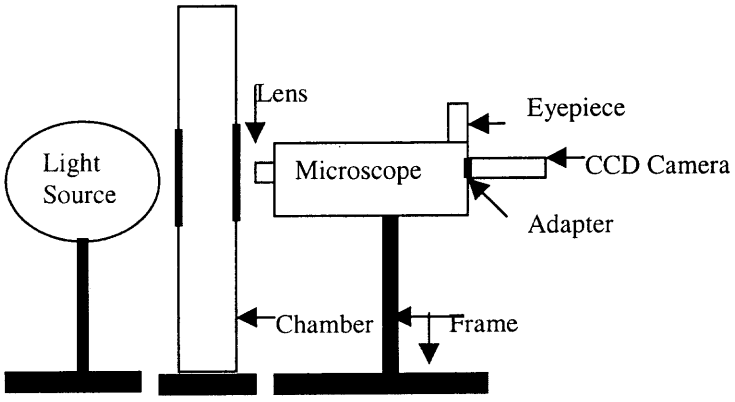

Figure 4.7 Microscope and Light Source

4.5 Recording and Image Capturing

A color camera with charge coupled device (CCD); NEC model NX18A was fixed to the microscope through a specially built metal adapter (Figure 4.7). The CCD camera has two video out connections. One connection from the camera was connected to a TV/VCR for video recording. The other was connected to a Gateway 2000 P5-120 computer for digital image capturing and analysis using WinTV 32. Figure 4.8 shows the arrangement of the connection from the CCD to the TV/VCR and the computer.

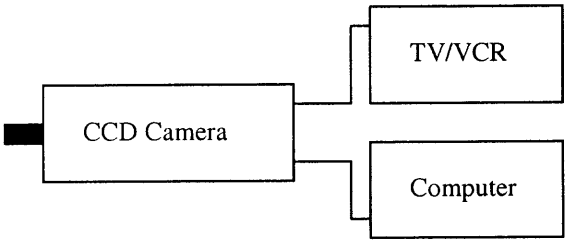

Figure 4.8 CCD Camera Connections for Recording and Capturing

4.6 Image Analysis

A WinTV32 card and associated software were installed in the computer. Digital motion video of the particles movement before and during the experiments were recorded using the image dimensions of 320X240 and image format of 24 bit RGB, at 30 frames per second. The video images were stored as AVI (Audio/Video Interleaved) files. With the above setting, a video of 8 seconds requires about a 60 M bits of file size.

For the analysis of images, Adobe Premiere software was used. Adobe Premiere 5.1 transfers the digital video, AVI files, into GIF individual frames. Thus every second of video run produced 30 frames or GIF files. Each frame was analyzed using Adobe PhotoShop 5.5. Photographs of a horizontal and vertical radical scale of total 0.1 mm with subdivision of 10 micrometers where captured using the same setting of Figure 4.8, WinTV32 captured and Adobe software analyzed images of radical scale are shown in Figure 4.9 and 4.10. X and Y pixels on Adobe Photoshop 5.5 images were calibrated using each division correspond to 12 micrometers in Figure 4.9 and 4.10. Positions of different particles at different locations were measured using the x and y pixel coordinates in the software and compared to the radical horizontal and vertical scale. Movements of individual particles were tabulated using the above techniques.

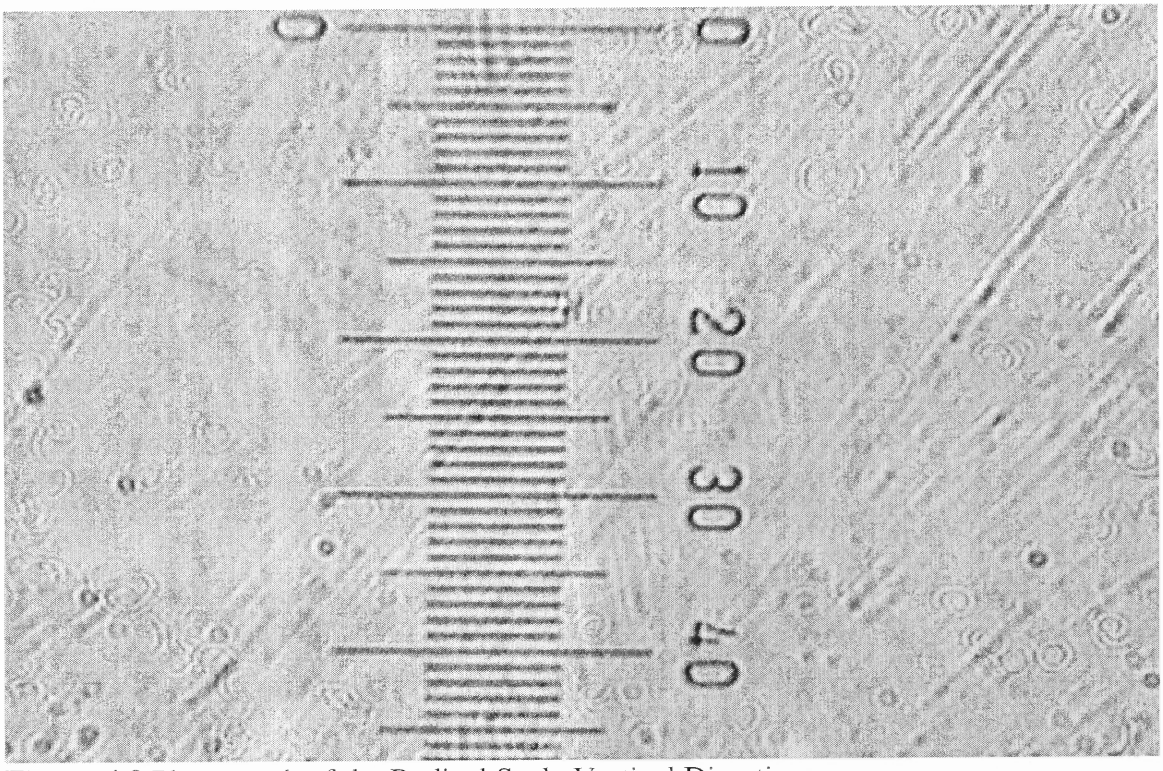

Figure 4.9 Photograph of the Radical Scale Vertical Direction

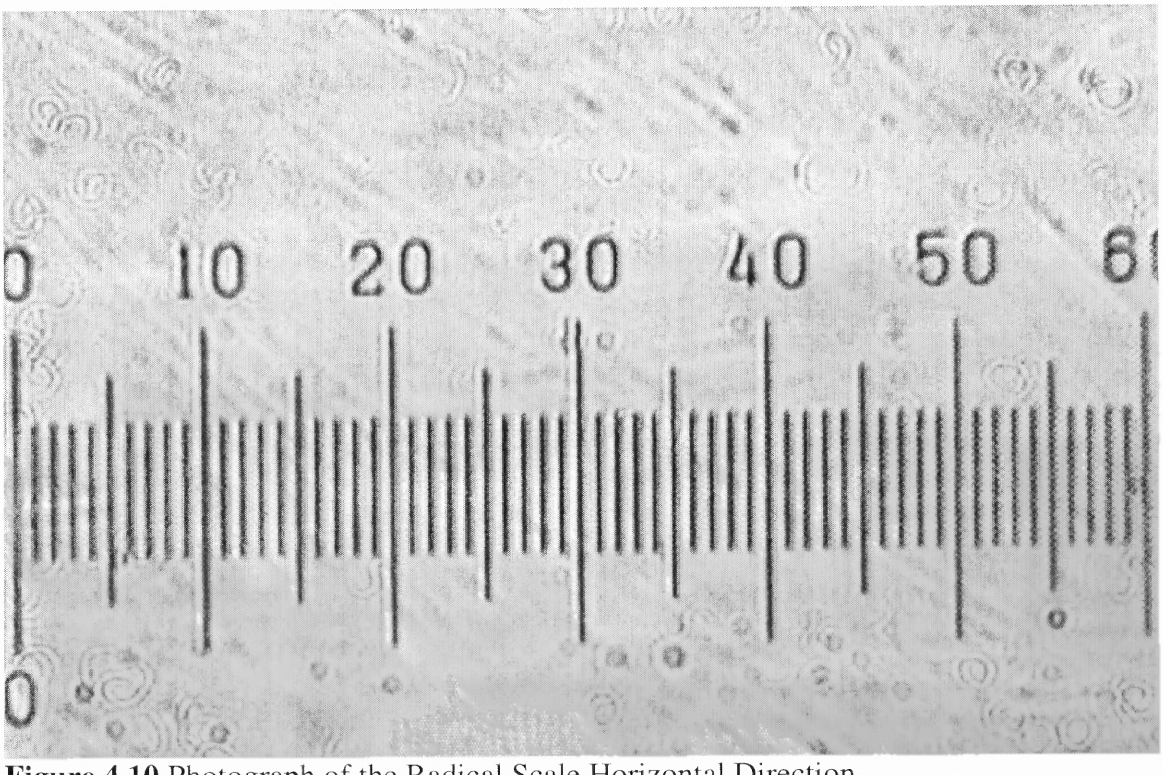

Figure 4.10 Photograph of the Radical Scale Horizontal Direction

4.7 Conclusions

A complete experimental setup was built and details are discussed in this chapter. This includes the electrical equipment used, the acoustic chamber built, sediments used, recording/image capturing and electrical connections. Figures 4.11 through 4.22 show the photographs of different equipment and their connections used in this research. Every time before an experiment the apparatus was leveled in all direction to make sure the chamber was standing perfectly upright. The electrical equipment was calibrated in the laboratory for accuracy.

A discussion of the experimental results using the above equipment and units is given in next chapter, Chapter 5. Conclusions and some future recommendations for studies are discussed in Chapter 6.

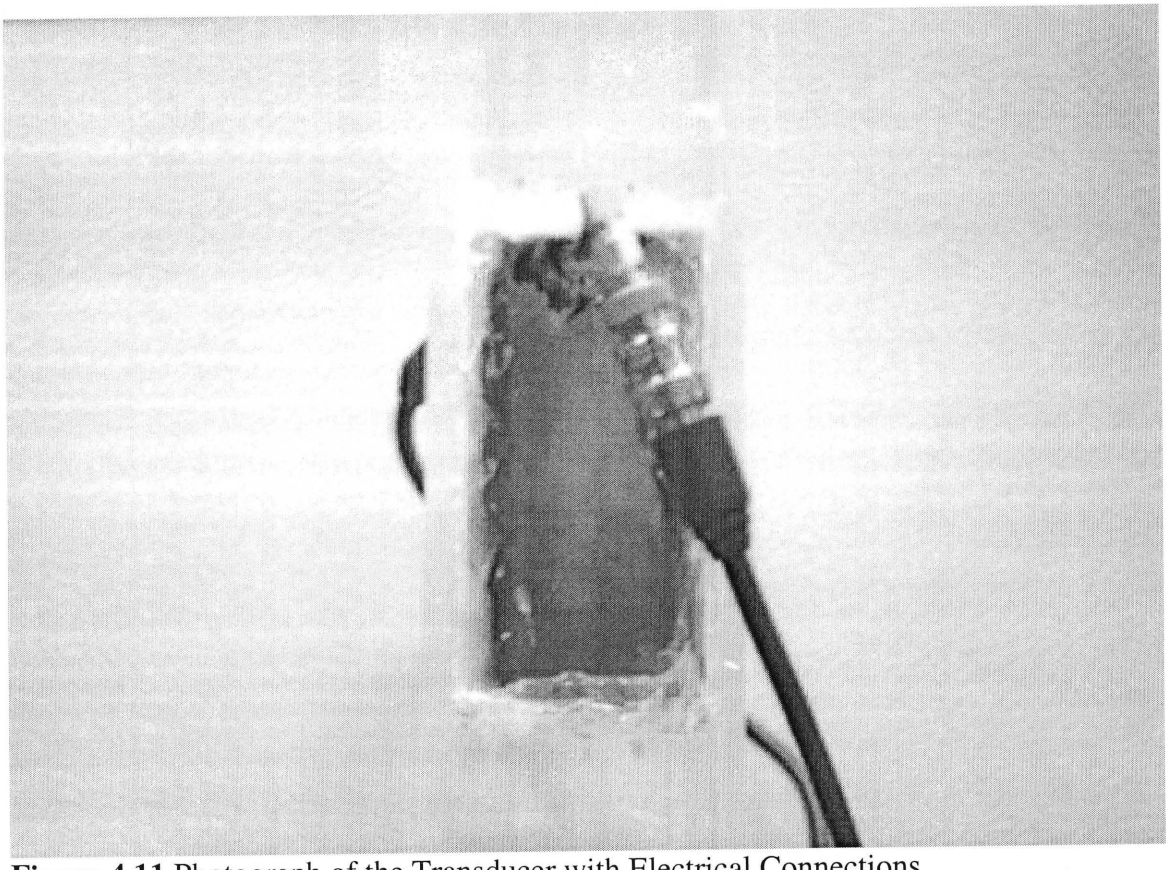

Figure 4.11 Photograph of the Transducer with Electrical Connections

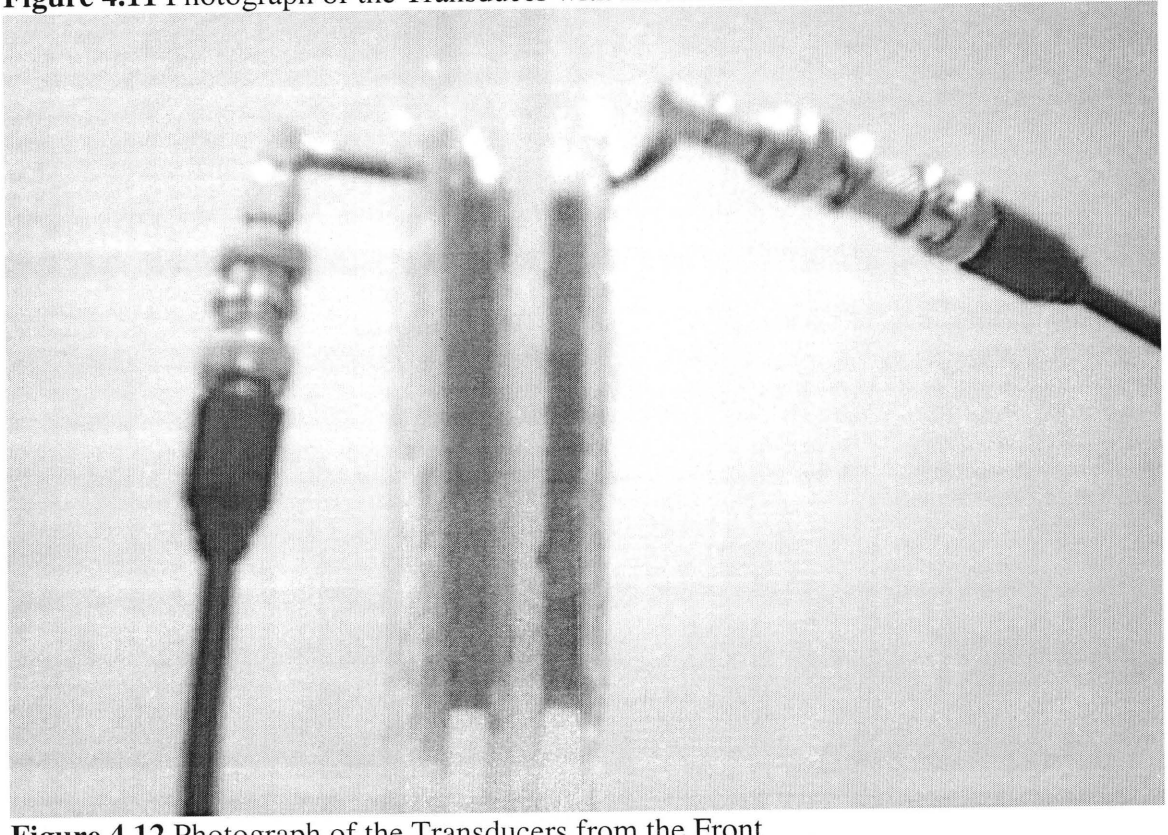

Figure 4.12 Photograph of the Transducers from the Front

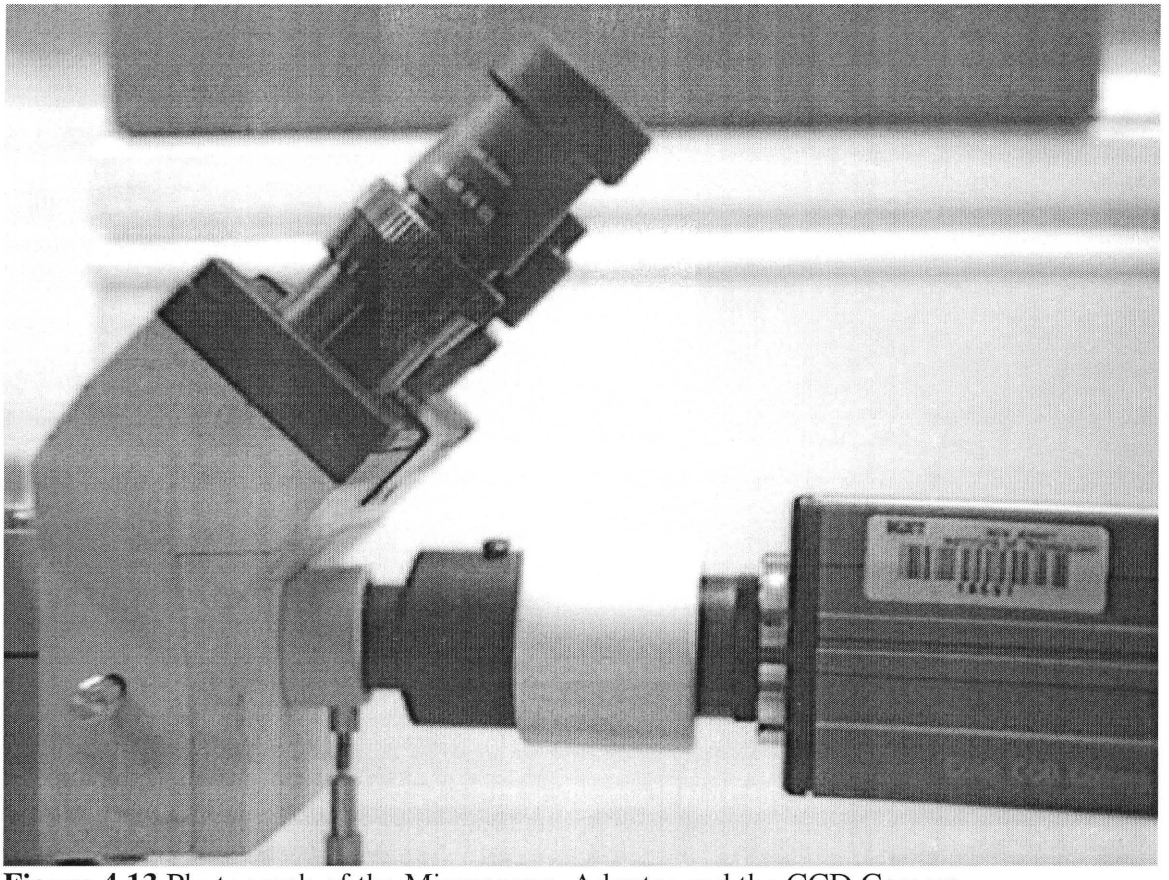

Figure 4.13 Photograph of the Microscope, Adopter and the CCD Camera

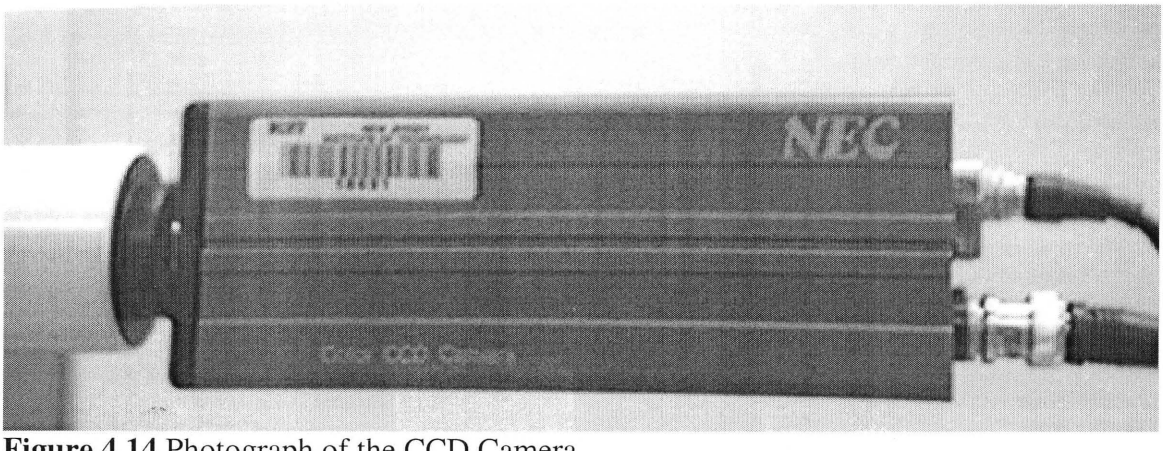

Figure 4.14 Photograph of the CCD Camera

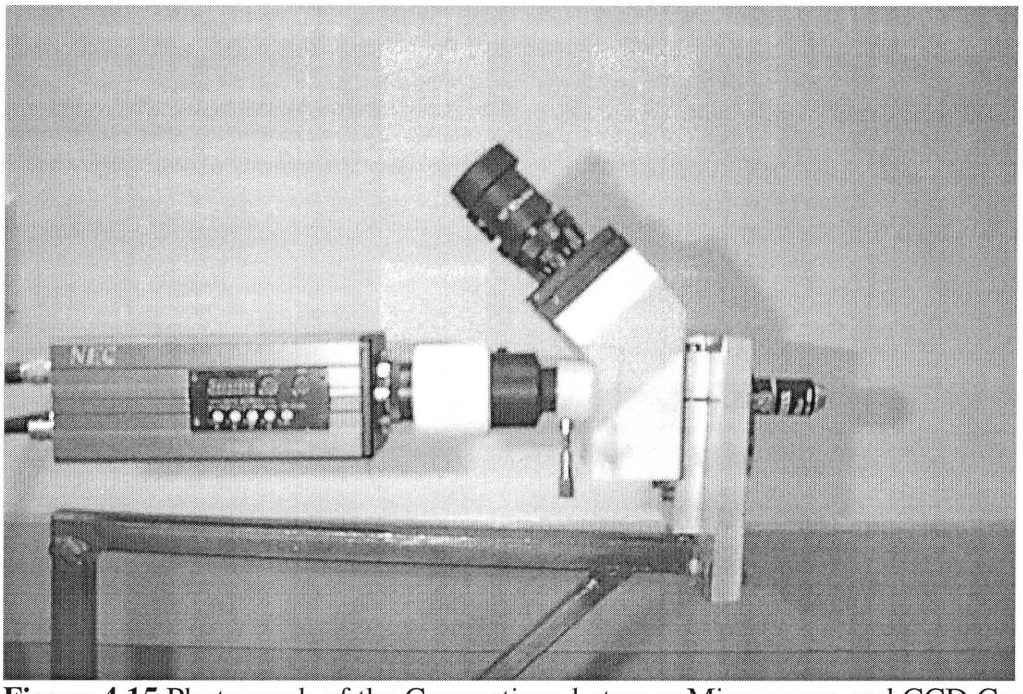

Figure 4.15 Photograph of the Connections between Microscope and CCD Camera

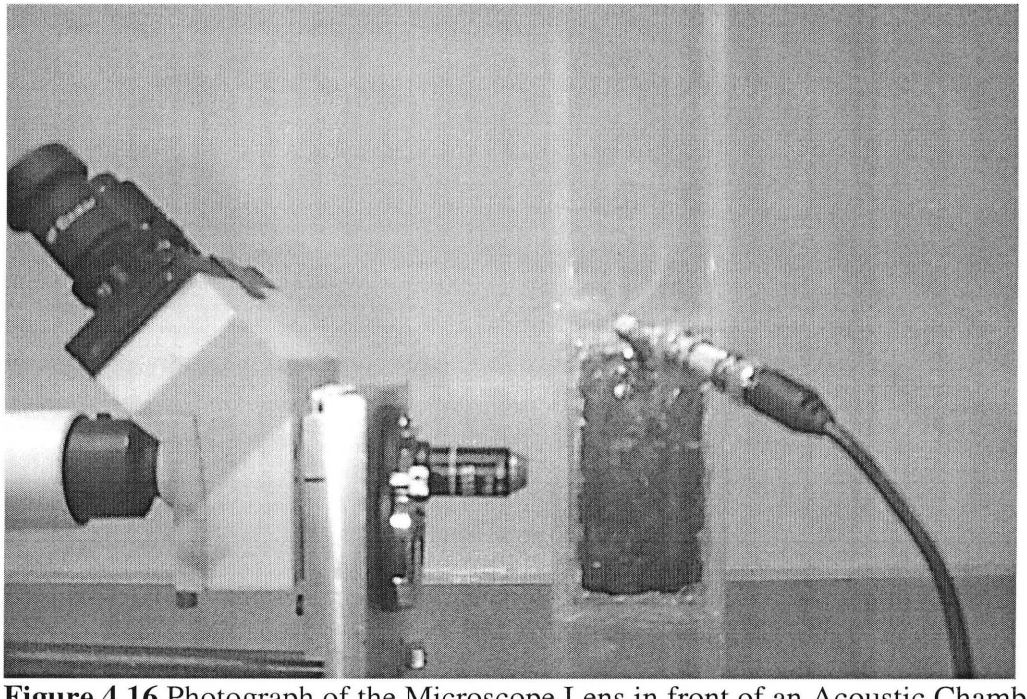

Figure 4.16 Photograph of the Microscope Lens in front of an Acoustic Chamber

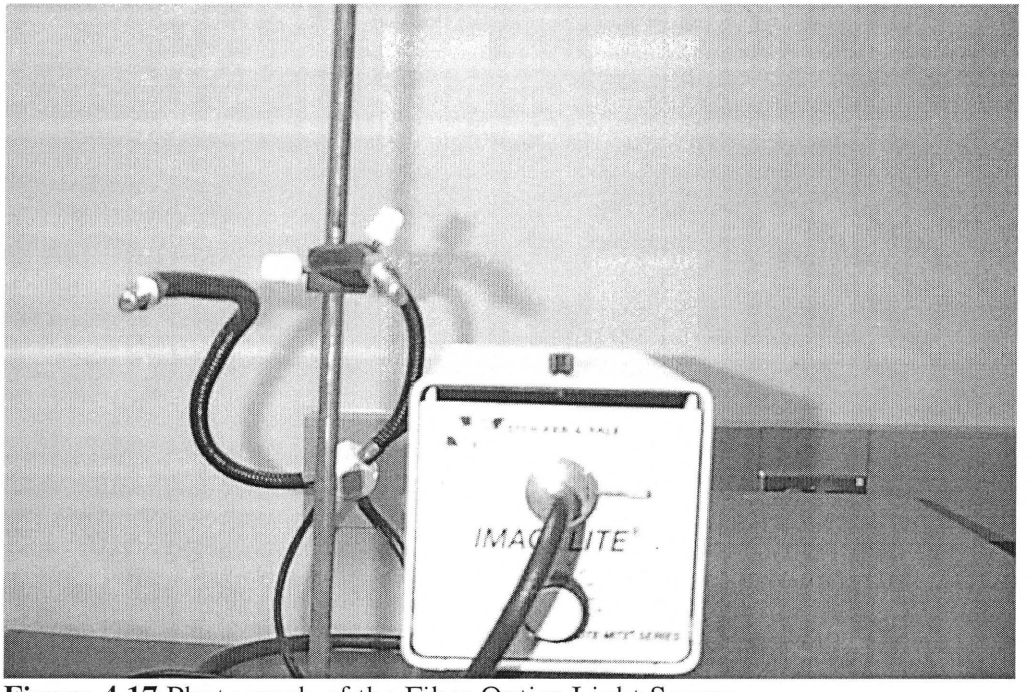

Figure 4.17 Photograph of the Fiber Optics Light Source

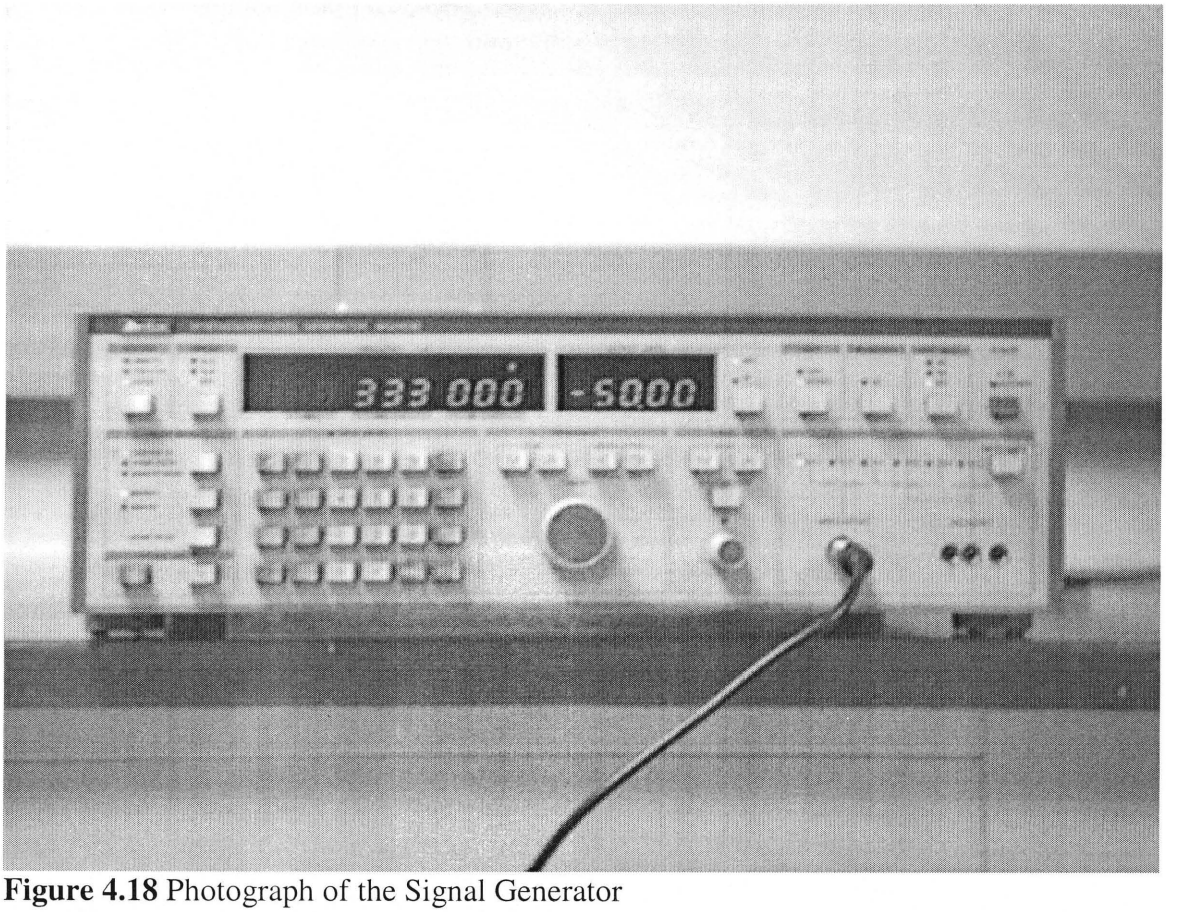

Figure 4.18 Photograph of the Signal Generator

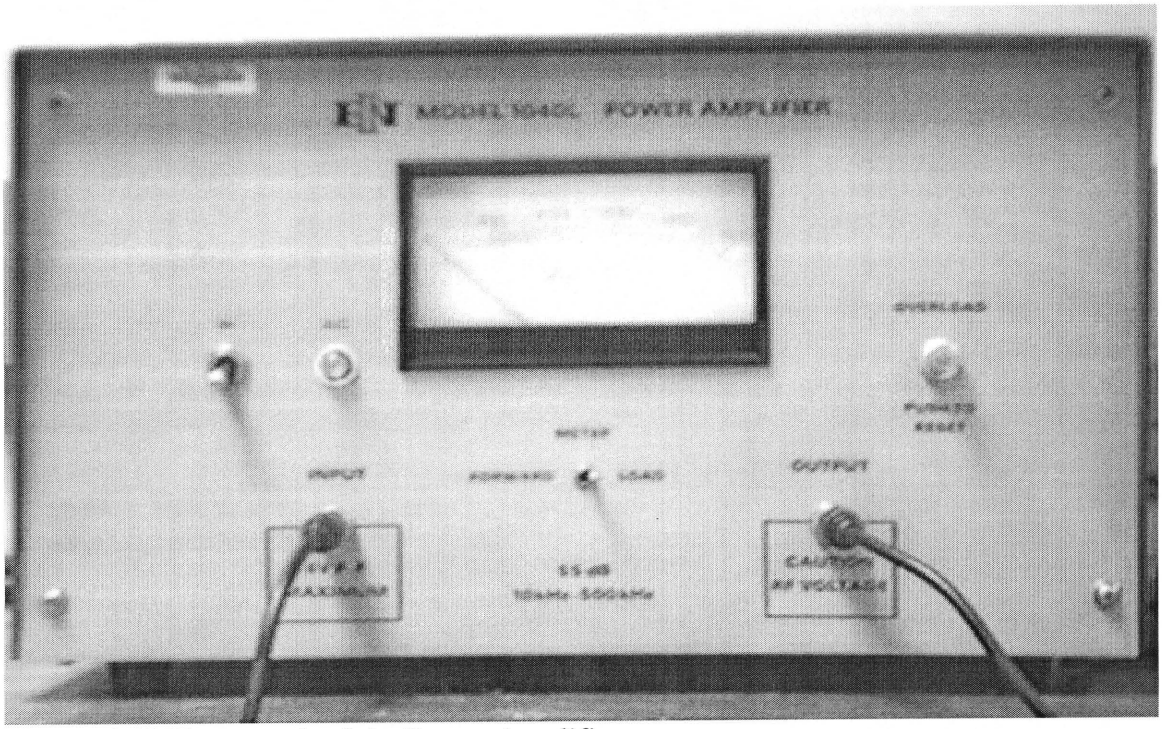

Figure 4.19 Photograph of the Power Amplifier

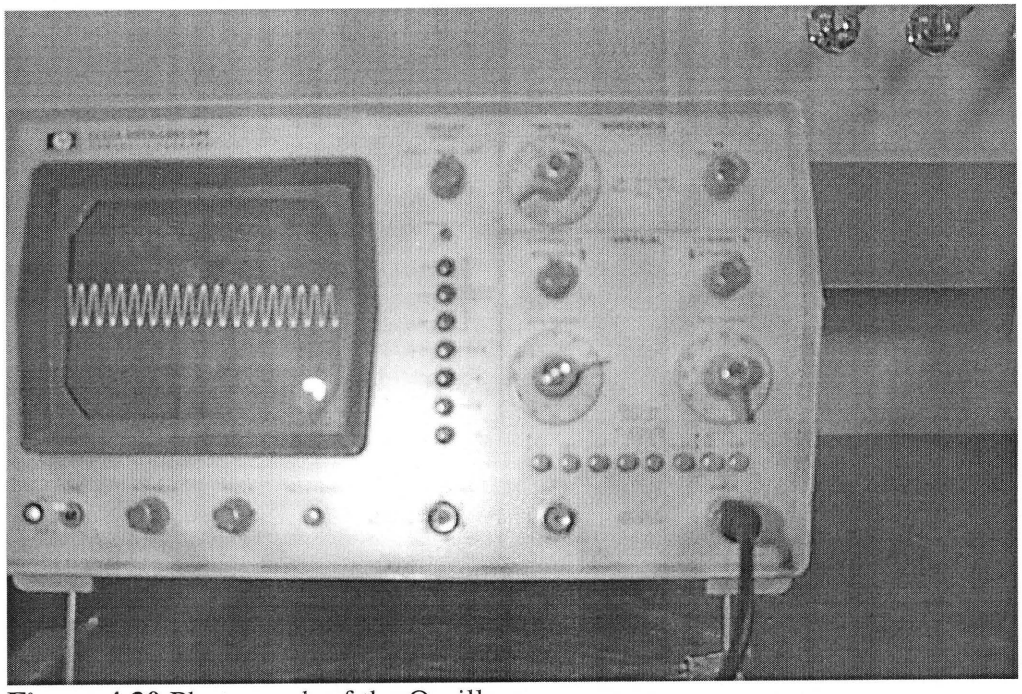

Figure 4.20 Photograph of the Oscilloscope

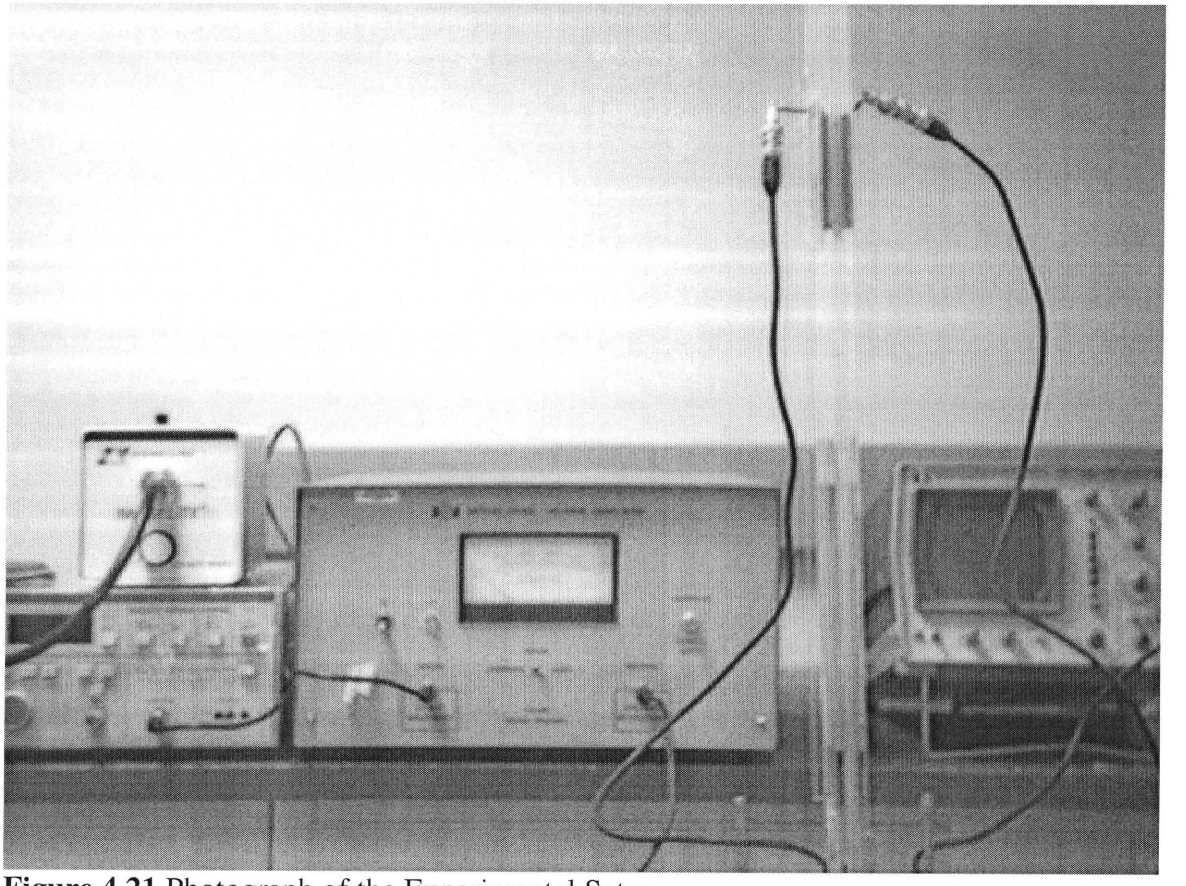

Figure 4.21 Photograph of the Experimental Setup

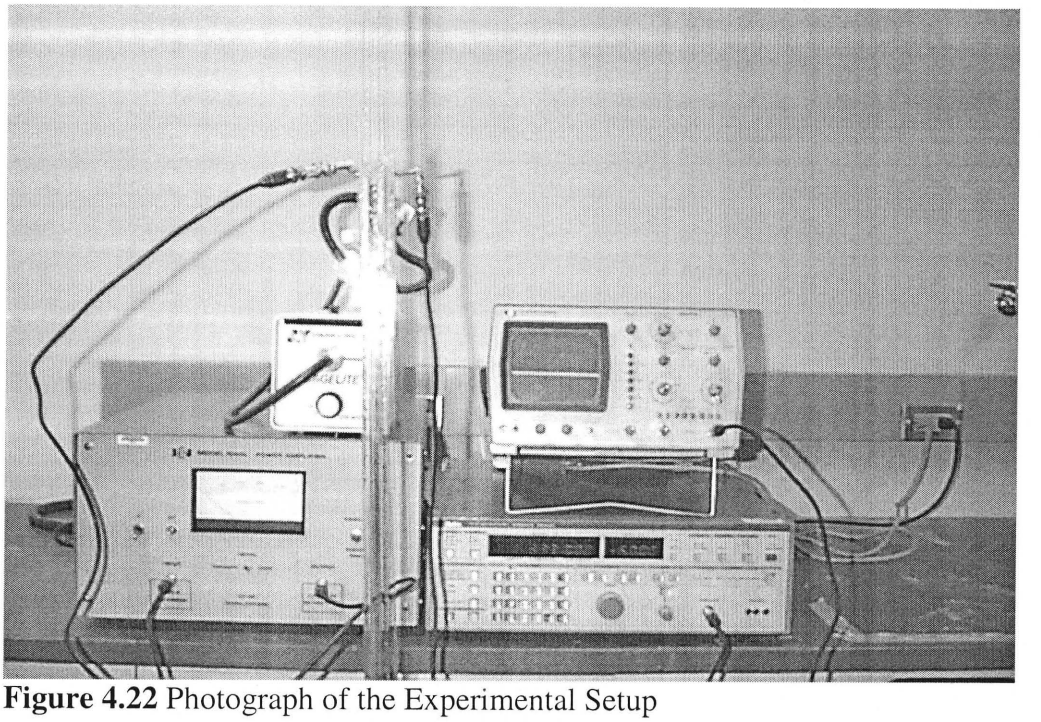

Figure 4.22 Photograph of the Experimental Setup

CHAPTER 5

EXPERIMENTAL OBSERVATIONS

This chapter contains detailed investigations of motion of suspended particles in an acoustic field. From literature search and the theory explained in previous chapters, it was concluded that under certain acoustic conditions, particles would move towards pressure nodes or antinodes depending on contrast factor G. The collection of suspended particles due to the acoustic radiation force and its relationship to the stability of the sound field distribution was investigated utilizing ultrasonic transducers mounted at two sides of the plexiglas chamber. The distance between the two transducers was made equal to two wavelengths. The ultrasound transducers were activated at different power input levels and the motion of suspended particles were observed, tracked and recorded. The results are then compared to the mathematical prediction model that was presented in Chapter 3. A discussion of test results and chapter summary is provided at the end.

5.1 Experimental Observations

The experimental observations are divided into two sections. The first section deals with the formation of particle columns with silicon dioxide (SiO_2). The second observation section deals with the individual particle movement and tracking of silicon carbide (SiC) particles. Since SiO_2 particles are very fine and it was not possible to trace particle trajectories, hence larger particle size of SiC were used for tracking. The detail observation and discussion for the particle column with SiO_2 is discussed below.

5.2 Particle Column Formation with SiO_2

Silica fume of size 1 to 5 micrometer in diameter purchased from AEE Atlantic Equipment Engineering (SI-601) was first used. The dispersing agent used in ASTM method for hydrometer test was used to disperse particles in water. Approximately 0.2 grams of Silica fumes were added to a dispersing agent (4% Sodium Hexameta Phosphate solution made with deionized water). The mixture was kept at rest for approximate five minutes. Then the solution was mixed with 1000 milliliter of deionized water in a graduated one liter jar and was thoroughly shaken 60 times to disperse the particles in the water. This solution was introduced into the acoustic chamber from the bottom inlet using gravity. Vacuum was applied at the top outlet of the chamber to remove air bubbles and to avoid formation of cavities during chamber feeding.

Then a 333 kHz and 40 watts sound field was generated in the chamber. Four particle columns were observed at equal distances from the transducers after few seconds of sound application. The distances between the columns were approximately 2.5 mm equivalents to half wavelength at 333 kHz frequency. These columns were visible by naked eyes. The exact position of the collections of particles in planes of minimum pressure was not possible without a probe hydrophone. After five minutes, small air bubbles appeared with the above particle columns. The optimum power reading on the amplifier was 40 watts. Further continuation of ultrasound energy for additional 15 minutes caused the bubbles to increase in size and number, and started disturbing the particle columns. Once the power was turned off, the particle columns disappeared and reformed when power was turned on. When the frequency was changed slightly, these columns were still visible but not as clear as when the signal frequency was set

at 333kHz. This indicates the formation of a standing wave at a frequency of 333 kHz. In other words, it is necessary to have an exact standing wave in order to create an acoustic radiation force field on particles.

Repeated attempts to digitally capture the above column formation failed even with help of NJIT media service department with the use of a professional digital recorder. However, VHS video recording was possible and was achieved to confirm the applicability of the technology. Figure 5.1 shows schematics of four particle columns formed at 333 kHz frequency and 40 watts power.

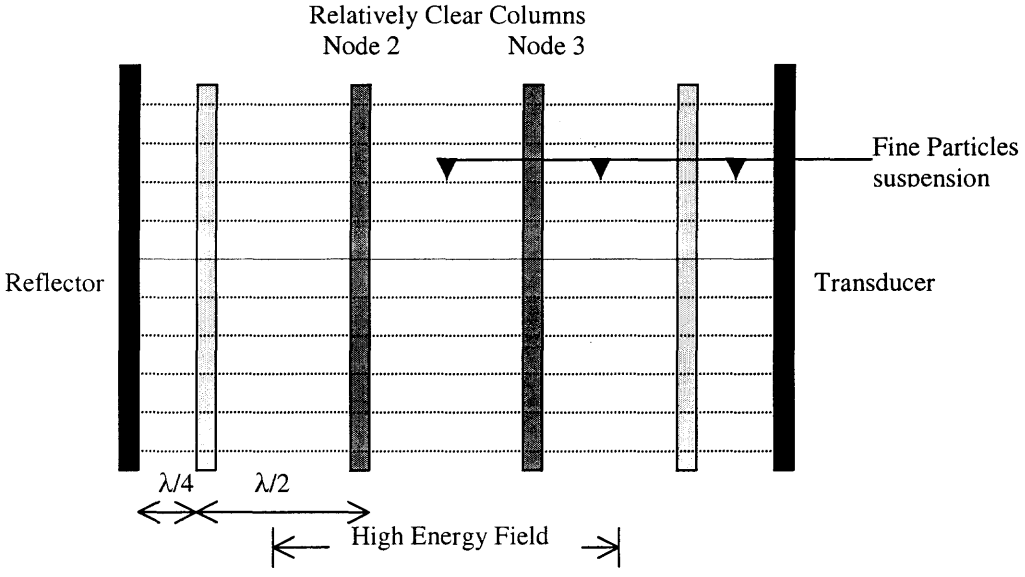

Figure 5.1 Formation of Particle Columns

According to the theory developed in Chapter 3, for an acoustic wave-guide of length 2λ between the transducer and reflector there are four nodes or minimum pressure nodes, repeated at every half-wavelength distance. The first and last nodes have to be at a distance of quarter wavelength from the face of the transducer and reflector respectively. This is schematically shown in Figure 5.2. However, video recording indicates two clearly visible columns corresponding to nodes 2 and 3 (Figure 5.1) and two faded columns corresponding to nodes 1 and 4.

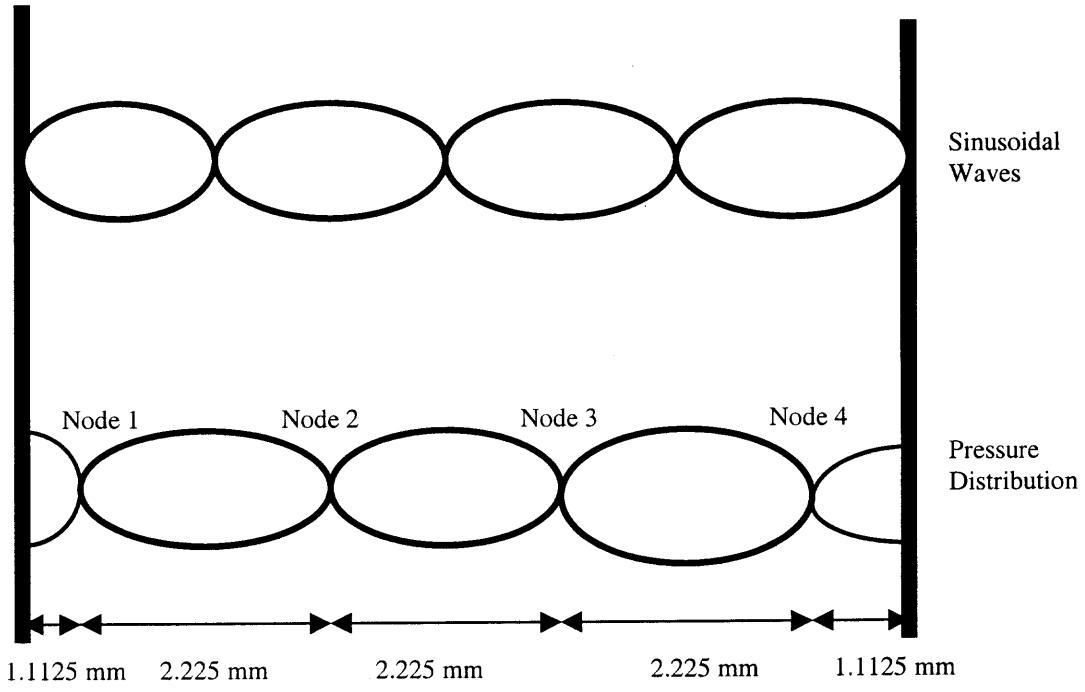

Figure 5.2 Positions of four Nodes in the Chamber

The reason for two clearly visible two-middle columns can be explained by reviewing Table 2.2. The maximum velocity amplitude occurs near center of the

wave-guide and decreases to minimum at the two boundaries, at the transducer and reflector. The occurrence of maximum velocity causes minimum pressure. Hence, the magnitude of pressure is comparatively very low at nodes close to the fixed boundaries when compared to those in the center of the chamber. Thus, the particle columns at nodes 2 and 3 had the highest visibility with more particles.

When the application of ultra sound energy continued beyond five minutes, air bubbles generated. Initially, those air bubbles were small and did not move, but once they got larger, they started moving rapidly from points of formation to fixed preferred positions. The movement of bubbles was horizontal rather than vertical (the direction of the gravity). This indicates the formation of bubbles at pressure antinode and later with the growth of their size and their movement towards the pressure node. After further bubble growth they started moving upward following one straight path probably along the node. Figure 5.3 shows bubbles even after the power was shut off. While the power was on, particle columns were still visible for few a minutes after the formation of small air bubbles. When the energy in the chamber further increased, the bubbles formed throughout the chamber with no visible bubble or particle columns.

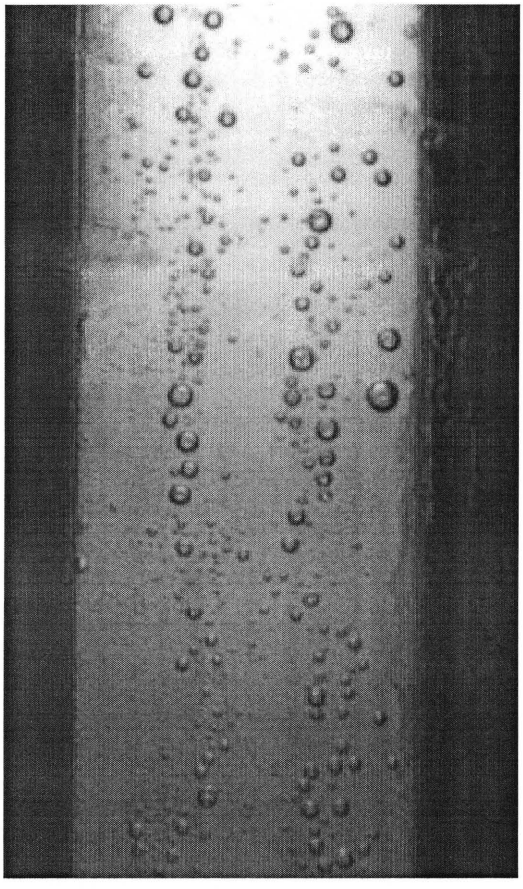

Figure 5.3 Chamber is full of Bubbles

To increase the contrast of particle columns, SiO_2 particles were mixed with water insoluble black dye. Eriochrome Black T, a liquid black dye, was added to Silica fume, mixed and dried in a vacuum oven. When this particle suspension was introduced to the chamber, the black dye colored the water and there was no improvement in the particle column visibility. In another effort, large size particles were separated from the bulk solution by removing the suspended particles at the top and collecting particles at the bottom. These large size particles were used in the experiment; still there was no significant improvement in the visibility to photograph the column. Then in another

attempt, particles were coated with florescence powder to be illuminated with a black light. When these coated particles were introduced to the sound field, the coating disintegrated and contaminated the chamber. Therefore, further experimentation using silica was suspended.

5.3 SiC Particles Sedimentation

As stated before, due to the small size of SiO_2 particles, it was not possible to trace the particle trajectories even a microscope. Hence, larger particles of SiC were used and the above experiment was repeated.

Approximately 0.2 grams of Silicon Carbide (SiC) with particle sizes of 5 to 20 micrometers were added to a dispersing agent made of 4% sodium hexametaphosphate in deionized water. This suspension was kept at rest for few minutes. Then it was mixed with 1000 milliliters of DI water in a graduated one liter cylinder and shaken 60 times thoroughly for complete dispersion of particles. The solution was introduced into the acoustic chamber from the bottom inlet of the acoustic chamber using gravity. Vacuum was applied at the top outlet of the chamber to remove air bubbles and to avoid cavitation.

Several experiments were performed to demonstrate the effectiveness of the fractionation technique and to obtain data to compare with the theoretical formulation. The resonant frequency for the acoustic chamber was experimentally determined to be 333.676 kHz using SiO_2 particles. Individual SiC particles were tracked and their positions were recorded, so that experimental data can be compared with mathematical model predictions.

Particles displacement can be documented by having a low concentration of uniformly dispersed particles in an acoustic field and recording the particle trajectories. Particle movements were captured using a digital video. The digital video was converted into individual frames using Premiere 5.0 and movement of number of individual particles in each frame was analyzed using PhotoShop 5.5. Figure 5.4 shows the photograph of the particles in the acoustic chamber before application of the acoustic energy. Figure 5.5 shows photographs of four consecutive frames from captured videos showing vertical displacements of particles (sedimentation) at 0.30 second intervals. The vertical displacements of particles were recorded and positions were estimated with the aid of radical scale. The time between the two consecutive frames was 1/30 seconds. The falling velocities of particles were calculated by dividing the vertical displacement by the time. Table 5.1 shows vertical velocities of a single particle at different time intervals from the experimental analysis.

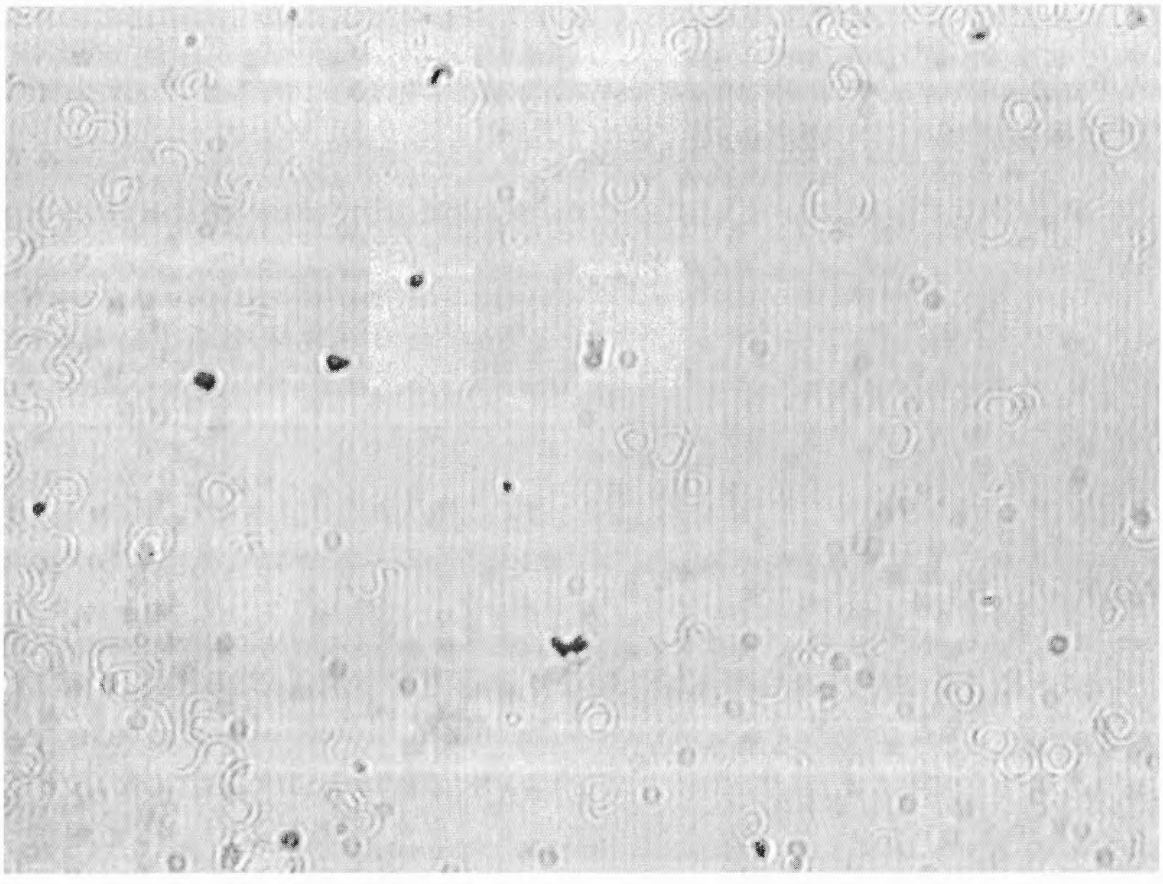

Figure 5.4 Photograph of the Particles in an Acoustic Chamber before Energy

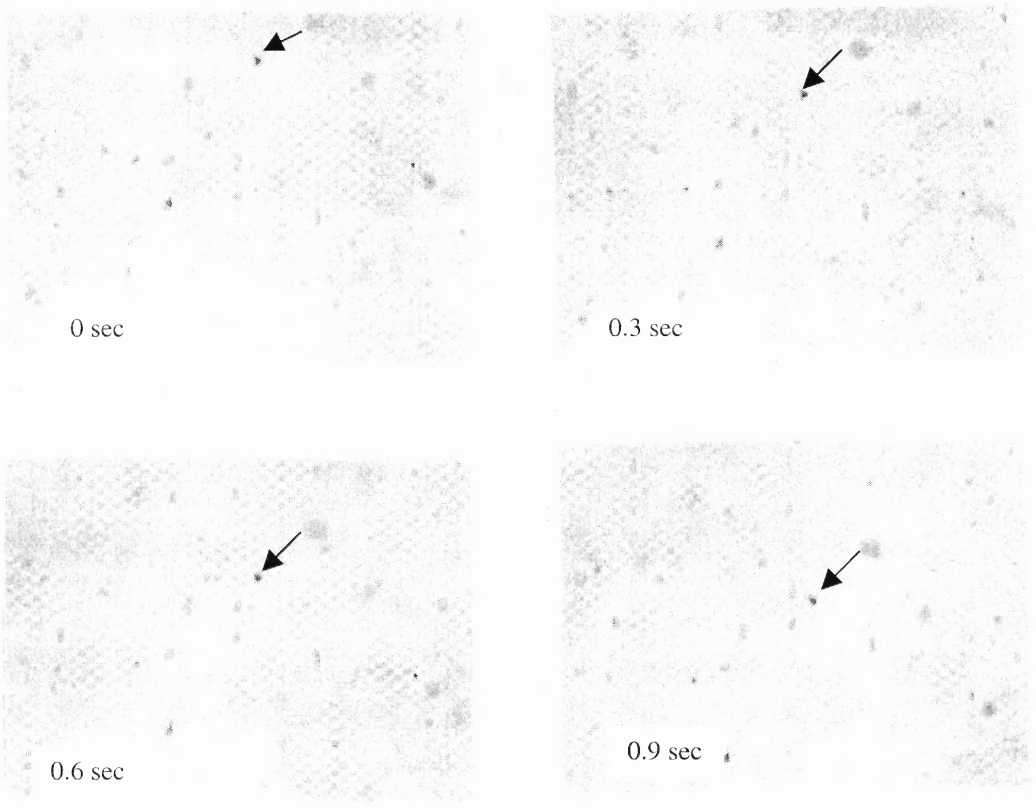

Figure 5.5 Photographs of the Particles during Sedimentation at 0.3 Second Intervals

Table 5.1 A Single Particle Velocity (sedimentation) by Experiment

Particle Positions	Time (seconds)	Displacement (micron)	Velocity (micron/sec)	Average Velocity (micron/sec)
1	0	0		
2	0.0999	53	530.53	530.53
3	0.1998	105	520.52	525.52
4	0.2997	160	550.55	533.86
5	0.3996	216	560.56	540.54
6	0.4995	266	500.5	532.53
7	0.5994	320	540.54	533.86
8	0.6993	380	600.6	543.4

From the above table the average particle velocity was approximated to be 530 micron/sec. Using the sedimentation velocity, the particle diameter was calculated using the Stokes' law:

$$v = \frac{2}{9}(\rho_p - \rho_f)\left(\frac{(D/2)^2}{\mu}\right)g \tag{5.1}$$

or,

$$D = \sqrt{\frac{18v\mu}{g(\rho_p - \rho_f)}} \tag{5.2}$$

Where, v is the particle velocity, ρ_p and ρ_f is the density of the particle and the fluid respectively, μ is the viscosity of the fluid, D is the particle diameter and g is the acceleration due to gravity.

It was difficult to estimate the exact size of the particles from the frames of video capture during sedimentation. The diameter of SiC particles used for this research were in the range of 5 to 20 micron with a density of 3.21 E-12 g/micon^3. Using the sedimentation velocities in Table 5.1 and Equation 5.2, the particle diameters were calculated and listed in Table 5.2.

Table 5.2 Diameter of Particle by Stokes' law

Particle Velocity (v) from Table 5.1 (micron/sec)	Particle Diameter (D) by Stokes' law (micron)
530.53	21.39
520.52	20.74
550.55	21.355
560.56	21.52
500.5	20.34
600.6	22.28

From Table 5.2, the particle diameters were found to be approximately 24 micrometer, which is above the upper limit of the SiC particle size distribution shown in Chapter 4. Since the average size of the particle from particle size analysis is around 9 micrometers, it can be concluded that the estimated diameter from the Stokes' law is more than twice that of measured. The only reason for the above discrepancy between the observed and the calculated velocities should be due to the assumption of spherical shaped particles in deriving Stokes' law. SiC particles are not spherical but rather cubical crystals. Thus, it is not logical to compare the experimental velocity with that obtained from Equation (5.1). Different particles that were tracked and recorded the positions during the experiment and they all had velocities in the same range as those in Table 5.1. This concludes that the observation technique used in this research for the individual particles is correct and can be used for recording particle trajectories in an acoustic field for different energy levels.

5.4 SiC Particle Trajectories in an Acoustic Field

A solution of SiC particles in DI water was prepared as described previously and fed into the chamber from the bottom inlet using gravity. The CCD camera attached to the microscope was brought close to the chamber as shown in Figure 4.16. The microscope was moved backward and forward to focus. Digital video capture started using WinTV capture board and accompanying software to read particle movements in the fluid at different acoustic energy levels. The signal generator produced a 333.676 kHz sinusoidal signal. Table 5.3 lists the power input from power amplifier to amplify the sinusoidal signal into the chamber and corresponding dB values. These different power levels were

introduced gradually into the chamber. Digital capturing at a rate of 30 frames per second was made at all these power levels and each capture was stored in separate AVI file. Thus, for 12 power levels 12 AVI files were obtained.

Table 5.3 Different Power Ranges used in the Experiment

Input form signal generator (before amplification) dB	Equivalent Power (after amplification) Watts
-50	0.003
-30	0.3
-28	0.5
-25	1.0
-23	1.5
-22	2.0
-21	2.5
-20	3.0
-19.5	3.5
-19.0	4.0
-18.5	4.5
-18.0	5.0

The Adobe Premier 5.0 software was used to convert each AVI file into individual frames and stored as separate JPEG files. After converting AVI files into JPEG frames, Adobe PhotoShop 5.5 was used to obtain particle displacements for each frame at 1/30 second intervals. The particle position were calibrated using radical (Figure 4. 10). Figure 5.6 shows photographs of particle movement from four consecutive frames with 0.30 second time intervals.

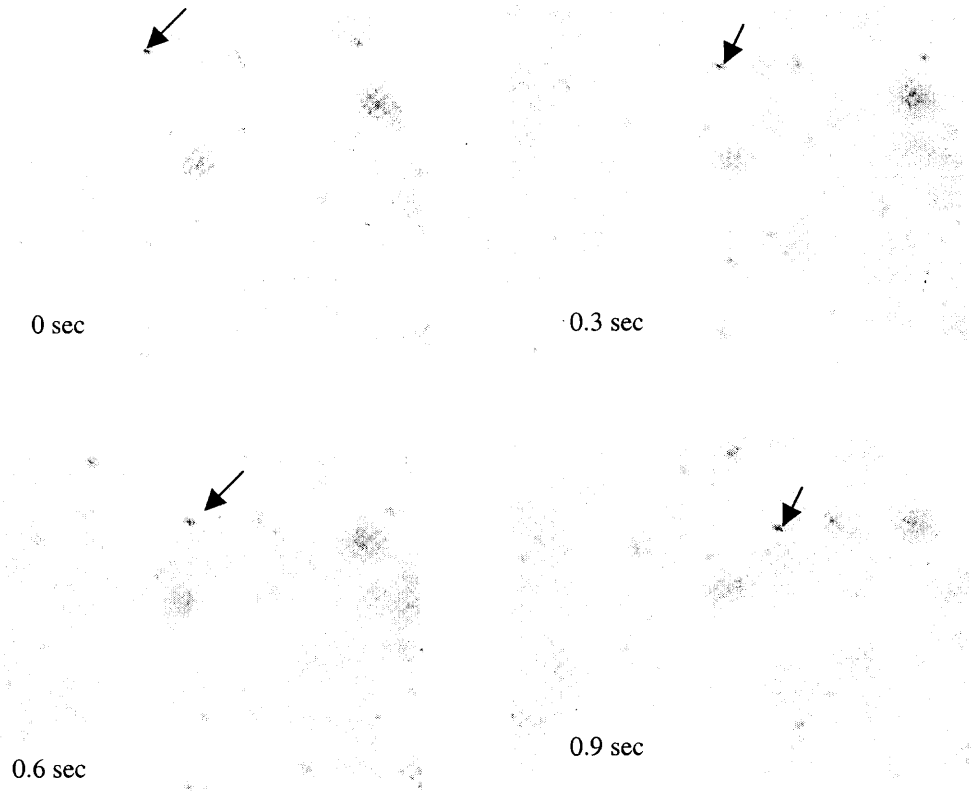

Figure 5.6 Photographs of the Displacement of SiC Particles in an Acoustic Field

The experiment was repeated a number of times and every time fresh sample was prepared and introduced into the chamber as discussed earlier. Graphs were produced for the experimental axial displacement verses time as shown in Figure 5.7 through 5.9.

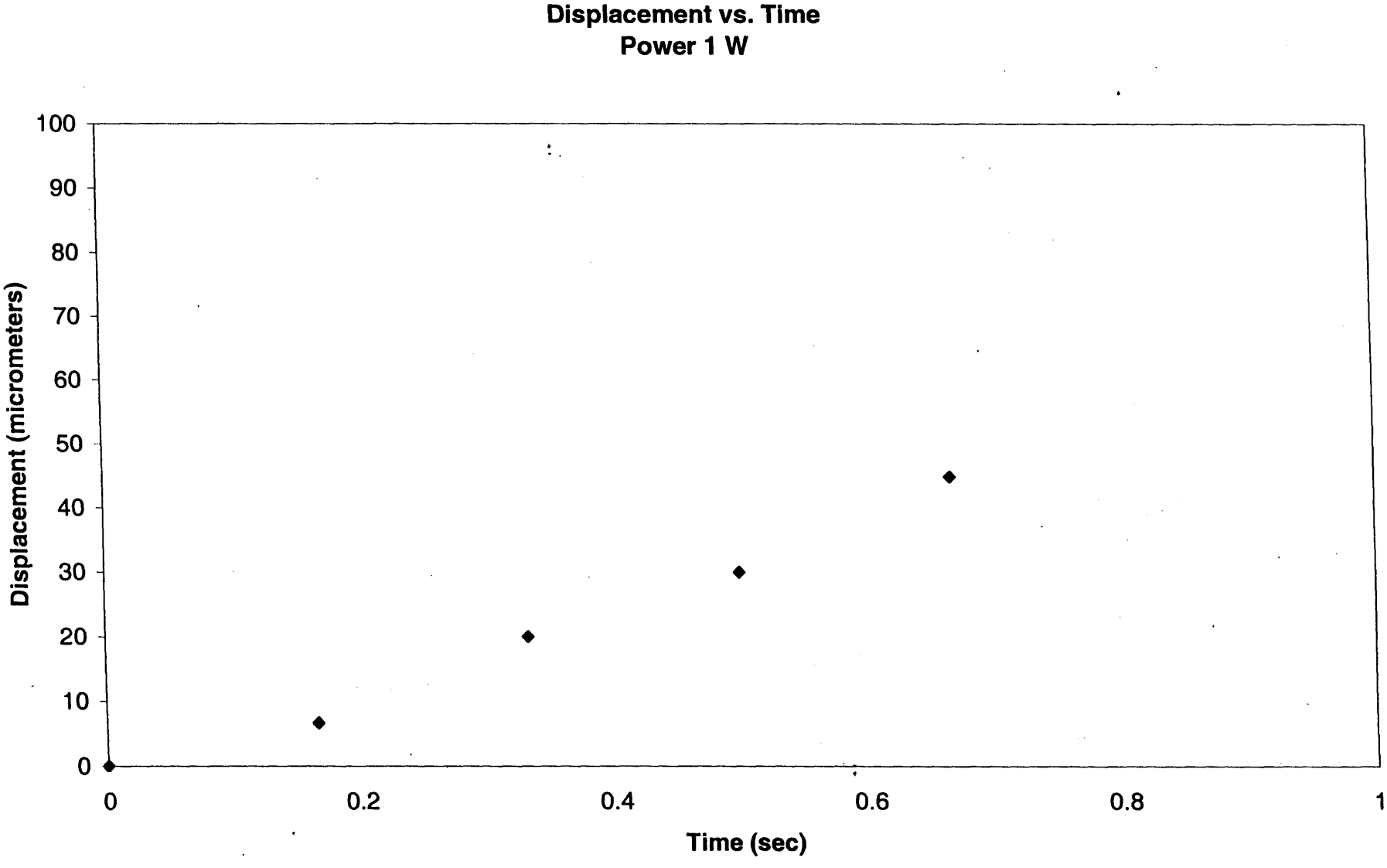

Firgure 5.7 Experimental Data at 1 W

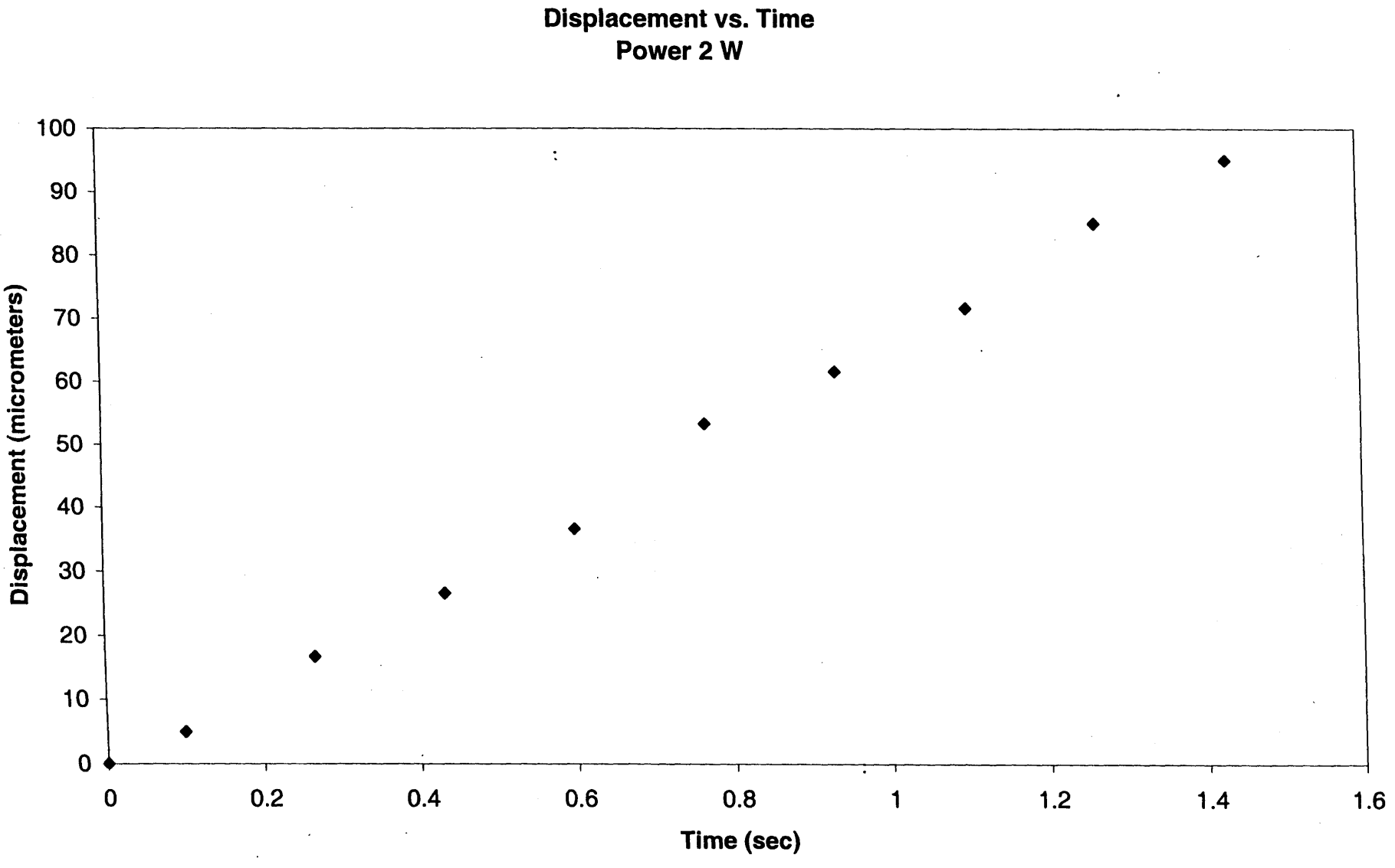

Figure 5.8 Experimental Data at 2 W

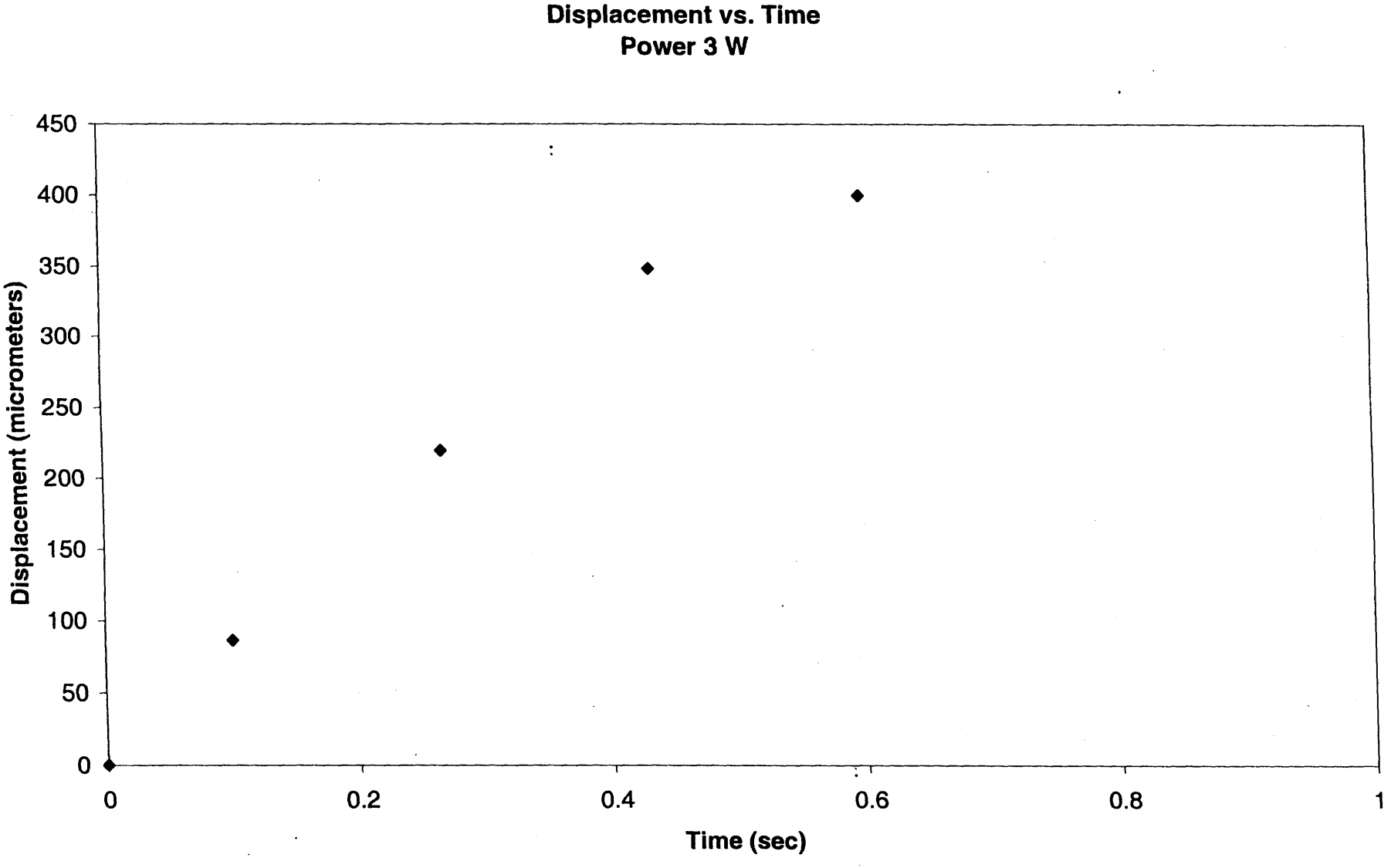

Figure 5.9 Experimental Data at 3 W

5.5 Comparison between Experimental Data and Mathematical Model predictions

After gathering displacement verses time data for different energy levels using the capturing technique discussed earlier, the next step was to compare the experimental data with particle trajectories obtained from the mathematical model in Chapter 3. The JPEG frames converted from AVI files were recorded as pixels. Those pixels were whole numbers (on or off); hence, the coordinates of the particle displacement were not very accurate as we were looking for on or off pixels. That is the length corresponding to the width of one pixel was the experimental error, which was quite significant for 320×240 pixel JPEG files. In order to correct the above error a statistical package was used. After smoothing the data, an optimization technique was used to evaluate the unknown parameters of the experiment. Both these techniques are discussed below.

5.5.1 Statistical Analysis

To obtain meaningful data from low-resolution experimental data in JPEG files, a statistical analysis was performed using S_Plus 2000 software. There are different smoothing techniques to improve data. The most commonly used smoothers are Friedlman Super smoother, Locally weighted regression smoother (LOESS), Spline smoother, and Kernel smoother. In order to select and use one of the above, one needs to understand how each smoothing technique works.

LOESS: in locally weighted regression smoothing, the smooth function is built by first taking a point say $x_{0,\ which}$ constitutes a neighborhood N (x_0). The number of neighbors k is specified as a percentage of the total number of points. This percentage is called the

span. The largest distance between x_0 and another point i in the neighborhood is calculated next;

$$\Delta(x_0) = \max_{N(x_0)} \left| \frac{x_0 - x_1}{\Delta(x_0)} \right| \tag{5.1}$$

Weights to each point in $N(x_0)$ using the tri_cube weight function is assigned:

$$W\left(\frac{|x_0 - x_1|}{\Delta(x_0)} \right) \tag{5.2}$$

Where,

$$W(u) = \begin{cases} (1-u^3)^3 \\ 0 \end{cases}$$

for $0 \leq u < 1$, other wise the weighted least squares fit of y on the neighborhood $N(x_0)$ is calculated. Then the fitting value $y_0 = s(x_0)$ is taken. This is repeated for each predicted value.

Friedlman Super Smoother: with LOESS, the span is constant over the entire range of predictor values. However, a constant value will not be optimal if either the error variance or the curvature of the underlying function varies over the range of x. An increase in the error variance requires an increase in the span whereas an increase in the curvature of function requires a decrease. The super smoother uses local cross_validation to choose the span.

Kernel Smoother: a kernel type smoother is a type of local average smoother that for each target point x_i in predictor space, calculates a weighted average value y_i of the observations in a neighborhood of the target point:

$$y_i = \sum_{j=1}^{n} w_{ij} y_j \tag{5.3}$$

where,

$$W_{ij} = K\left(\frac{x_i - x_j}{b}\right) = \frac{K\left(\frac{x_i - x_j}{b}\right)}{\sum_{k=1}^{n} K\left(\frac{x_i - x_j}{b}\right)} \tag{5.4}$$

are weights which sum to one:

$$\sum_{j=1}^{n} w_{ij} = 1 \tag{5.5}$$

Spline Smoother: a smoothing spline behaves approximately like a kernel smoother, but it arises as a function that minimizes the penalized residual sum of squares (PRESS) given by:

$$PRESS = \sum_{i=1}^{n} (y_i - f(x_i))^2 + \lambda \int (f''(t))^2 dt \tag{5.6}$$

over all functions with continuous first and intergrable second derivatives. The parameter λ is the smoothing parameter, corresponding to the span in Loess or Super smoother.

To select the best smoother for this research, several experimental data sets were smoothened using all four smoothers. The graphs in Figure 5.10 through 5.12 show the experimental data with the above four smoothers.

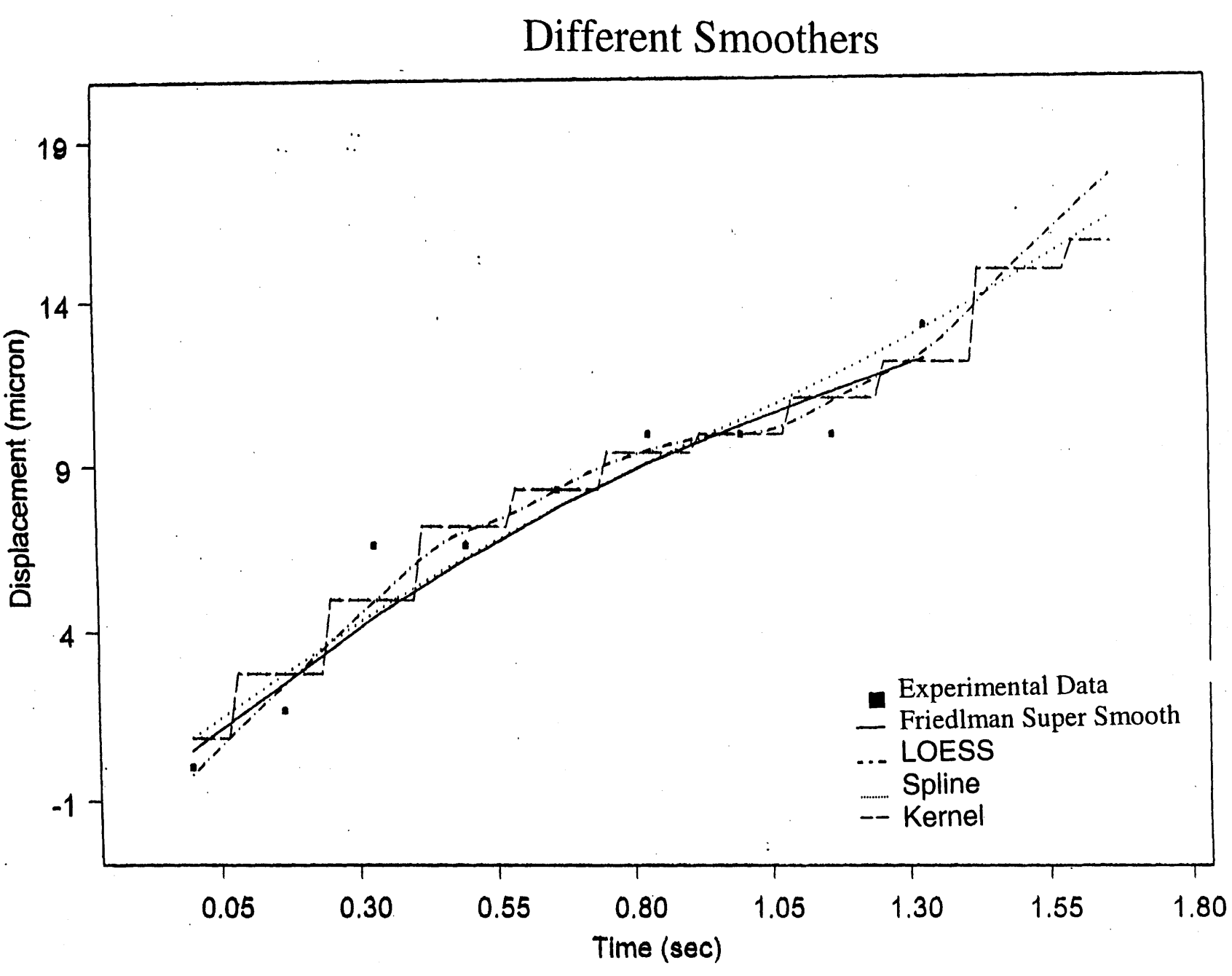

Figure 5.10 Different Smoothers, Sample 1

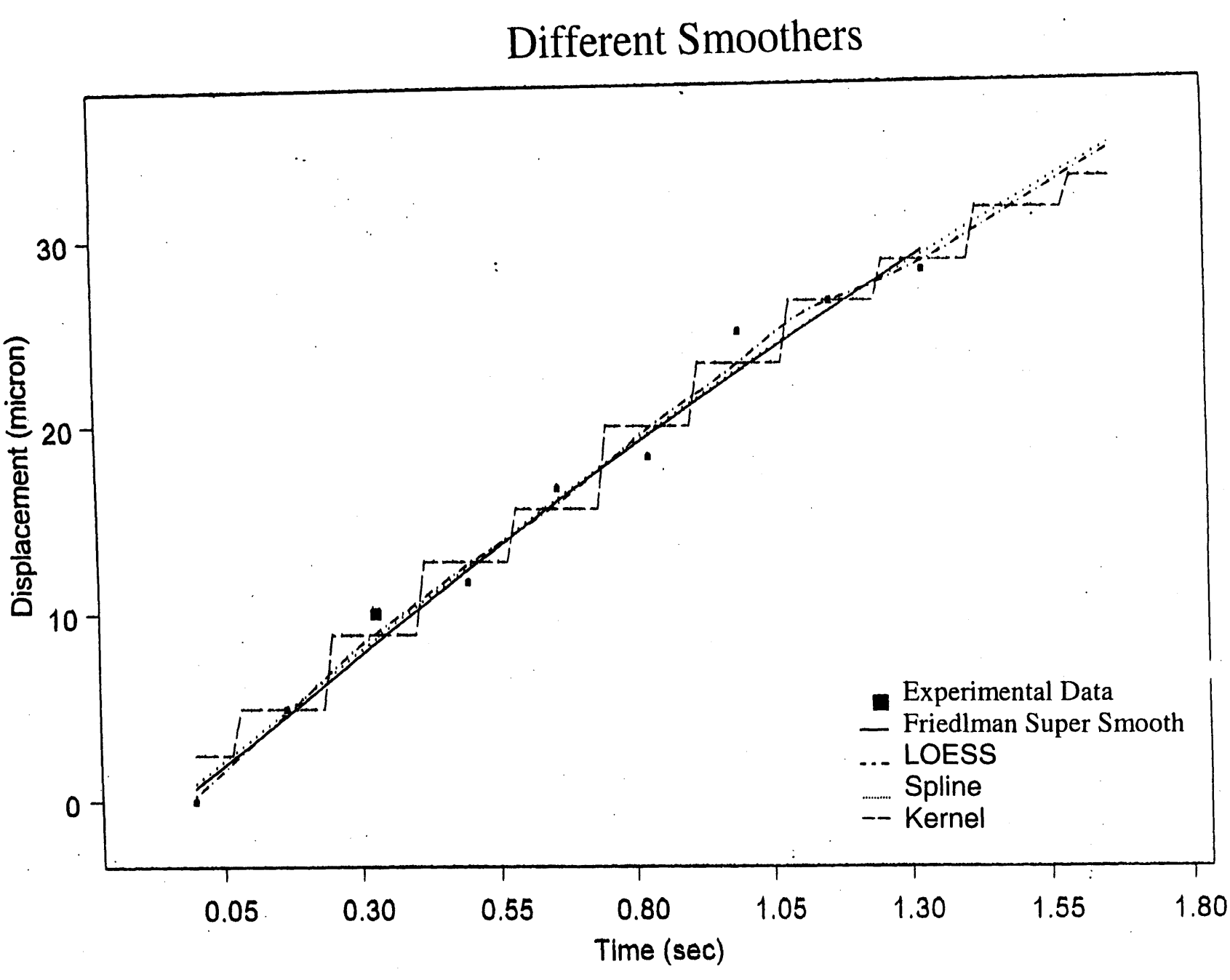

Figure 5.11 Different Smoothers, Sample 2

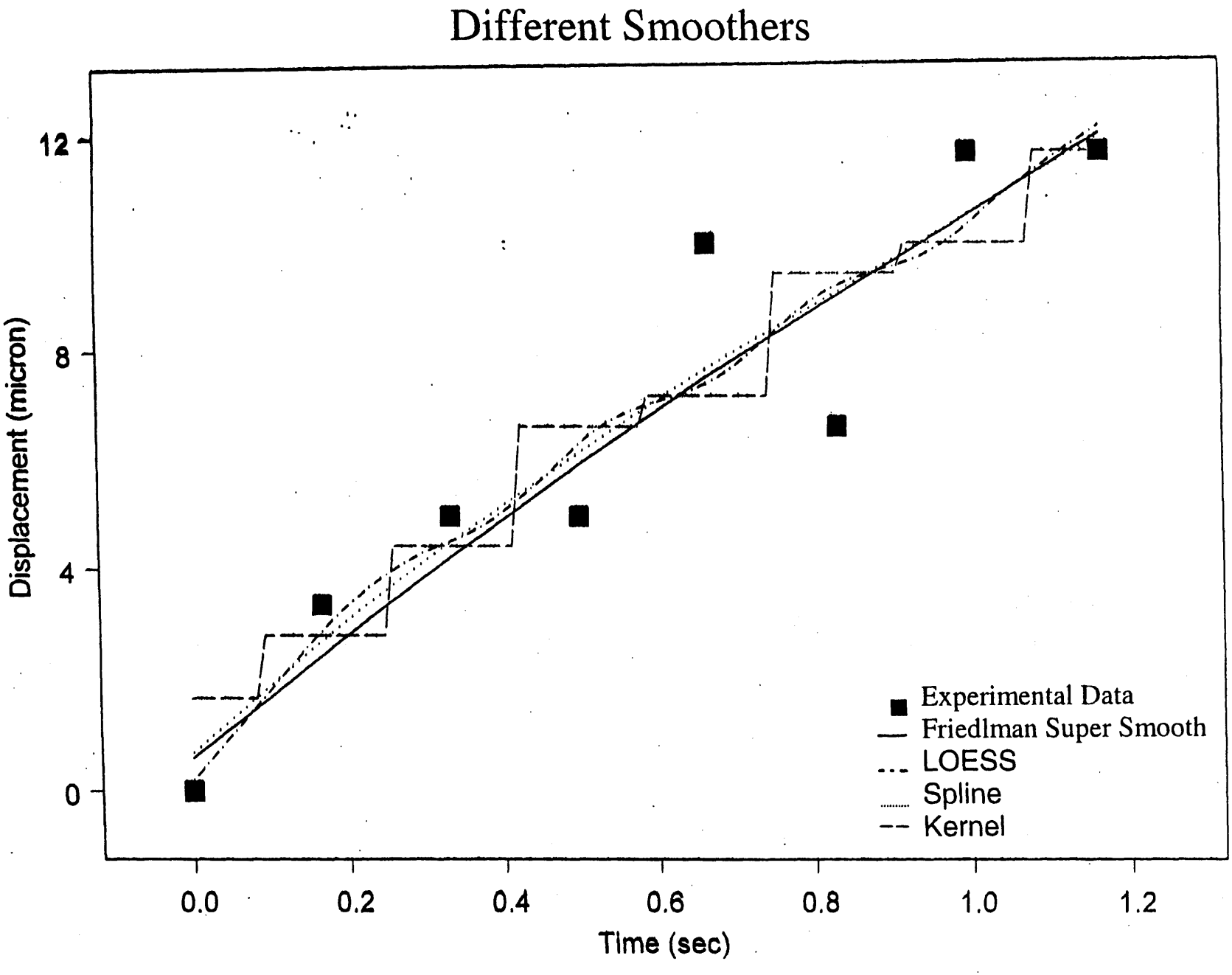

Figure 5.12 Different Smoothers, Sample 3

By observing the predicted values from different smoothers, the super smoother was chosen for this research because the deviation of the experimental error is minimum. Figure 5.13 through 5.15 shows the graph of the experimental data for different energy levels after using the super smoother.

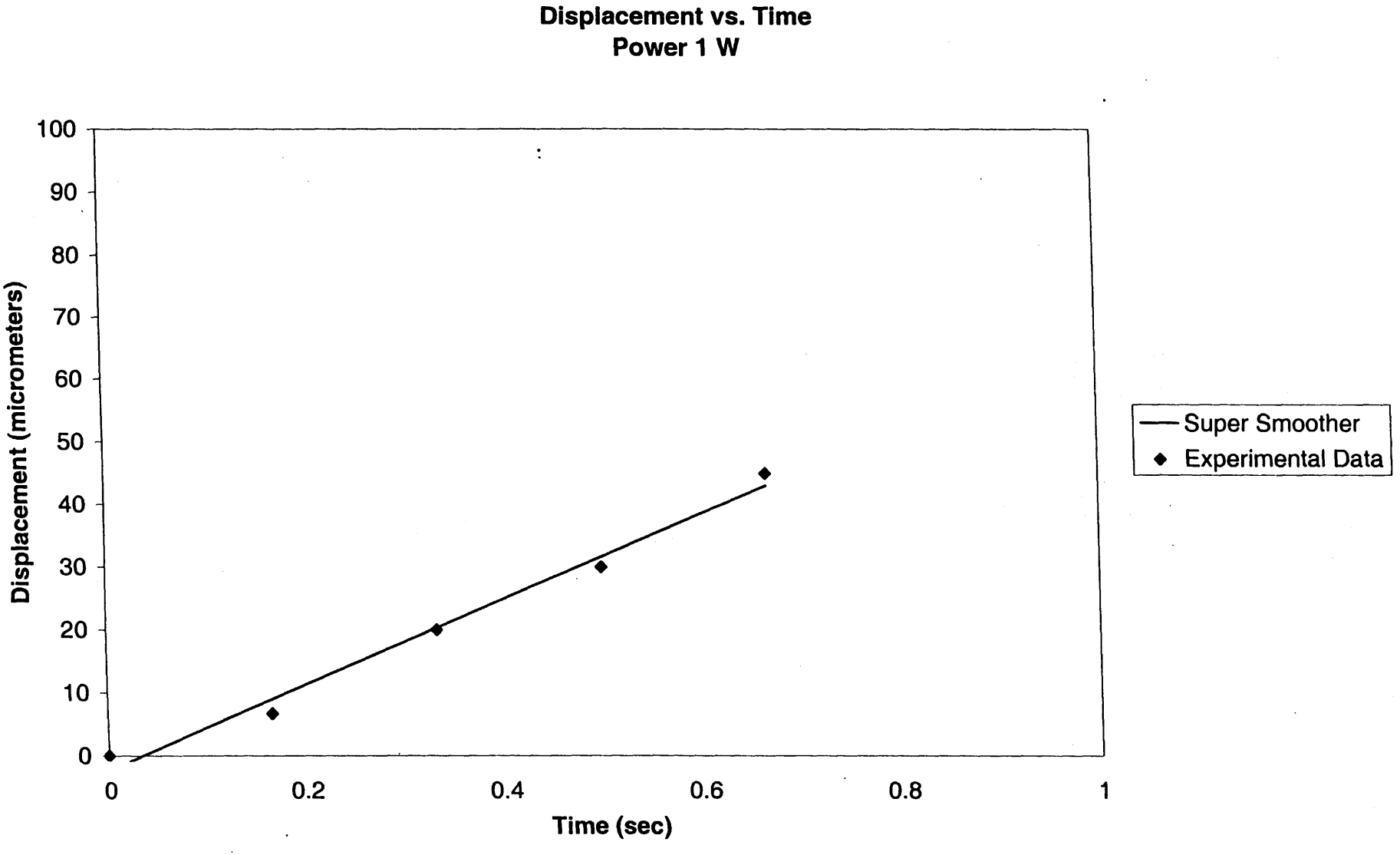

Figure 5.13 Experimental Data at 1W after using Super Smoother

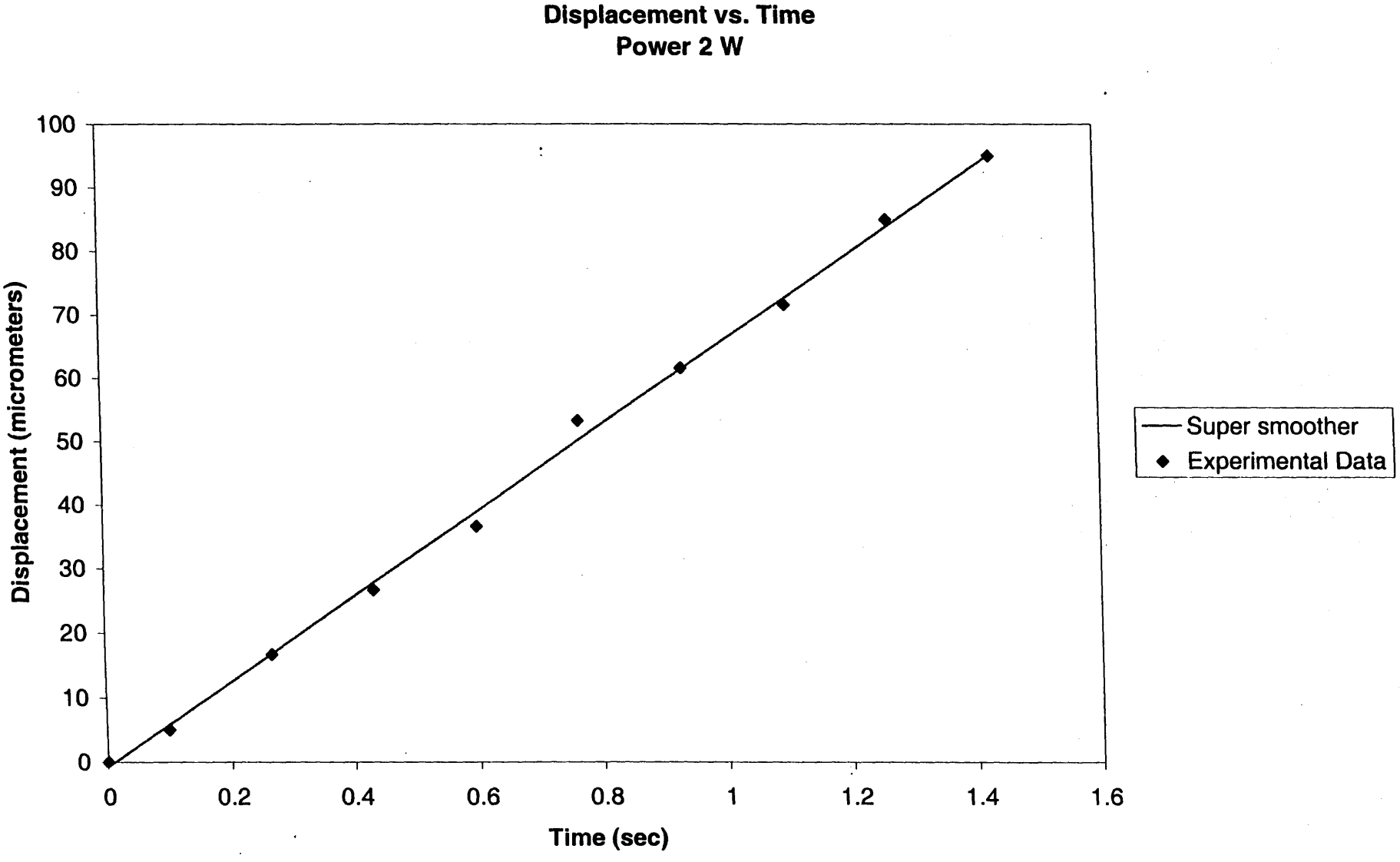

Figure 5.14 Experimental Data at 2 W after using Super Smoother

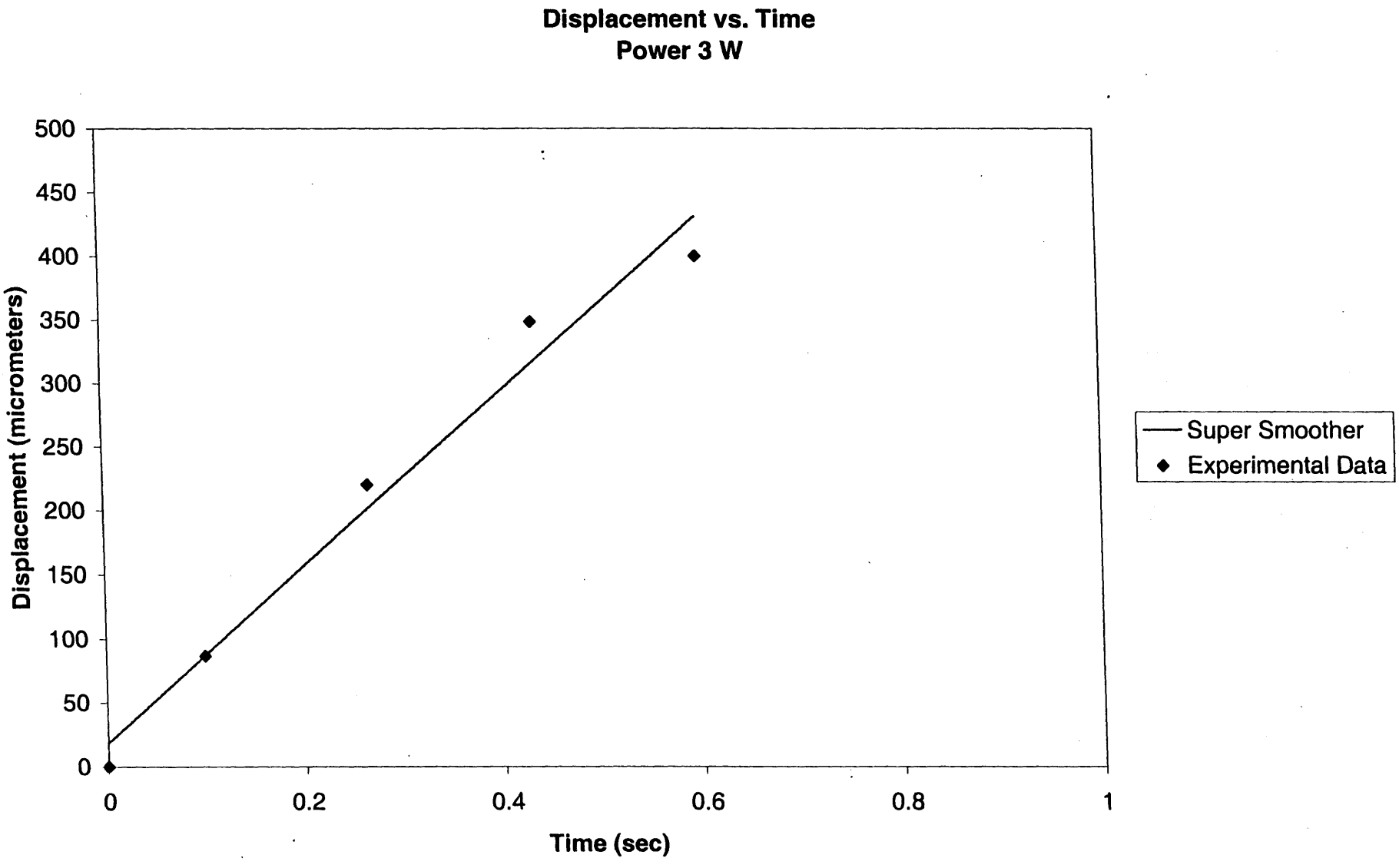

Figure 5.15 Experimental Data at 3 W after using Super Smoother

5.5.2 Data Optimization

In order to predict the motion of particles using mathematical model, four input parameters that should be known. They are the radius of the particle, initial position of the particle from the pressure node, particle compressibility of SiC, and acoustic energy in the fluid.

The compressibility of SiO_2 was known to be 2.75E-11 m^2/N. The compressibility of SiC was assumed to be in the range of 2.75E-11 ±1E-11. Therefore, the corresponding contrast factor (G) for SiC was calculated to be 1.83 for 2.75E-11 +1E-11 and 1.85 for 2.75E-11 –1E-11. Since the variation of G was not significant, the G value for SiC was selected as 1.85.

Three other variables that were not known for comparing the predicted data with the experimental data were radius of the particle (r), initial starting position of the particle (x_0) and acoustic energy in the field (E). The acoustic energy in the medium can be estimated by using known values of input power form the power amplifier and assuming a quality factor (Q) of 5000 using Equation (2.13). The mathematical equation of the particle trajectory (Equation 3.40) was rewritten in terms of unknown variables of r, x_0, and E. In order to compare the mathematical model predictions with the experimental results, data optimization was performed for the data collected from the experiment to obtain the best r, x_0 and E values. Matlab 5.3 was used for the optimization using minimization function in the package.

Different combinations of these unknown variables were used as initial guesses for the displacement function and corresponding optimized values were generated by the fminsearch function in the Matlab Optimization software. Appendix B provides the

computer code that was incorporated to fminsearch function for optimization. Any optimization value with radius greater than 6 micrometer and initial position less than zero or grater than half wavelength were discarded since the maximum probable size of the SiC particle is less than 12 microns. Some possible combinations for these three variables obtained from the optimization program are given in Table 5.4.

Table 5.4 Possible Combinations of the Three Variables

Radius of the Particle (r) micrometers	Initial starting position of particle (x_0) micrometers	Acoustic Energy (E_{ac}) 10E-17 J/micron^3
5.0	2.0	20
3.0	6.0	20.7
6.0	6.5	32
4.5	1.8	20
4.7	12	17.5

The above procedure for optimization was repeated for each experimental data set at different input power values from 0.5 to 5.0 W. Since the energy in the system is directly related to the input power through the quality factor, one could expect trend such as linear or exponential variation. Hence, the proper energy values from optimized data sets were selected in an increasing trend as the input power data. Then the selected energy values from the optimized data, listed in Table 5.5, were plotted against input energy to establish the trend as shown in Figure 5.16.

The relationship between the input power and acoustic energy in the medium appeared to be exponential. But according to literature (Equation (2.13)), it is linear. With increase of power the Q values are not constant but may be increasing, resulting in nonlinear rise of energy with increase of power. It was found that the relationship between power and energy can be expressed as $E=12.68e^{0.3011P}$.

Table 5.5 Acoustic Energy Corresponding Power input after Smoothing

Power (W)	Acoustic Energy after Optimization (10E-17J/micron^3)	Acoustic Energy from Best Fitting Curve (10E-17J/micron^3)
0.5	17	14.68
1.0	18	17.06
1.5	21	19.84
2.0	20	23.06
2.5	25	26.81
3.0	26	31.16
3.5	32.55	36.22
4.0	45	42.11
4.5	47.5	48.95
5.0	70	56.9

Table 5.5 shows the relationship obtained between the power and the energy for this research from Figure 5.16.

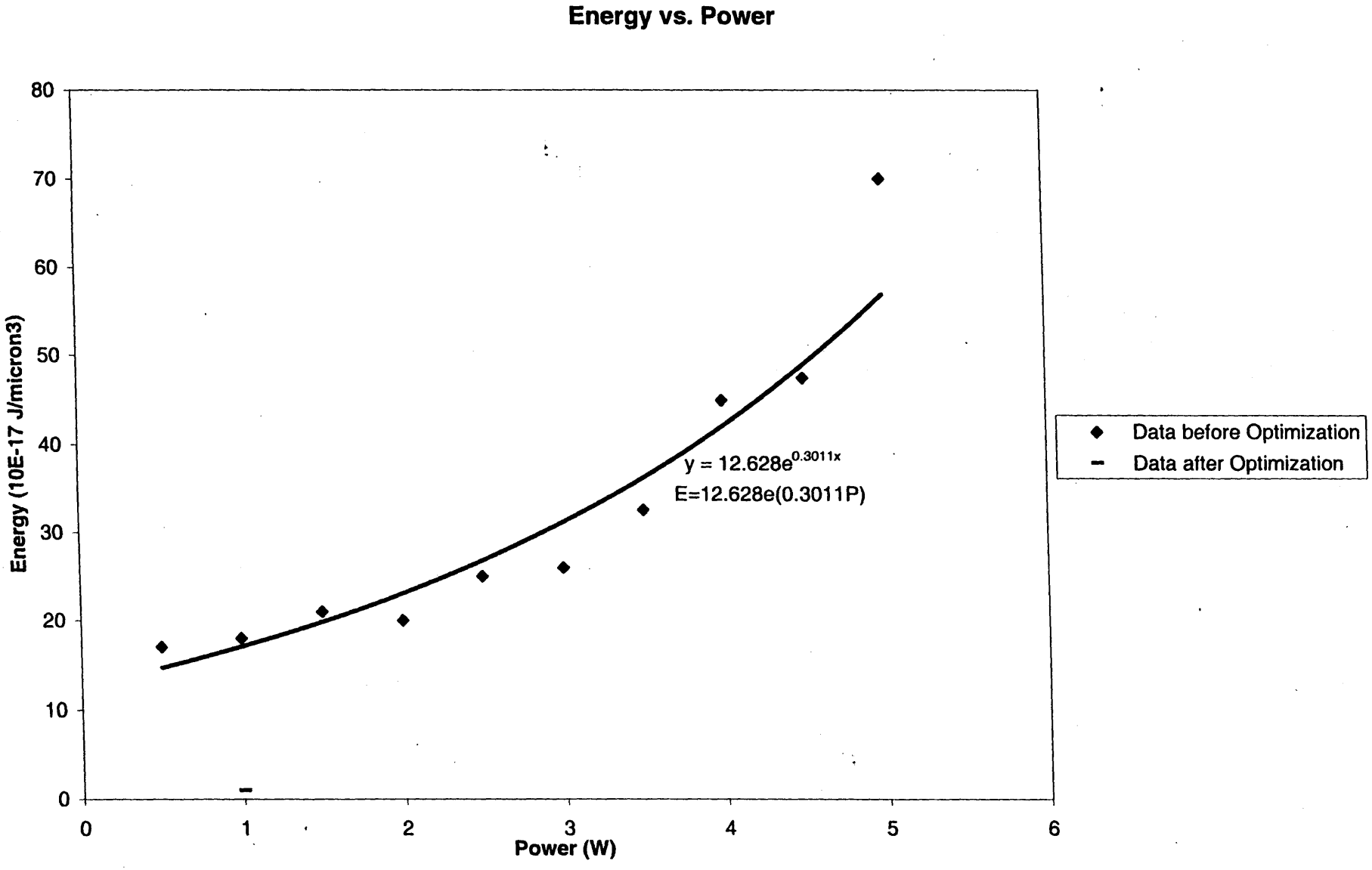

Figure 5.16 Relation between Input Power and Acoustic Energy

5.5.3 Particle Trajectories from Experimental and Optimization Technique

By knowing the acoustic energy, and the corresponding radius of the particle and the initial particle position, Equation (3.40) was used to calculate the displacement of particles at different time intervals. Figures 5.17 through 5.26 shows the measured and predicted particle trajectories.

Analysis of Figures 5.22 through 5.26 shows that above 3.0 W power, the particle trajectories from the experimental results are comparable to the mathematical model predictions using Equation (3.40). However, at power values below 3.0 W, there was a considerable deviation. Therefore, it can be concluded the mathematical model is applicable for higher energy levels but for lower energy levels further investigation is required. The experiment was conducted for up to 5W power because above that it was not possible to capture the movement of individual particles due to extremely high particle speeds.

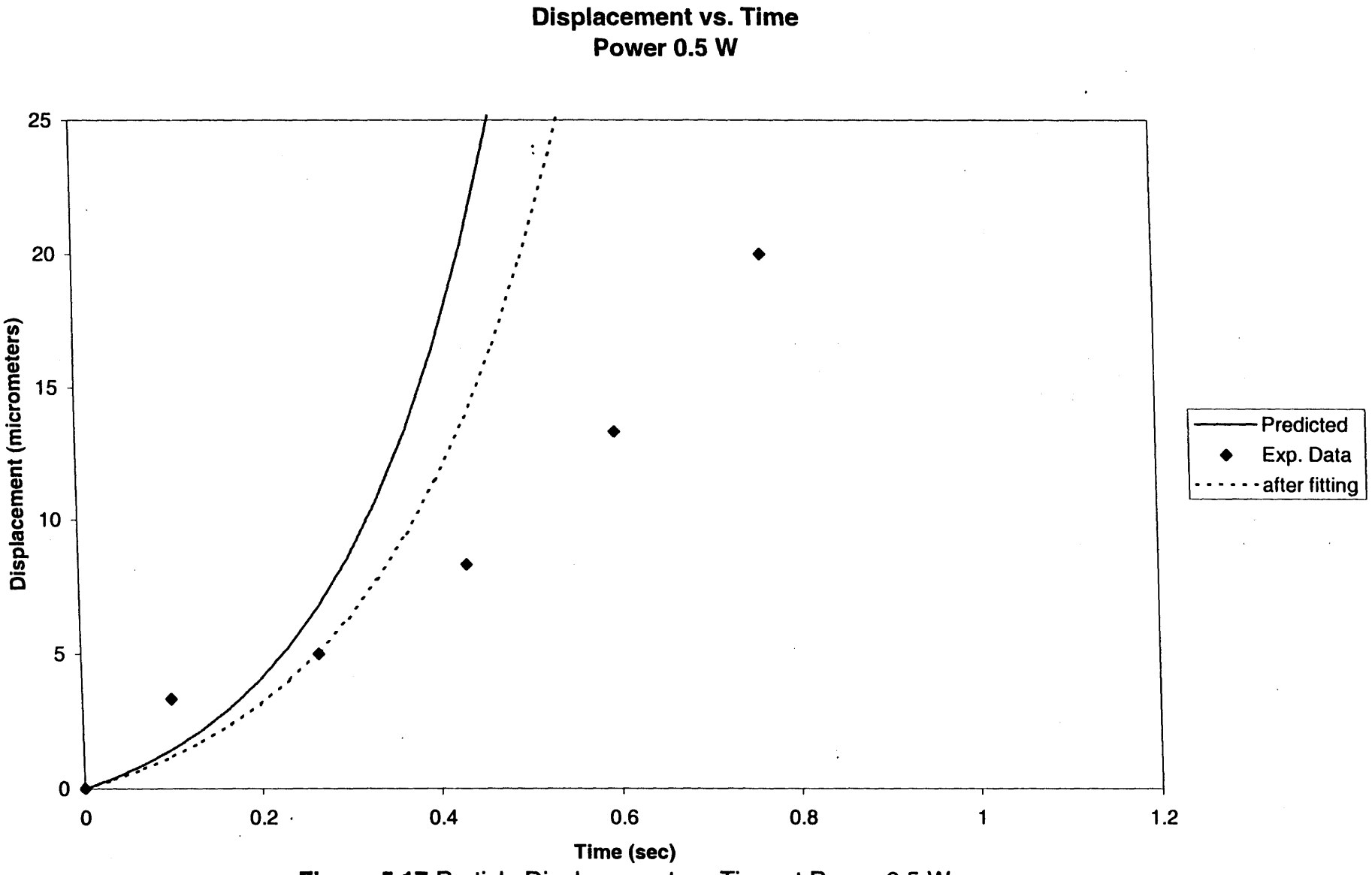

Figure 5.17 Particle Displacement vs. Time at Power 0.5 W

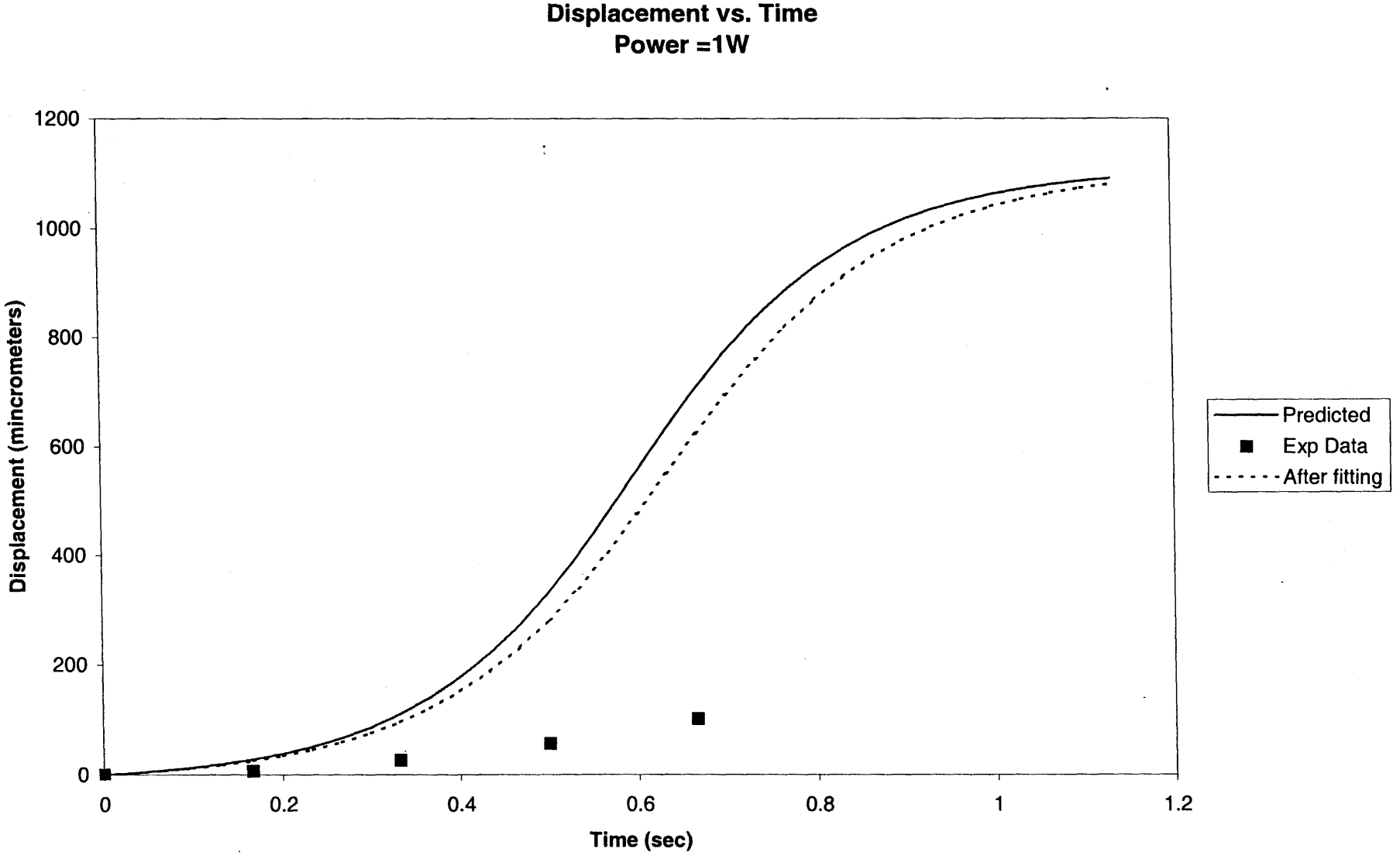

Figure 5.18 Particle Displacement vs.Time at Power 1 W

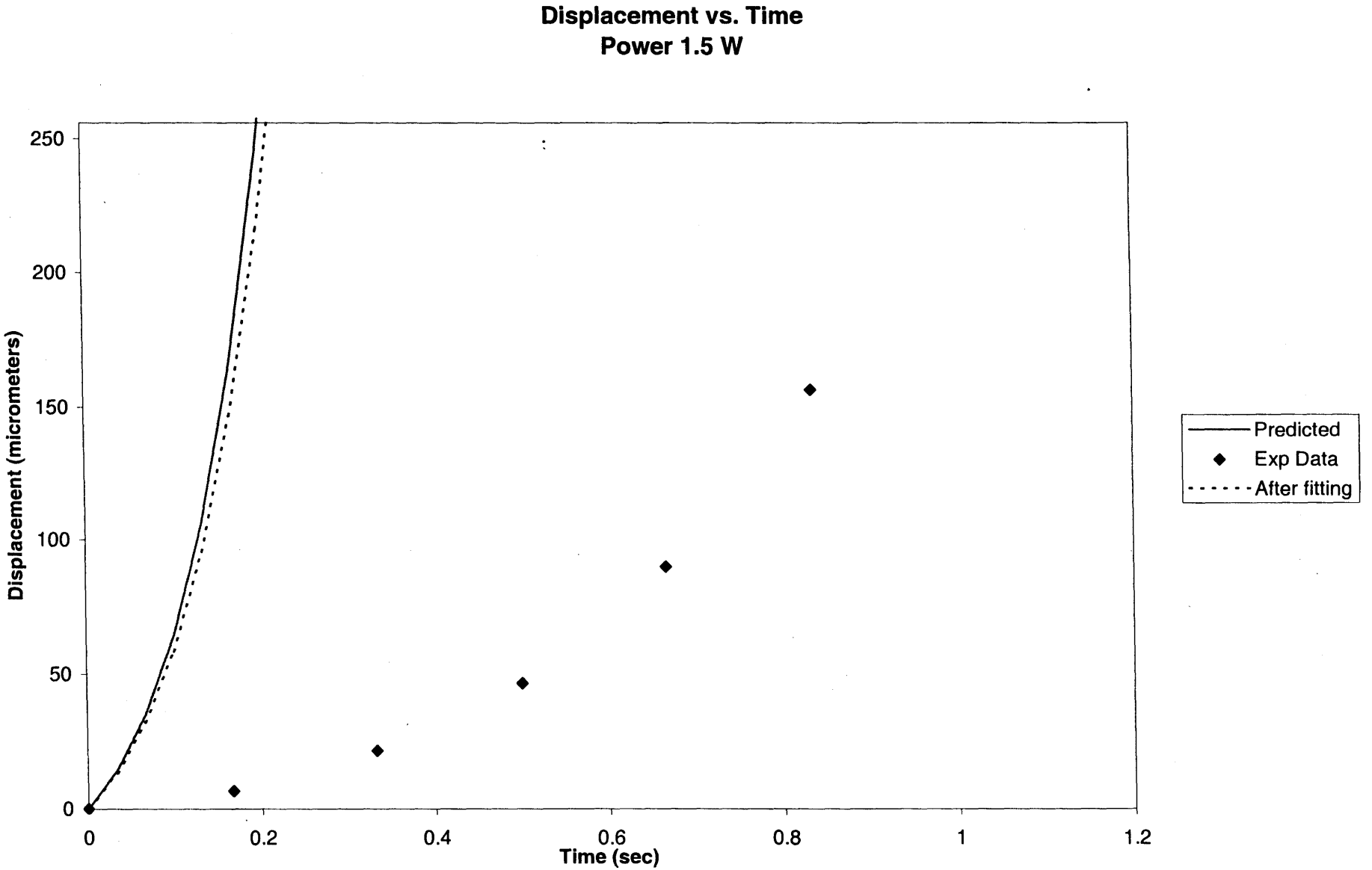

Figure 5.19 Particle Displacement vs. Time at Power 1.5 W

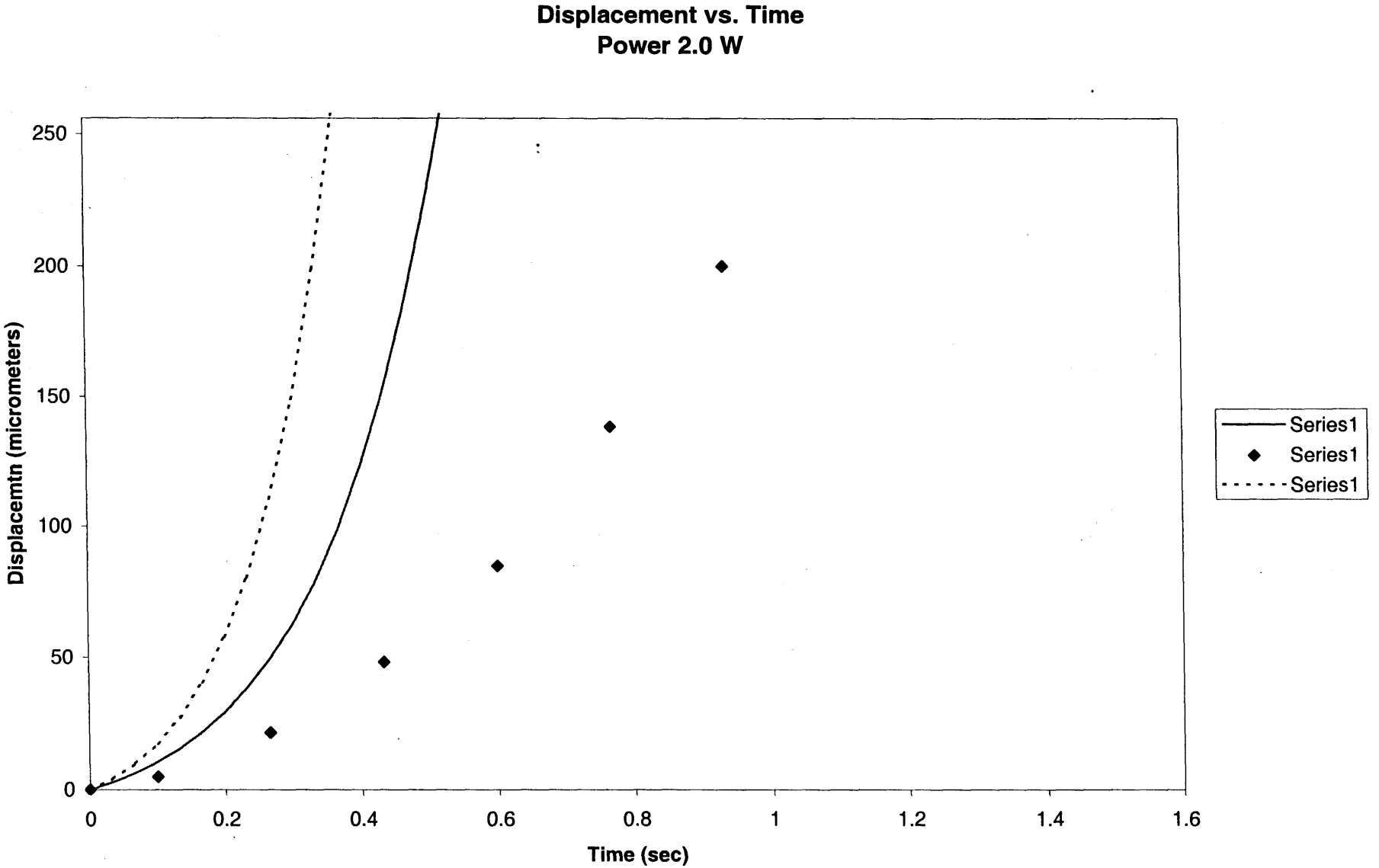

Figure 5.20 Particle Displacement vs. Time at Powe 2.0 W

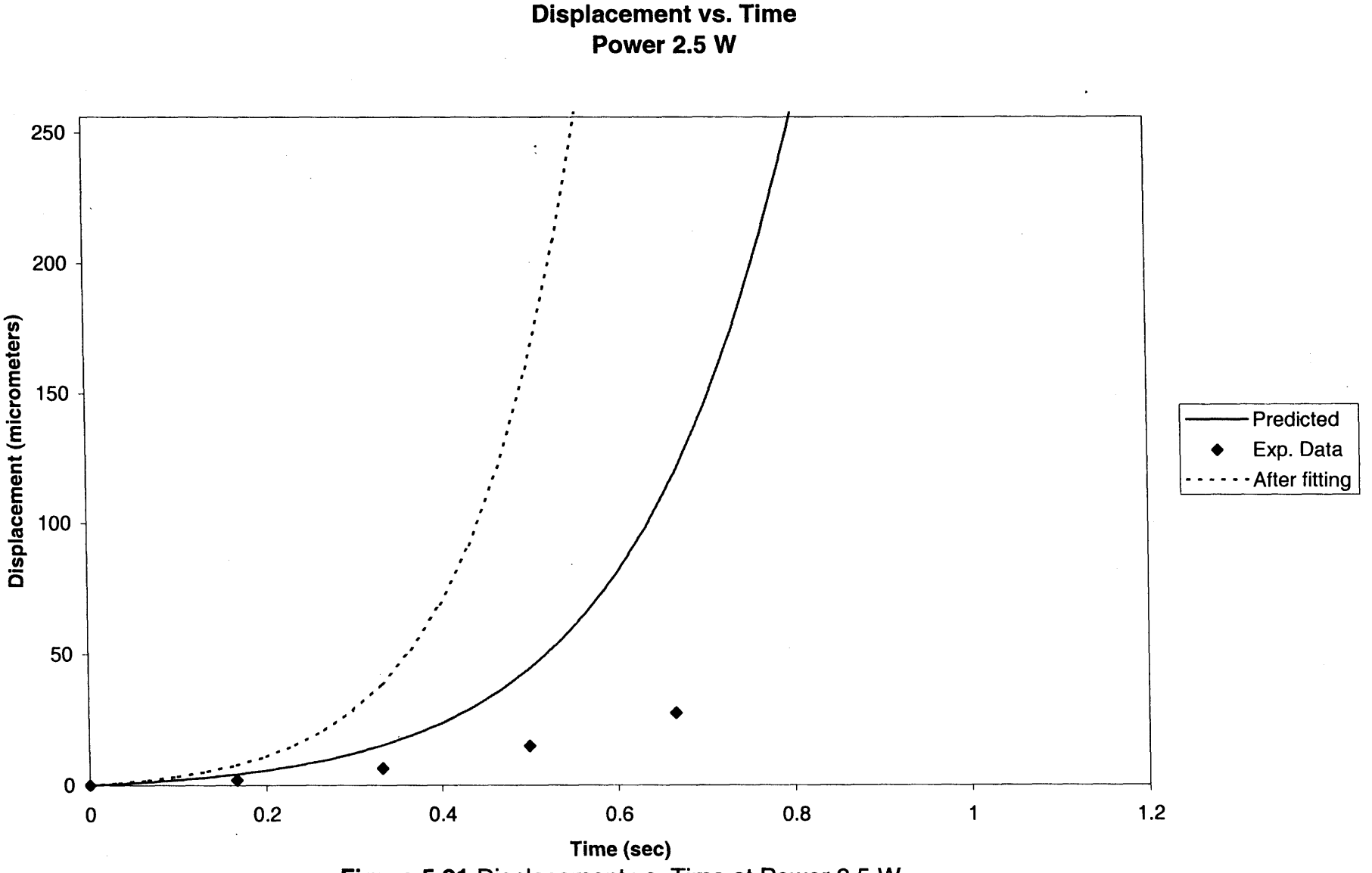

Figure 5.21 Displacement vs. Time at Power 2.5 W

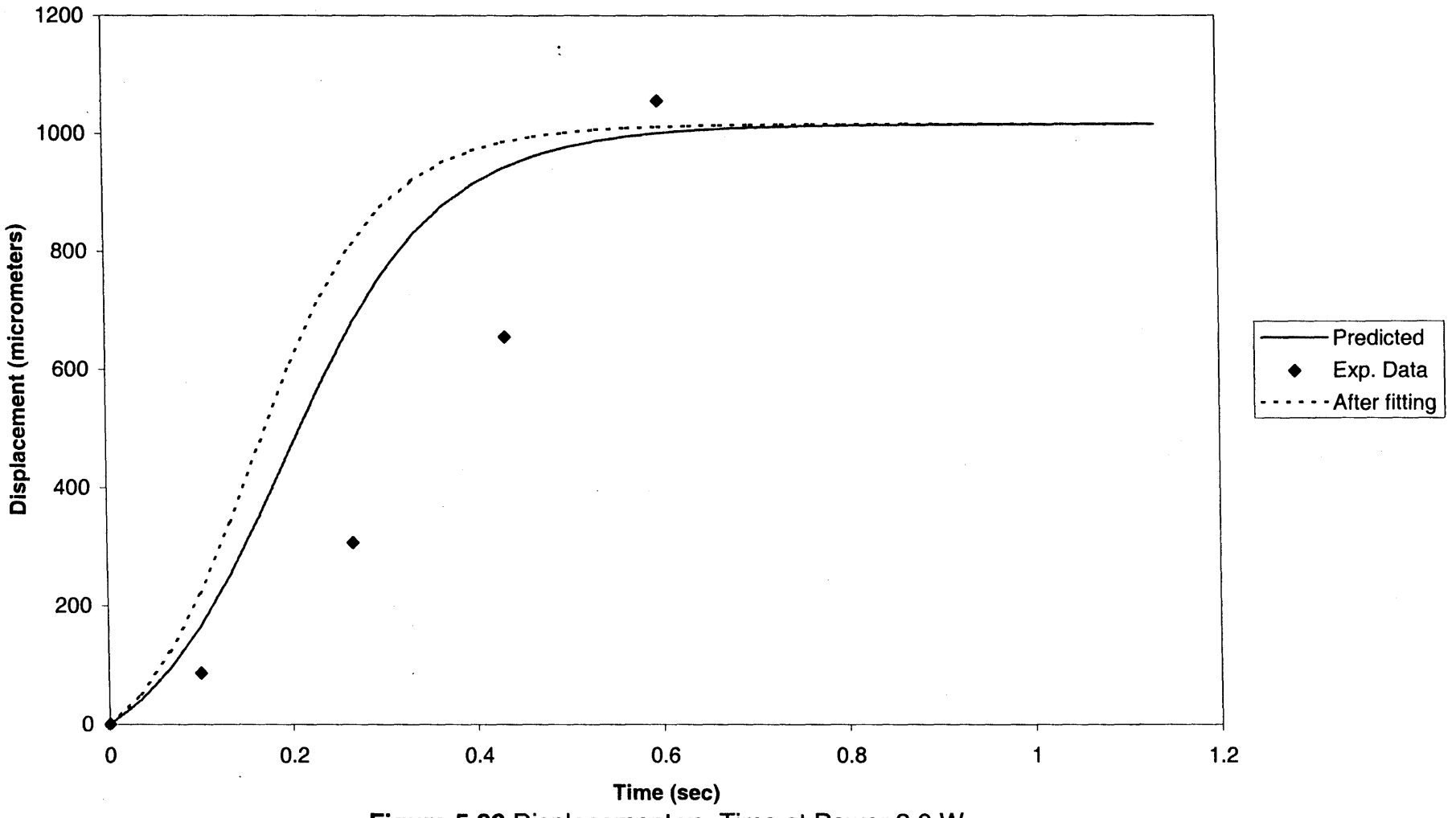

Figure 5.22 Displacement vs. Time at Power 3.0 W

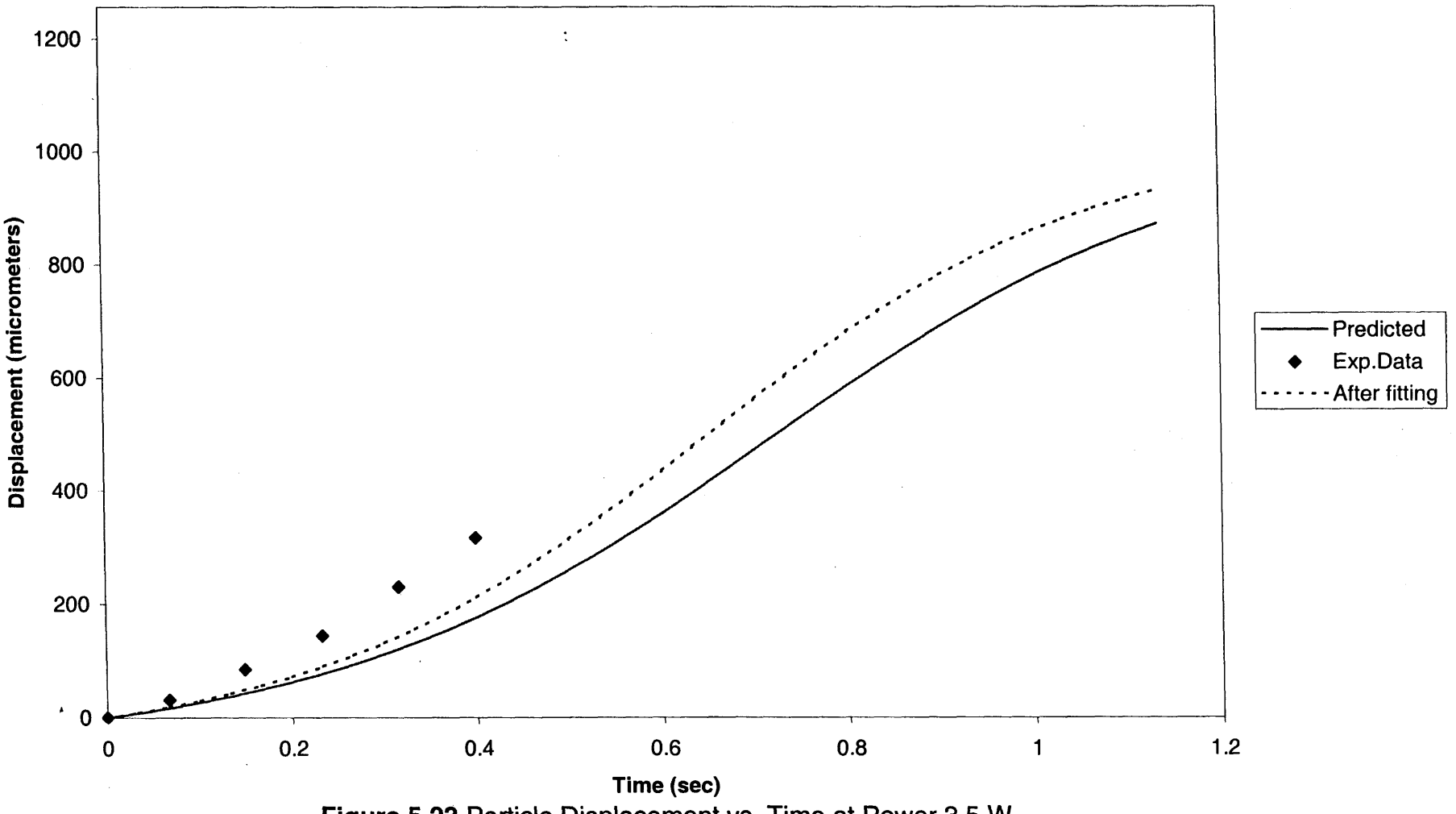

Figure 5.23 Particle Displacement vs. Time at Power 3.5 W

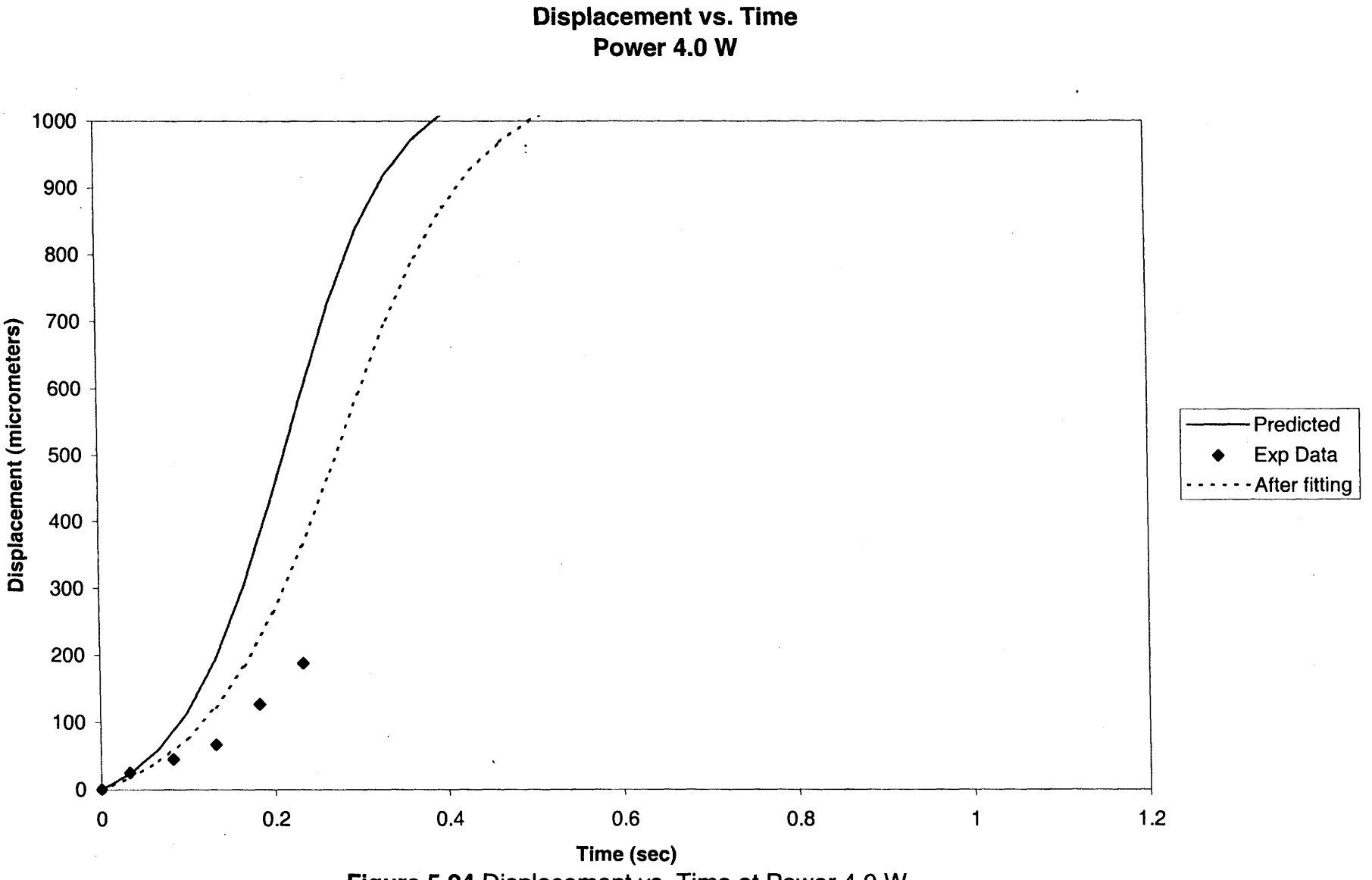

Figure 5.24 Displacement vs. Time at Power 4.0 W

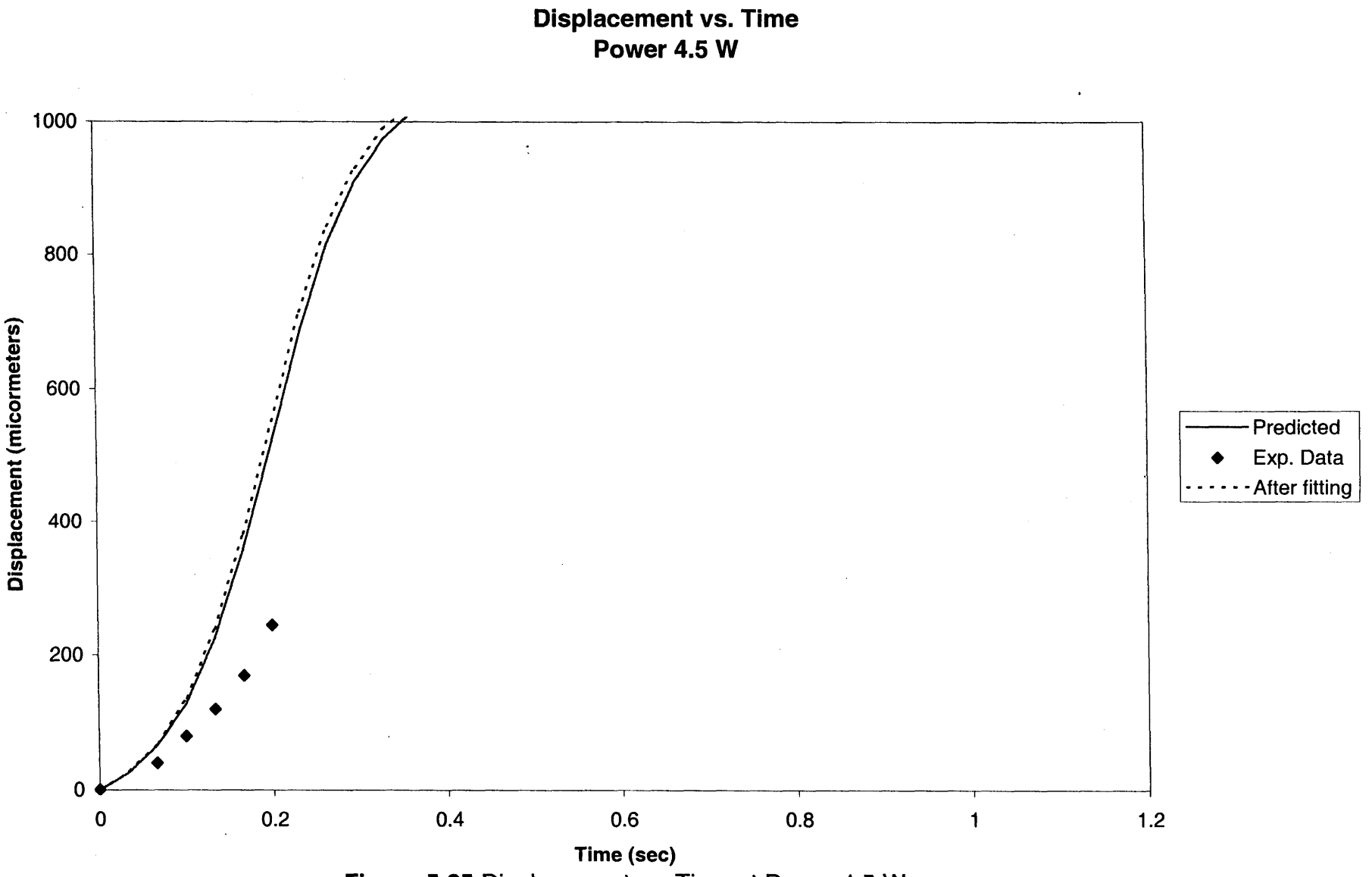

Figure 5.25 Displacement vs. Time at Power 4.5 W

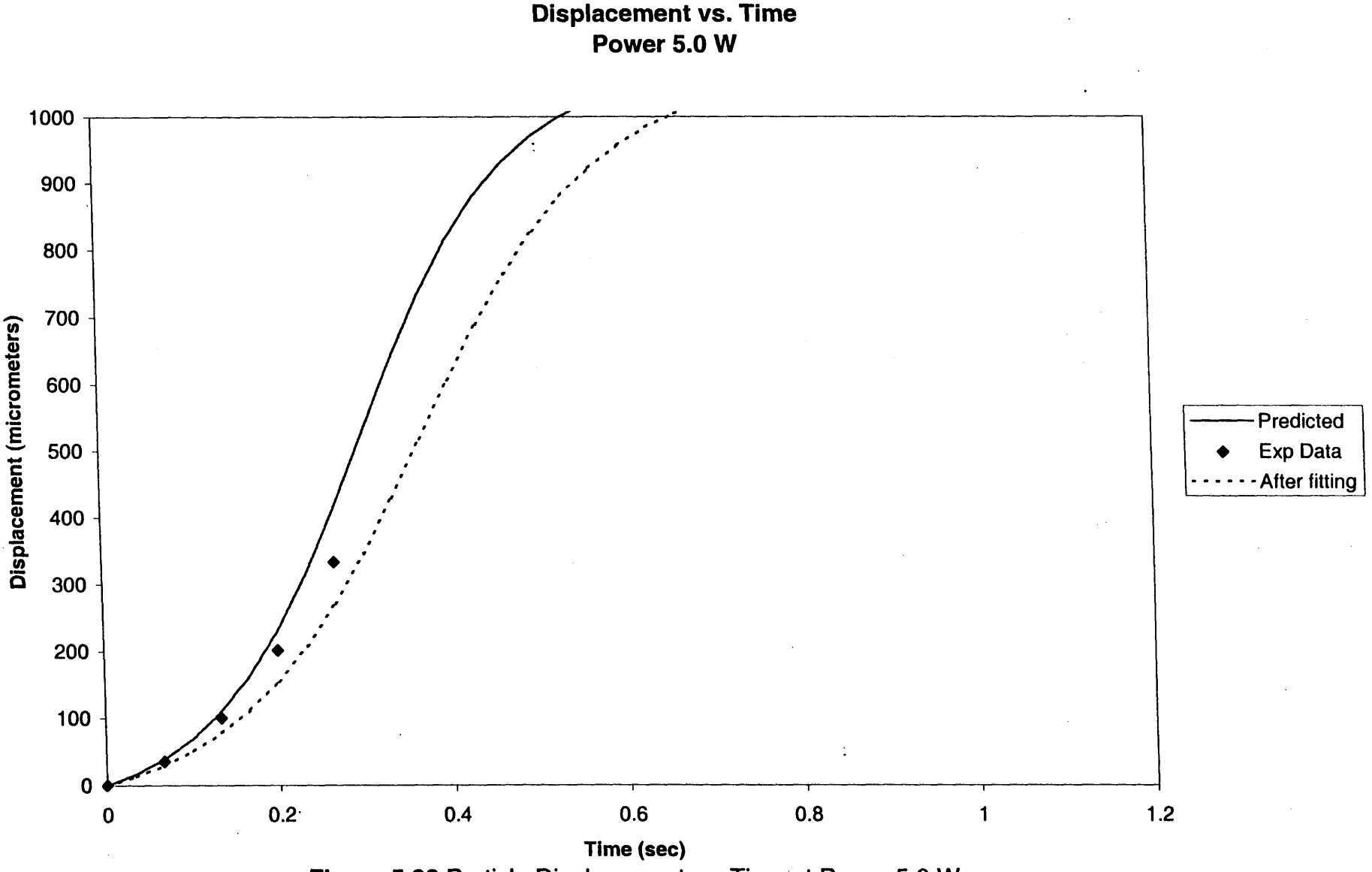

Figure 5.26 Particle Displacement vs. Time at Power 5.0 W

5.6 Conclusions

In this research both SiO_2 and SiC were used to investigate the particle aggregation due to acoustic energy. It was possible to fractionate the suspended particles in an acoustic energy using SiO_2 particles. However, because of the small size of these particles it was not possible to record the particle trajectories. Hence, a larger particle size SiC was used. The experimental data were smoothen and compared with mathematical model predicted. The experimental data compared well with the theoretical prediction for higher power inputs.

Hence, it can be concluded, it was able to fractionate particles and the particle movement can be predicted from mathematical model derived in the research. The mathematical model is needed for process optimization. Some possible future study and recommendations are discussed in Chapter 6.

CHAPTER 6

CONCLUSIONS

This chapter contains a summary of the research conducted, including a brief explanation of the proposed technology and some closing remarks concerning the experimental results. Some cost estimates for basic equipment and operational limitation is also provided in this section. A discussion of some possible directions for future research is also included. Finally, a discussion of the implementation of the acoustic treatment process for contaminated dredged harbor sediment is included.

6.1 Summary

In this research, the application of an acoustic standing field for segregation and fractionation of suspended particles was investigated. Many separation methods are available for particle separation such as filtration, sedimentation, and magnetic/electrical methods. When particles of size smaller than several millimeters are to be separated, then non of the above methods can not be used efficiently. In such cases, the proposed technology for segregation and fractionation of fine particles using an acoustic standing field wave is an effective alternative. The feasibility of using the proposed technology for silica fume (SiO_2) and silicon oxide (SiC) in deionized water was studied.

It was shown that the particles, when subjected to an adequate acoustic energy field, migrate towards pressure nodes at half wavelength intervals for a positive contrast factor. This technology is based on the response of the particle to the acoustic contrast, which is a function of the particle and the fluid densities and compressibilities.

The particle response is very sensitive to the acoustic properties such as G and r, frequency and acoustic energy.

Silica fume (SiO_2) with a concentration of 0.01-0.02% by weight in DI water was used to study the migration of particles towards the pressure nodes to form particle columns. A plexiglas acoustic resonator chamber was built with two transducers fixed to opposite ends. One transducer was used as a load to transfer energy into the fluid, and the other transducer was used as a reflector or receiver to reflect the waves to produce standing waves. The load transducer was excited using a sinusoidal signal amplified using a power amplifier. The experimental setup for this research was described in Chapter 4.

While the acoustic energy was supplied, particles moved toward the pressure node forming four particle columns at half wavelength distances. These columns were visible to the naked eye. The optimum frequency and power for this particle formation was 333 kHz and 40 watts, respectively. These columns were sustained for a few minutes after which air bubbles formed and disturbed the standing field.

Mathematical models for the particle trajectories and concentration were obtained using the acoustic force acting on the particle proposed by King (1934), drag force by Stokes' law, and equation of equilibrium of a particle in a medium. It was not possible to find a closed form solution for the equations so approximate solutions were derived in Chapter 3.

SiC particles were used to capture the individual particle displacements since SiO_2 particles were so small it was not possible to capture the particle trajectories even using 100 $\times$ magnification. The setting for capturing particle displacement in an acoustic

field was described in Chapter 4. After using statistical analysis and a data optimization, acoustic energy in the fluid as a function of power input was obtained (Figure 5.16). This relationship was nonlinear which was different from that linear relationship sited in the literature (Equation 2.13). For input power levels between 3 W up to 5 W experimental data matched the predicted trajectories.

Acoustic standing fields can be advantageous for separation of particles in liquid suspensions. When compared to the available methods such as filtration and sedimentation, the proposed method has a much higher resolution. The cost of operation and maintenance is less because this method does not have any moving parts. This technology can be used as long as the contrast factor for the particle and suspending medium is not zero and the particle size is much smaller than the sound wavelength. Also, there is no need for the particle to have any special properties such as an electrical or magnetic surface charges, nor is there a need for any chemical agents.

The cost of basic equipment used in this research includes the power amplifier about $4000.00, and each transducer $300.00 for a dimension of 76.2mm x 38.1mm. The cost of the transducer per square centimeter is then 300/7.62x3.81 =$10.33/cm^2. For particle size of one micrometer to be fractionated at an assumed flow rate of 100 ml/min or 0.006m^3/hr, then per unit width the flow rate is 0.006/0.06 =0.1 m ^{3} /hr/unit width (two wavelength distance). For scale up operation with ten-wavelength distance between transducer and the reflector and a one meter wide chamber, the flow rate will be 0.5 m^3/hr. For five micrometer particle size, the flow rate would be (0.5 ×5× 5) 12.5 m^3/hr.

For scale up, a transducer of same the height (7.62cm) and one meter, wide the cost will be $10.33/cm^2 x762cm2 =$7871. The cost of operating the fractionation

technology for one micrometer size silica fume, for 0.1 $/kWh power cost, 0.02% w/w concentrated solution at a density of 1000 Kg/m^3, and power 40 W ($40/7.62x3.81=1.377W/cm^2$) will be:

($0.1\$/kWhr$ x $0.001377\ W/cm^2$ x $762cm^2$)÷(0.0002 w/w x 0.1 m^3/hr x$1000Kg/m^3$)=$5/Kg of one micro silica fume; and for 5 micron, 5/25=$0.2/ Kg of 5 micro silica fume.

6.2 Future Research

To fully understand the behavior of the silica fume particles in an acoustic field, further study is required. This research lacks the quantitative analysis of the separation efficiency, the concentration of the particle, effect of temperature change, and the flow rate. The experimental data suggested that the technology is quite encouraging and hence, should be further investigated. This research is at a point where it needs further support both technically and financially for a comprehensive investigation of acoustic segregation and fractionation. For the real world application of the technology, some of the recommendations for further research are:

1. Have transducers with attached connections at the back from the manufacturer. This is to avoid destroying the crystal behavior at the time of soldering of cables.
2. Use thinner transducers less than 6.25 mm and thinner plexiglas frames to obtain a better magnification.
3. Use transducers with wider range of resonance frequency for better performance.
4. Have a moving reflector rather than a stationary to control the standing waves in the field.
5. Have a closed system to avoid air entrance that causes cavitation inside the medium.

6. Computer to control the steady flow into the chamber.
7. Some automatic control to extract samples from the chamber at the exact position of pressure nodes for analysis.
8. A hydrophone pressure probe to measure pressure at different locations along the sound wavelength. This will provide information on the position of the pressure nodes and the distance between them.
9. Monitor temperature inside the chamber to control the standing wave frequency.
10. Cool the system to control the heat dissipation inside the chamber, for example having a temperature bath..
11. Automatic computerized system to adjust the frequency of the sound field with changing temperature.
12. Powerful and stable microscope with high field of view (greater than 0.5 mm) capable of horizontal and vertical adjustment for focussing and better resolution.
13. Repeat the experiments and analysis for power less than 3 W to confirm the particle trajectories in an acoustic field.
14. Location of the collection plane at exact position of pressure nodes for collecting samples.
15. High-resolution camera for taking pictures and movies from the microscope.
16. Scale up of the laboratory model for actual implementation of the technology.
17. Application of the technology for the actual dredged sediments and the study of the behavior of organic compounds and metals in the acoustic field.
18. Have a person with an electrical engineering background in the team to better understand the circuits and different electrical units.

19. Evaluate the technology with more than one transducer for continuous treatment.

In conclusion, the proposed technology is an innovative way to separate fine particles. Complete understanding of the phenomena will provide greater efficiency for technology implementation.

6.3 Implementation of the Proposed Technology for Dredged Sediments

From the morphology of the dredged sediment obtained by using ESEM and X-ray diffraction, the main constituents of the sediment are silica and oxygen. The sediments contain large quantities of organic material and heavy metals. In this research a representative sample of silica fume in DI water was investigated. Cleaning of dredged sediments can be accomplished by first removing the organic material by applying ultrasound to the sediments and then by diluting the sediments to very a light concentration to allow non-viscous flow.

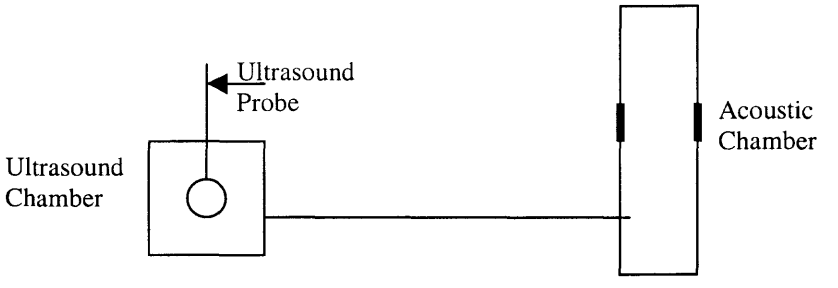

Figure 6.1 Implementation of the Technology

Figure 6.1 shows schematic diagram drawing how the proposed technology of acoustic separation can be implemented. The contaminated dredged sediment is first subjected to an ultrasound field at high energy to remove all the organic material and metals from fine soil particles. The diluted sediment will be fed into an acoustic chamber at the bottom for segregation. This method will provide continuous treatment of dredged sediments.

APPENDIX A

In appendix, element composition and Environmental Scanning Electron Microscope (ESEM) micrographs of the contaminated dredged sediments from New York harbor are presented. The morphology of sediments was analyzed using Energy Dispersive X-Ray (EDX) attached to the ESEM. The sample was thoroughly mixed for uniform consistency. Dry sample was prepared by oven drying the sediments at 500 °C for 24 hours to remove all organic compounds. The dry sediments were sieved using sieve No. 40, 70, 140 and 200 after drying.

By analyzing different samples, some of the elements that were detected are; Si, O, Al, Fe, Na, Mg, k, Ti, S, K, P, and Ca. These form part of the composition of the contaminated dredged sediment because EDX can detect only elements lighter than oxygen. The elements with energy less than oxygen are not included and hence it can not be concluded that these are the only element present in the sediments.

The main elements found in most of the analyzed area are oxygen and silica. The oxygen content however differs at different EDX analysis locations. The oxygen element estimated by EDX is not exactly for the sample because the chamber which holds the sample contains water vapor. Therefore, the amount of oxygen in the area analyzed is just the comparative or qualitative amount. The composition of the sample also differs with the location of the focus point and the magnification used. The overall study of dredged sediment confirms the high concentration of silt and clay as observed by Brookhavan National Laboratory, about 45% and 27% respectively. The ESEM micrographs also revealed the presence of irregular shaped dredged sediments. The sediments dredged from the NY/NJ harbors are a complex mixture of soil and contaminant and the cleaning

process proposed here can segregate and fractionate and eventually recycled the clean soil back into the ocean.

Figure A1 was taken at a magnification of 180X for the dry dredge before sieve analysis. It gives some idea of the main element composition of the analyzed area. From Table A1, the main composition is oxygen 39%, and silica 57%. This indicates when the organic contaminants are removed, only silica and oxygen is present in the form of silicon dioxide, SiO_2.

Table A1 Composition of Dredged Sediments for Figure A1

Element	Weight %
O	39.51
Al	3.36
Si	57.13

Figure A2 to A8 show the pictures at different locations for same sample and Table A2 to A8 are the corresponding element analysis. In all these pictures, small cluster of spherical, octagonal shaped structure, or disk shape objects are visible. These irregular shaped clusters are either filled with silica or hollow from the inside. But the common thing is the structural nonhomogenity. If by some treatment this composition can be broken, for example by the application of ultrasound, then it is easy to remove these impurities from the sediments by applying the proposed separation technique.

Table A2 Composition of Dredged Sediments for Figure A2

Element	Weight %
O	37.43
Na	3.56
Mg	4.07
Al	24.36
S	0.80
K	7.3
Fe	22.49

Table A3 Composition of Dredged Sediments for Figure A3

Element	Weight %
O	10.27
Na	1.11
Mg	1.99
Al	15.48
Si	39.41
K	396.39
Ti	2.79
Fe	22.55

Table A4 Composition of Dredged Sediments for Figure A4

Element	Weight %
O	18.63
Na	1.82
Mg	2.09
Al	10.92
Si	46.07
K	3.99
Fe	16.47

Table A5 Composition of Dredged Sediments for Figure A5

Element	Weight %
O	14.89
Na	.97
Al	6.90
Si	60.13
K	4.47
Fe	12.36

Table A6 Composition of Dredged Sediments for Figure A6

Element	Weight %
O	37.43
Na	3.56
Mg	4.07
Al	24.36
Si	22.49
K	7.30
Fe	0.8

Table A7 Composition of Dredged Sediments for Figure A7

Element	Weight %
O	6.63
Na	1.53
Mg	1.65
Al	7.19
Si	31.12
S	1.88
K	3.69
Ca	2.72
Ti	2.29
Cr	0.53
Fe	40.78

Table A8 Composition of Dredged Sediments for Figure A8

Element	Weight %
O	16.01
Na	3.66
Mg	3.98
Al	23.02
S	1.61
K	6.53
Ca	4.31
Ti	3.04
Fe	37.84

In Figure A9, an oblong structure about 2micormeter width might cause problem in the treatment because the proposed technology is more efficient for uniform circular objects. These oblong objects have to be broken into circular or irregular shape small pieces before the treatment process.

Table A9 Composition of Dredged Sediments for Figure A9

Element	Weight %
O	3.36
Al	6.81
S	0.11
K	1.75
Ca	0.7
Fe	87.26

The beehive shaped structure is shown in Figure A10 for sediment retained on No. 70 sieve, and with higher magnification of 4000X. The main composition of this structure is silica. The rings are made from the mixture of Na, Al, S, K, Ca, and Fe, and the center core is filled with the silicon dioxide.

Table A 10 Composition of Dredged Sediments for Figure A10

Element	Weight %
O	4.01
Na	0.85
Mg	1.38
Al	9.67
Si	33.43
S	0.99
K	7.35
Ca	3.16
Ti	1.9
Fe	37.27

Figure A11, shows the sediment also retained on No.70 sieve. The spherical shape object is in the range of 20 micrometer and the main composition is silica and oxygen (Table A11) forming silicon dioxide spheres with hollow inside. The proposed technology will be very successful for these shaped objects because of the uniform spherical shape. The beehive structure of sediments passing No. 200 sieve is given in Figure A12.

Table A11 Composition of Dredged Sediments for Figure A11

Element	Weight %
O	27.43
Na	1.70
Mg	2.11
Al	19.35
Si	37.24
S	0.99
K	3.69
Ca	1.59
Fe	5.90

The composition is still dominated by the element Si and O as shown in Table A12. The structure in Figure A12 for sediment passing 200 is similar to Figure A10 for retaining sieve No. 70. The same structure is repeated for sediments retained at different sieve size.

Table A12 Composition of Dredged Sediments for Figure A12

O	25.51
Na	1.65
Mg	1.90
Al	7.41
Si	53.03
S	1.82
K	2.17
Ca	1.10
Cr	0.00
Fe	5.39

From the above results this can be concluded that the main composition of the sediment is silica and oxygen and, silica fume can be used as representative sample for this research. The quantities in Table A1 to A12 provide an idea of the element composition rather than the actual composition. The sediment analysis by Brokhavan can be used as a result for the main composition of sediments. The spherical and regular shape of the objects shown in different figures in this chapter indicates a successful application of the proposed technology for separation.

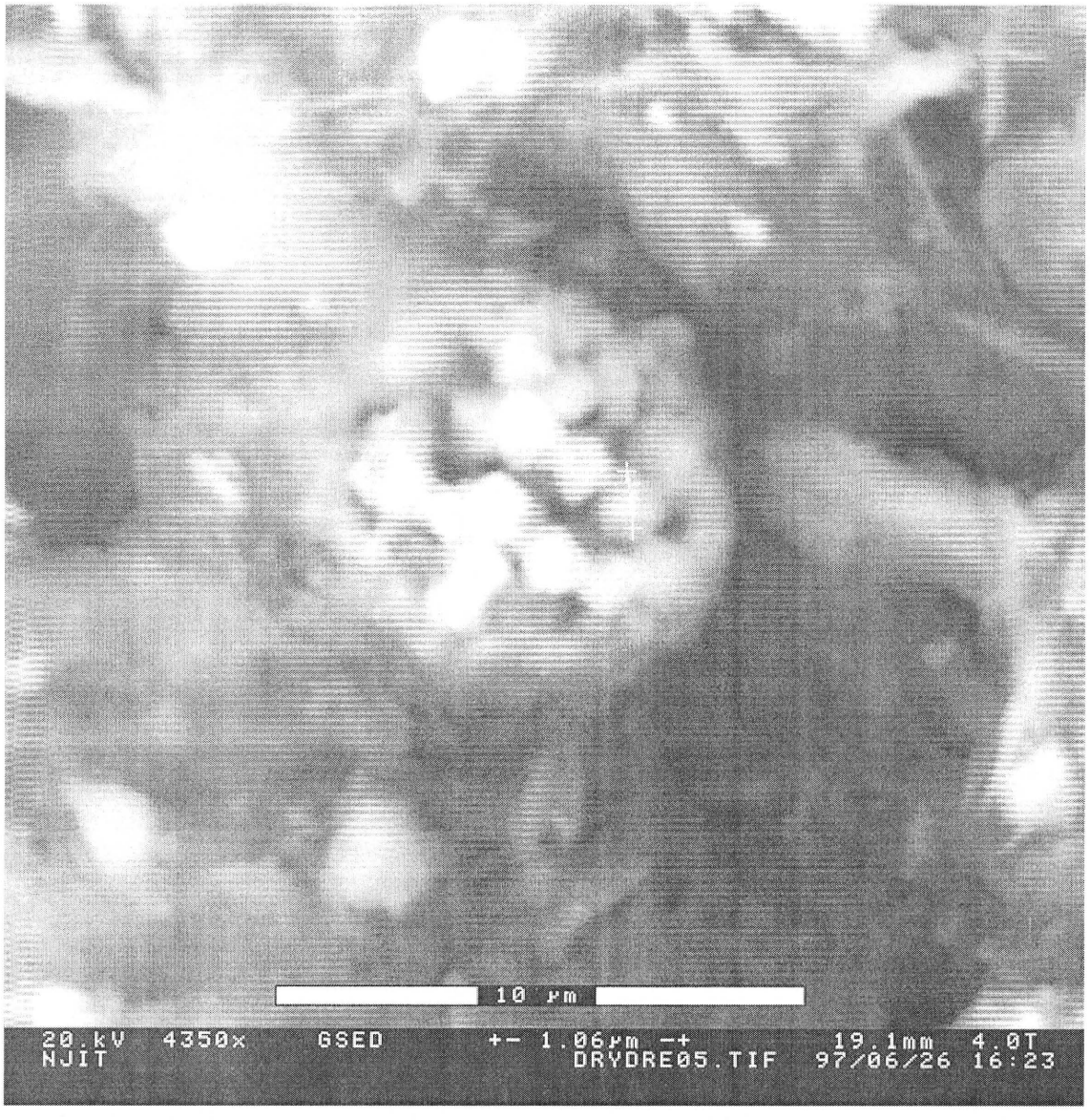

Figure A1 Morphology of Contaminated Dredged Sediment

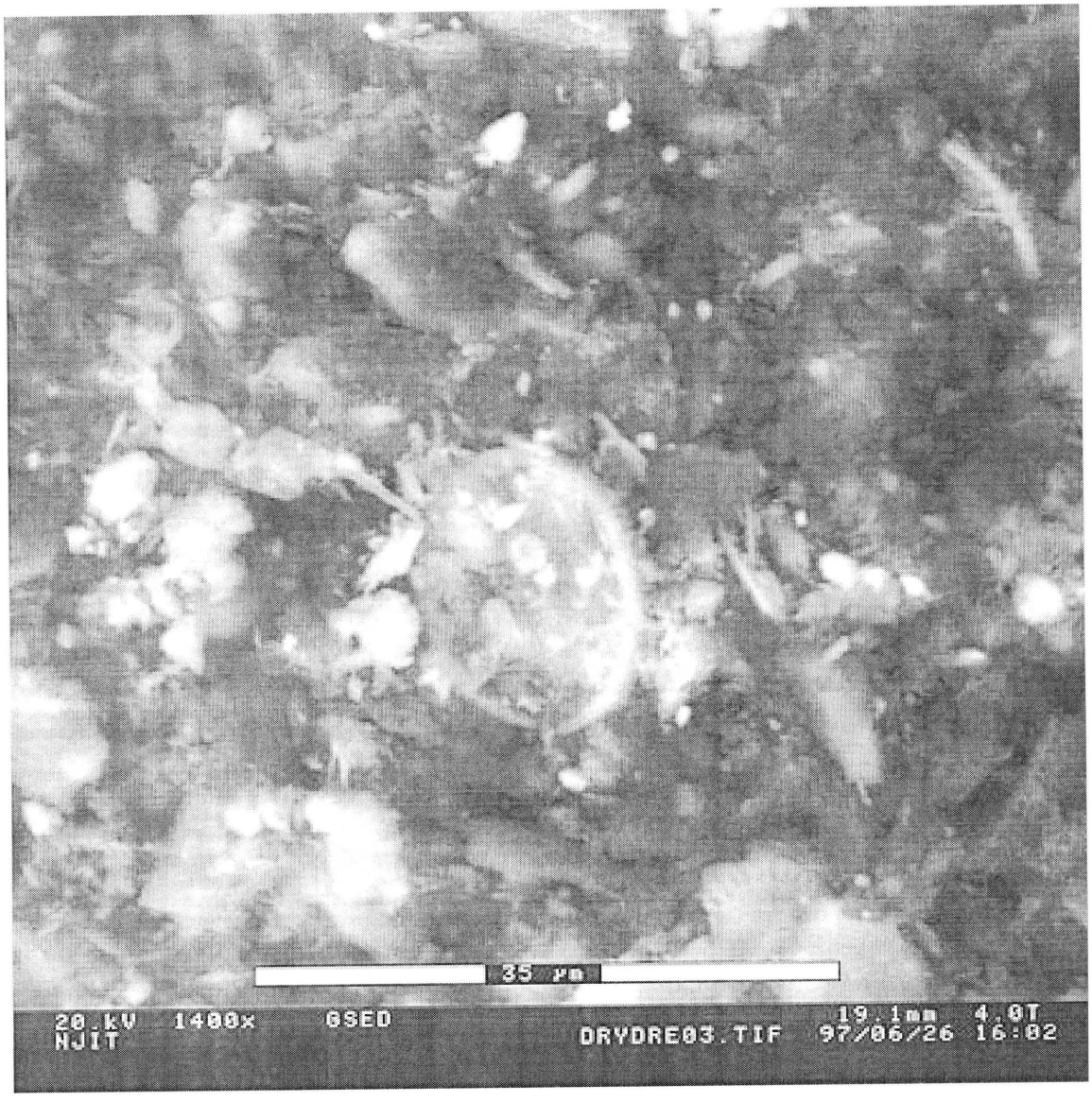

Figure A2 Morphology of Contaminated Dredged Sediment

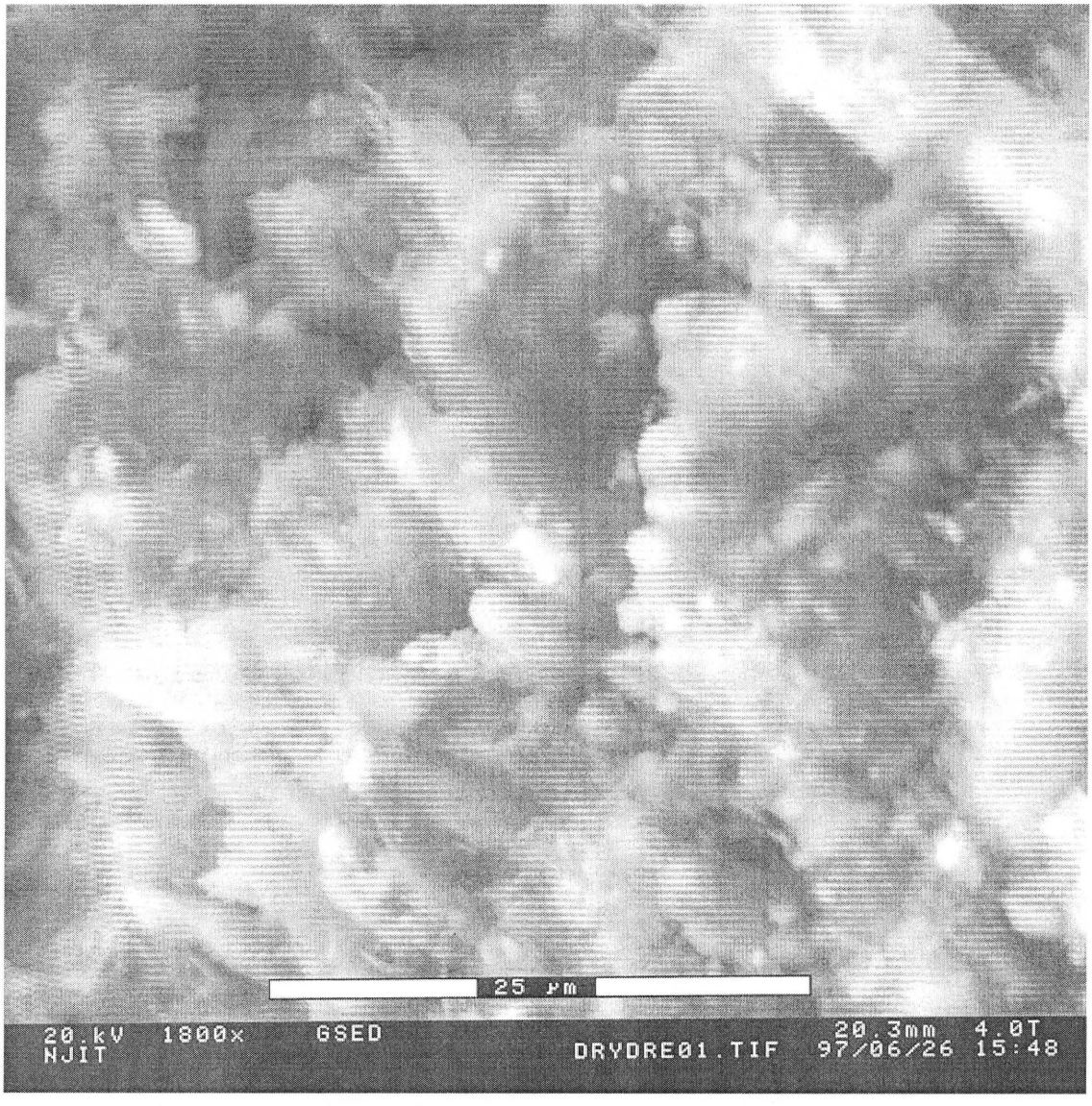

Figure A3 Morphology of Contaminated Dredged Sediment

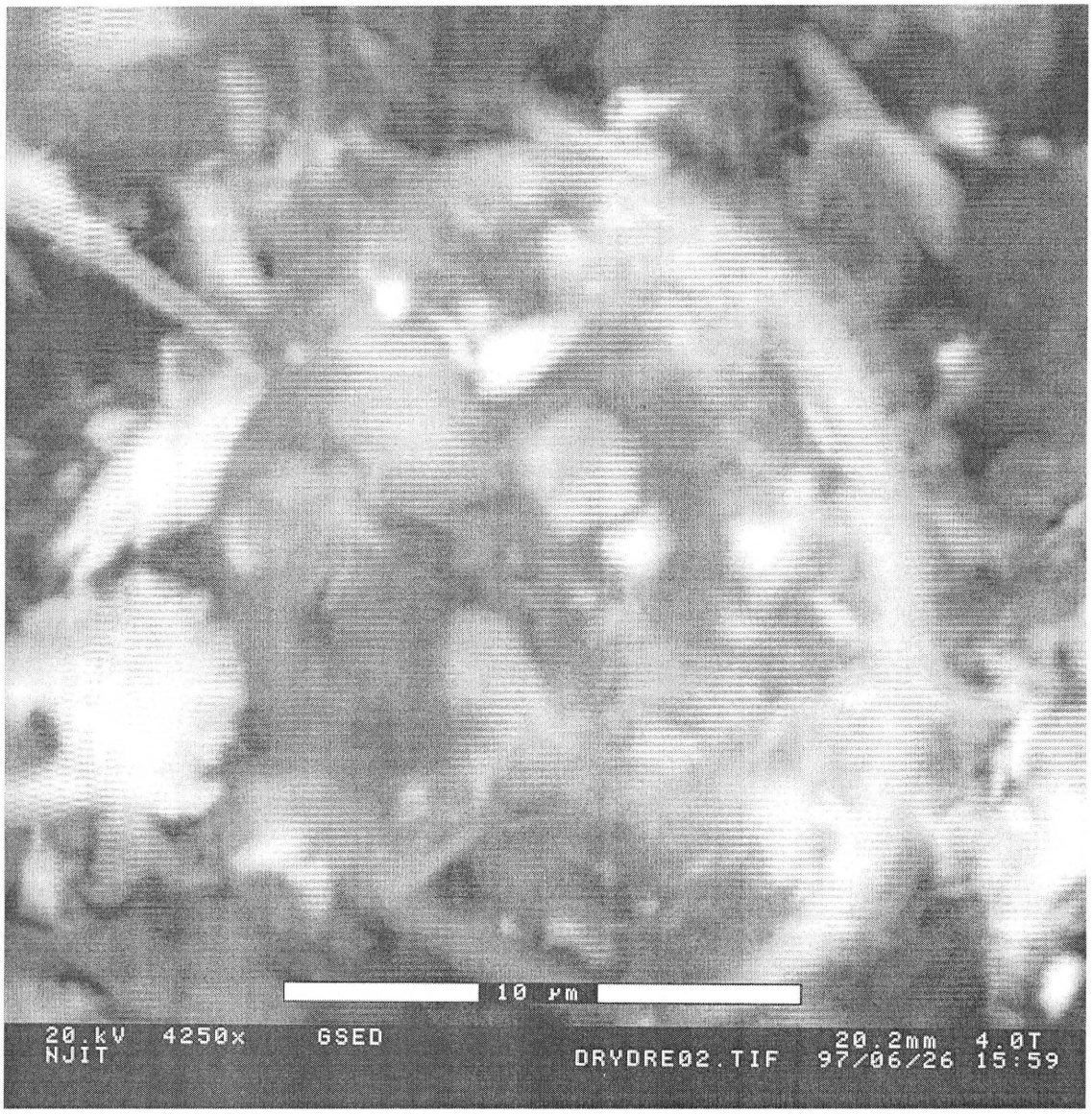

Figure A4 Morphology of Contaminated Dredged Sediment

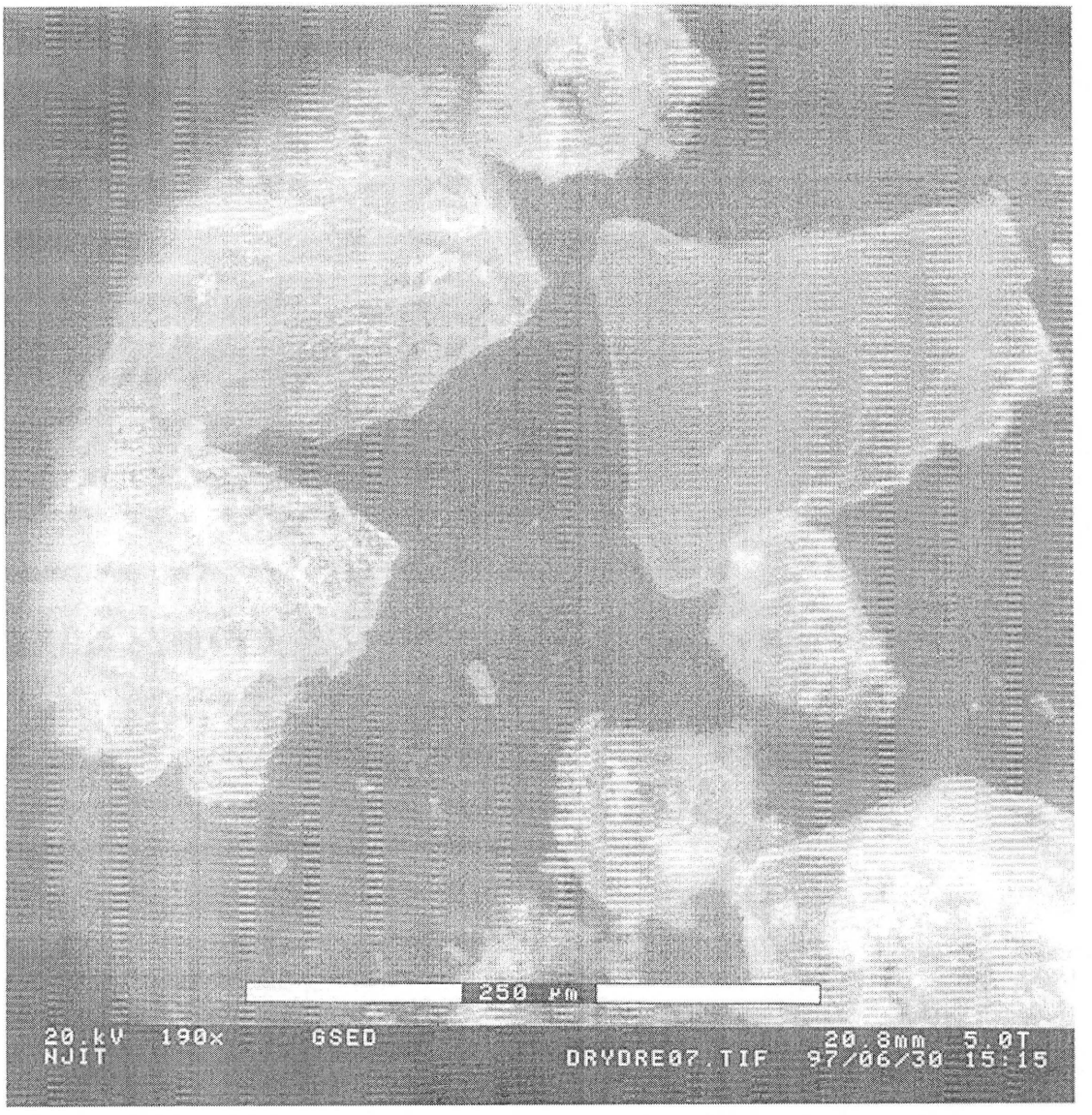

Figure A5 Morphology of Contaminated Dredged Sediment

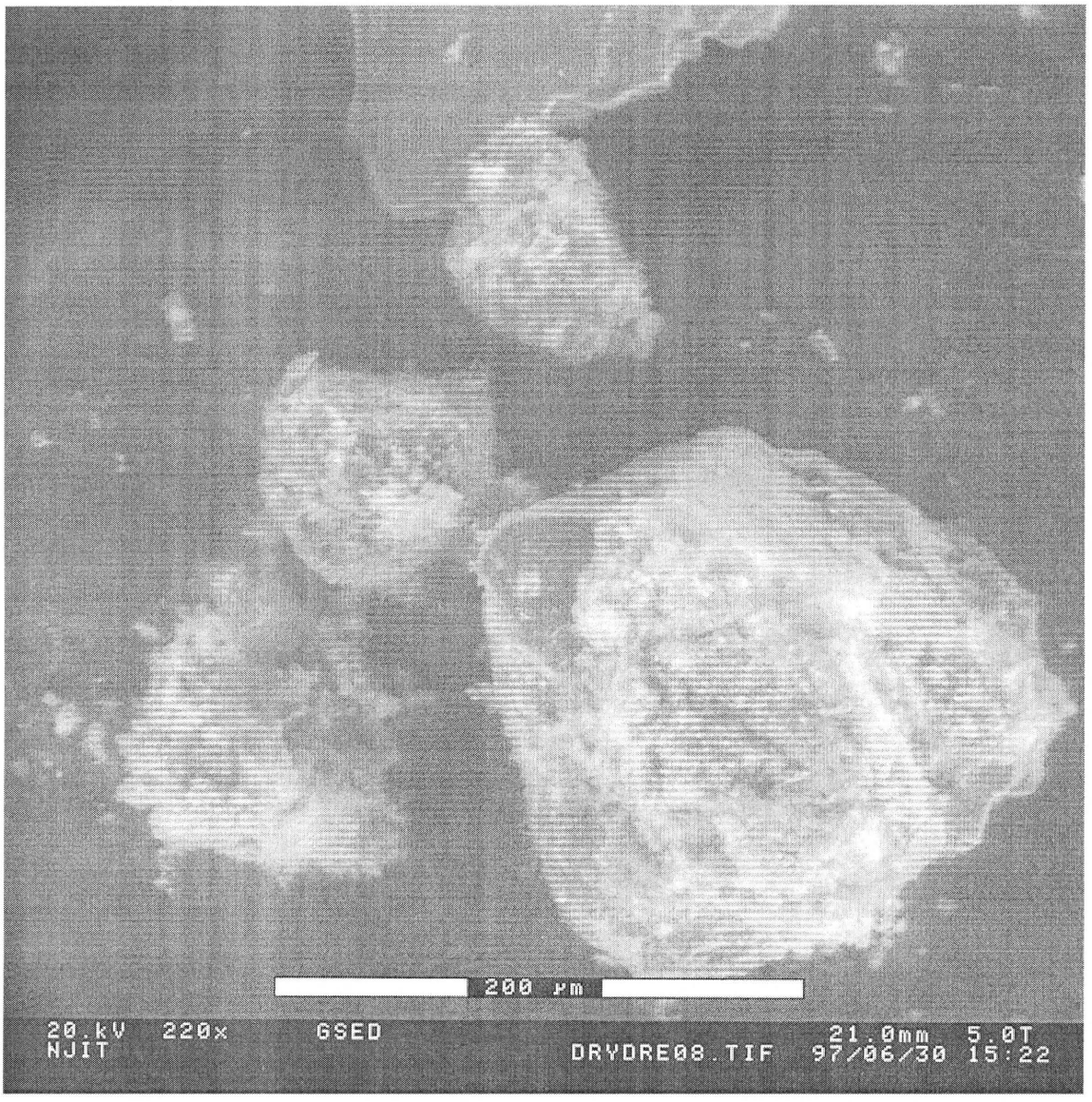

Figure A6 Morphology of Contaminated Dredged Sediment

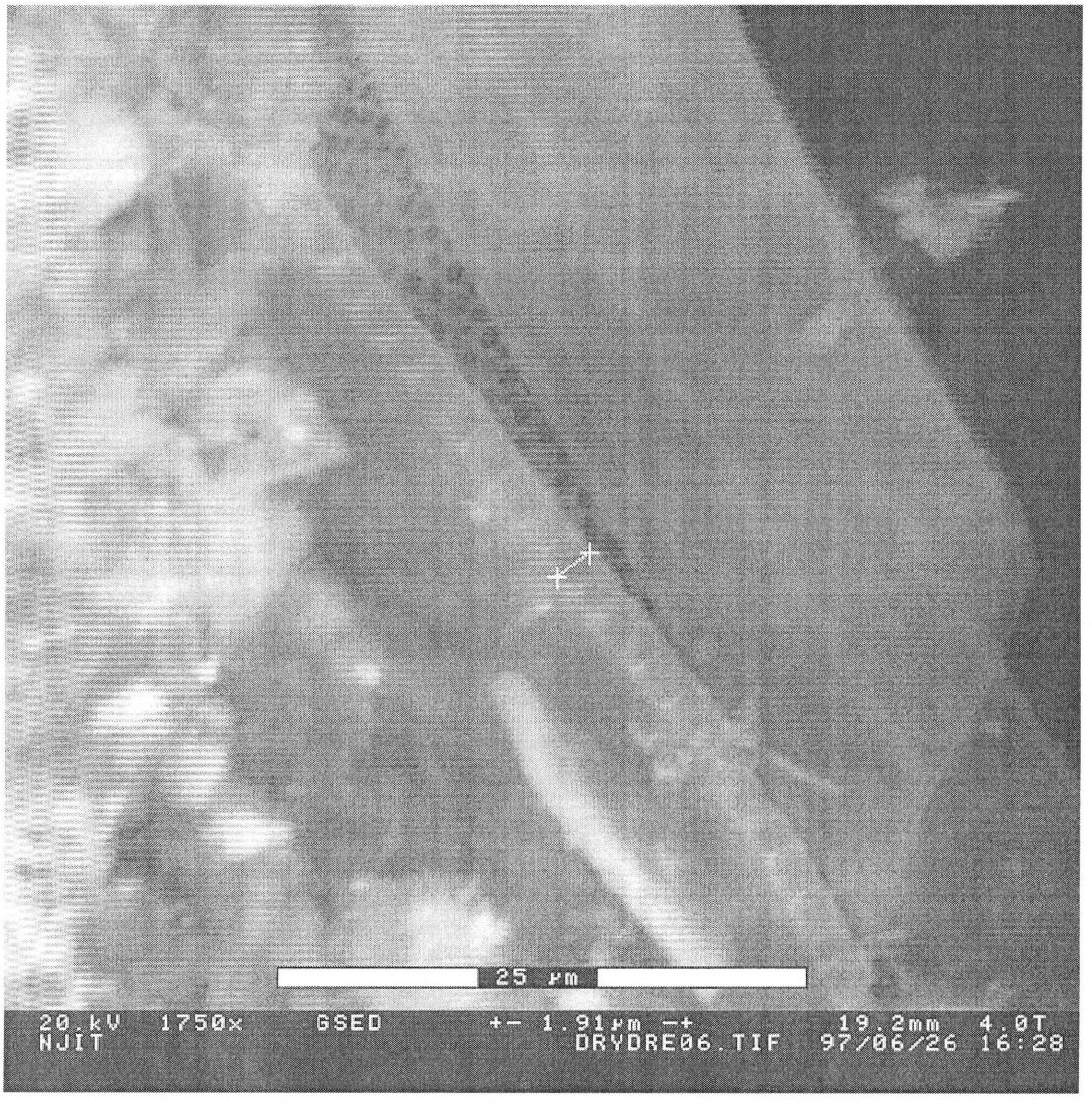

Figure A7 Morphology of Contaminated Dredged Sediment

Figure A8 Morphology of Contaminated Dredged Sediment

Figure A9 Morphology of Contaminated Dredged Sediment

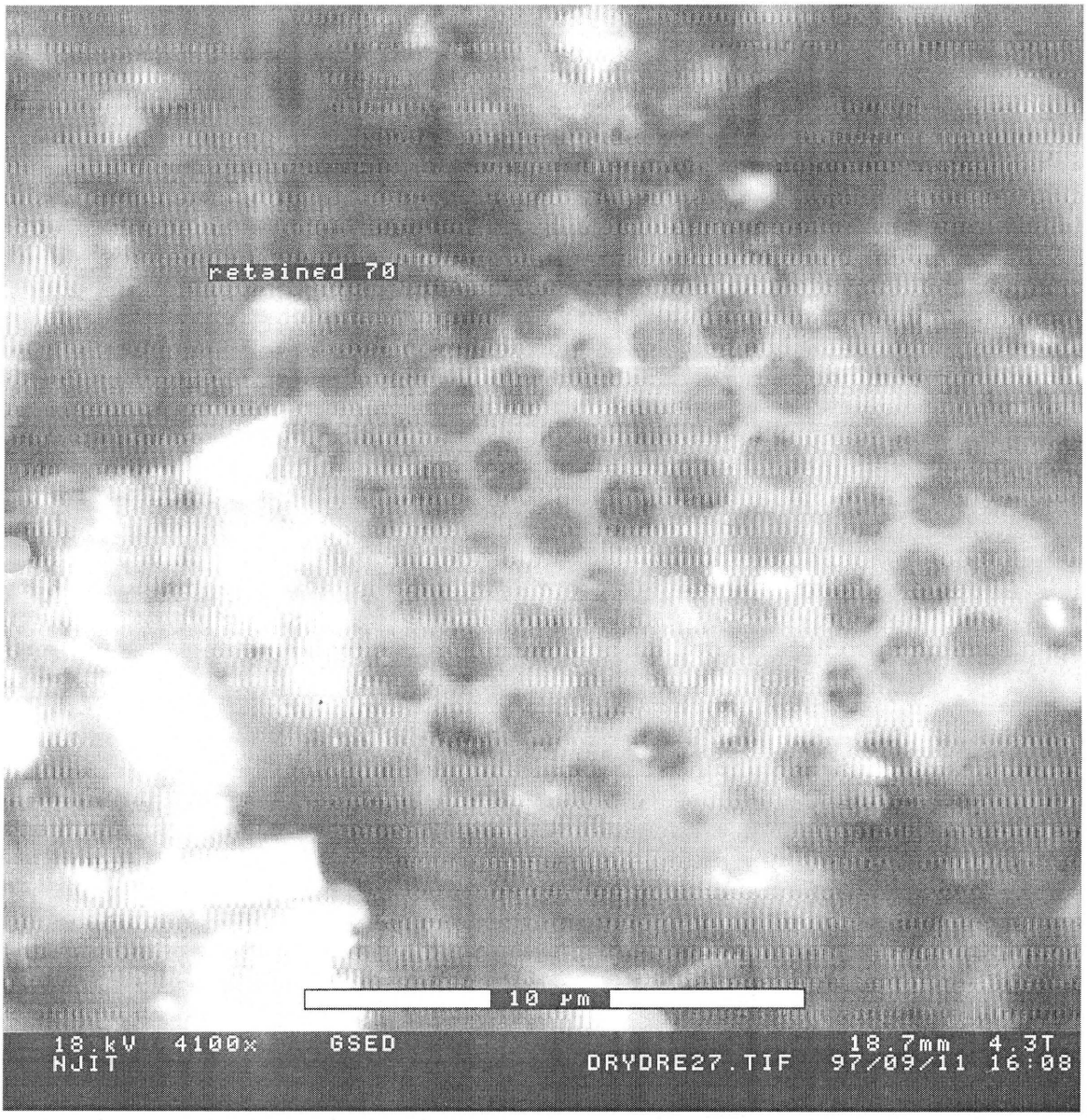

Figure A10 Morphology of Contaminated Dredged Sediment

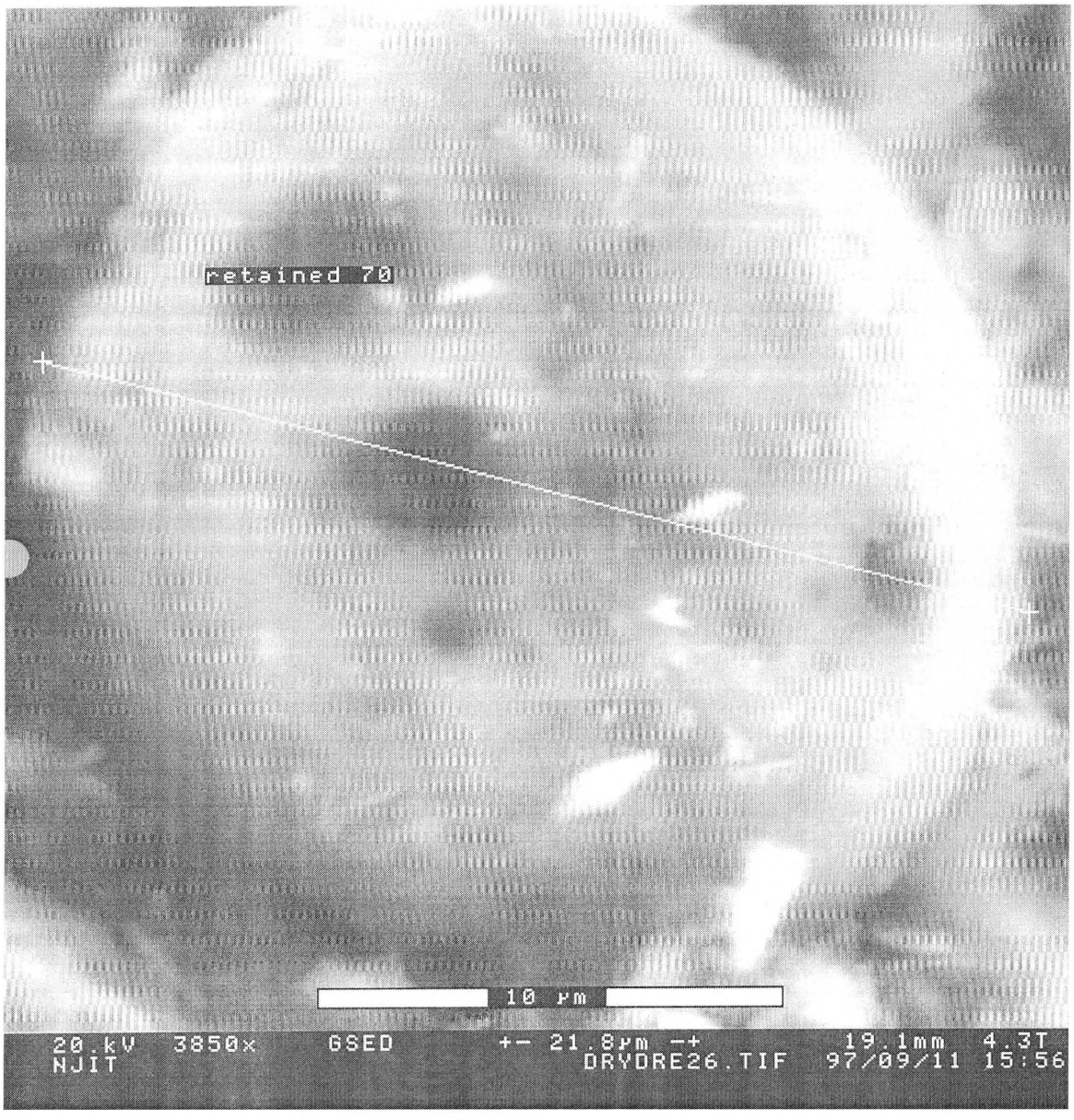

Figure A11 Morphology of Contaminated Dredged Sediment

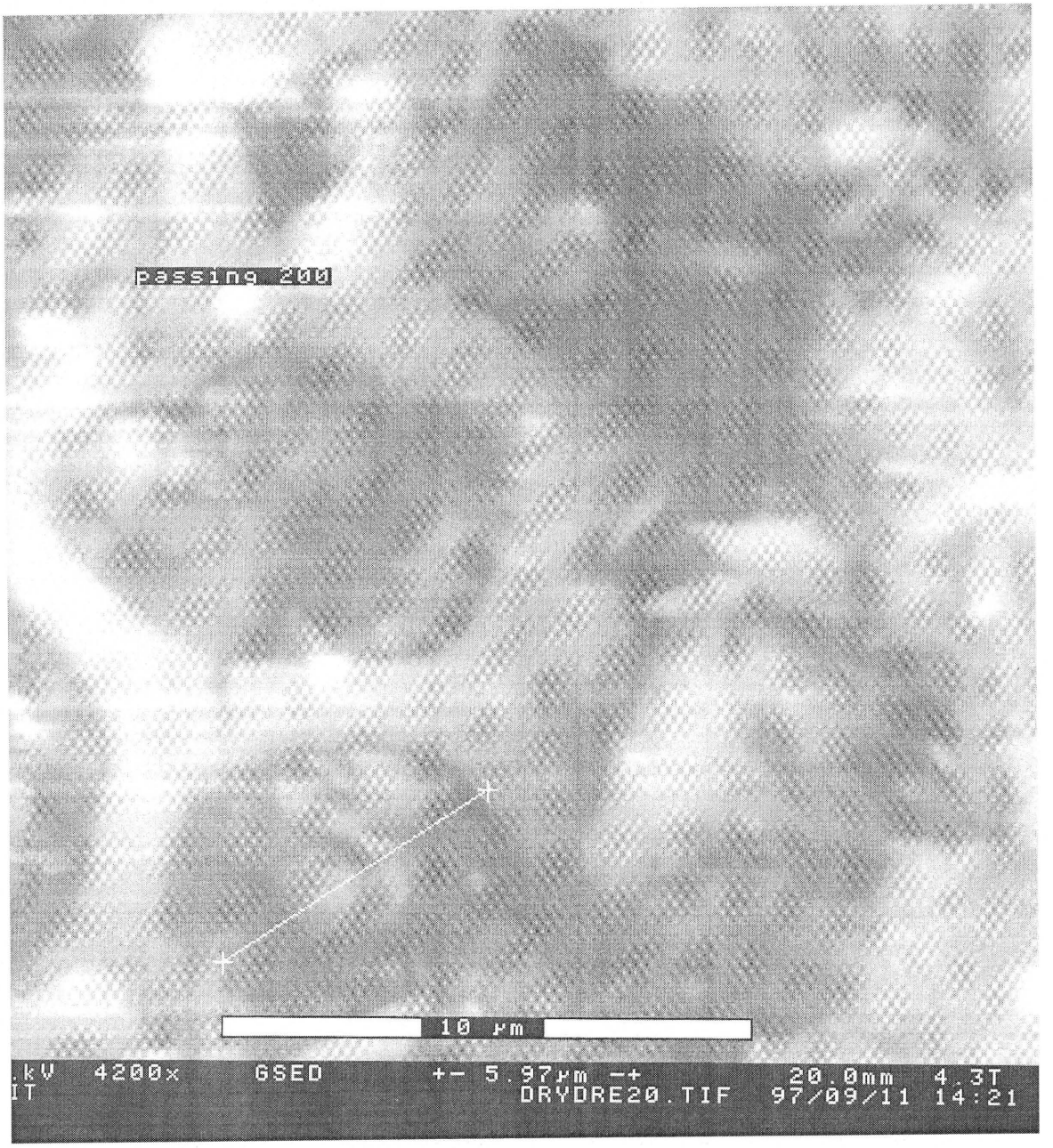

Figure A12 Morphology of Contaminated Dredged Sediment

APPENDIX B

This section deals with the method used to optimize the experimental data using the software Matlab. The SiC particles ranging from 5 to 20 μm in diameter were used in the experiment to track the particle trajectories in an acoustic field. Rewriting the dynamic particle equilibrium Equation (2.12):

$$(\rho_p V_0 + 0.5\rho_f V_0)\frac{dv}{dt} + 6\pi\mu r\frac{dx}{dt} - 4\pi r^3 KE_{ac} G\sin(2Kx) = 0 \qquad (2.12)$$

The unknown parameters for SiC were the radius of the particle (r), initial position of the particle x_0, and the acoustic energy in the fluid (E). The above equation was written with unknown parameters r, x_0, and E_{ac} and were simplified in terms of first and second derivative functions (as discussed in Chapter 3. These terms then were plugged in Equation (3.40) for particle trajectories:

$$x(t) = \frac{(r)\sin(2.78E-3\times(x_0))}{1.2E6}(-e^{1.58E-2(r)(E_{ac})t}) + \\ +719.4\tan^{-1}\left[(\tan(1.39E-3\times(x))e^{1.58E-2(r)(E_{ac})t}\right] \qquad (B.1)$$

A small program was written separately by declaring a function f:

function f = Displacement (x)

Least square function f_1 was written for particle displacement at time t= 0.0333 sec and with unknown variables r, x_0, and E_{ac}:

$f_{1=}$ (x(t) at time 0.033 sec – experimental value for displacement)^2

Similarly, functions f_2 through f_{10} were formed for time 0.06666 sec through 0.3sec, respectively:

$f_{2=}$ (x(t) at time 0.03333 sec – experimental value for displacement)^2

$f_{3=}$ (x(t) at time 0.06666 sec – experimental value for displacement)^2

$f_{4=}$ (x(t) at time 0.09999 sec – experimental value for displacement)^2

$f_{5=}$ (x(t) at time 0.13332 sec – experimental value for displacement)^2

$f_{6=}$ (x(t) at time 0.16665 sec – experimental value for displacement)^2

$f_{7=}$ (x(t) at time 0.19998 sec – experimental value for displacement)^2

$f_{8=}$ (x(t) at time 0.23331 sec – experimental value for displacement)^2

$f_{9=}$ (x(t) at time 0.26664 sec – experimental value for displacement)^2

$f_{10=}$ (x(t) at time 0.030000 sec – experimental value for displacement)^2

then a function f was assigned as:

$f=f_1 + f_2 + f_3 + f_4 + f_5 + f_6 + f_7 + f_8 + f_9 + f_{10}$

In Matlab optimization program, an initial guess for the stating points r, x_0, and E_{ac} were provided by the user and a function call for minimum was made to find the best possible combinations of these three parameters. This gives the least square error. The call for function minimum is given below:

[x, fval] =fminsearch ('Displacement',[r, x_0, E_{ac}]);

x

fval

Different initial guesses for r, x_0 and E_{ac} were tried and output for all the optimization were recorded. The optimization was repeated for all experimental data sets at different input power levels. Any optimized outputs for r less than zero or greater than 6 micrometers were discarded because the radius of the particle can not be zero or grater than 6 micrometers. Similarly, unreasonable values for x_0 and E_{ac} were discarded too.

REFERENCES

Adler, R. J., Paleu, P. T. and Wu, C. K., "Periodic Flow Slurry Fractionation," *Chemeca* 88, Vol. 88, pp. 892-897, 1988.

Alex E. H, and Burling, R. W., "On Sound Scattering and Attenuation on Suspensions, with Marine Applications," *Acoustical Society of America*, vol. 73, No. 3, pp. 950-959, 1982.

Apfel, R. E., "Acoustically Induced Square Law Forces and some Speculations about Gravitation," *Am J Phys*, Vol. 56, pp. 726-729, 1988.

Ashkin, A., "Acceleration and Trapping of Particles by Radiation Pressure," Phys. Rev. Lett., Vol. 24, pp. 156-159, 1970.

Auld, B. A., *Acoustic Fields and Waves in Solids*, Vol.1, John Wiley and sons, New York, 1973.

Barmatz, M., Collas, P., "Acoustic Radiation Potential on a Sphere in Plane, Cylindrical and Spherical Standing Wave Fields," *Acoustical Society of America*, Vol. 77, No. 3, pp. 928-945, 1984.

Benson Carlin, *Ultrasonics*, McGraw-Hill Book company, Inc., 1960.

Brandshaw, P., Cebeci, T., Whitelaw, H. J., *Engineering Calculation Methods for Turbulent Flow*, Academic Press, 1981.

Burger, W., Groschl, M., Trampler, F., Benese, E., "Frequency Dependence of the Acoustic Loss Distribution in Piezoceramic/Liquid Resonators," Ultrasonic International Conference, Proceedings, Butterworth-Heinemann, Oxford, U.K, pp. 507-510, 1993.

Charless T. Lynch, *Handbook of Materials Science*, Vol. 1, General Properties, CRCpress Inc.

Collas, P., Barmatz, M., and Shipley, C., "Acoustic Levitation in the Presence of Gravity," *Acoustical Society of America*, Vol. 86, pp. 777-787, 1989.

Crum, L. A., "Bjerknes Forces on Bubbles in a Stationary Sound Field," *Acoustical Society of America*, Vol. 57, No. 61, pp. 1363-1672, 1975.

Danilov, S. D, and Mironov, M. A. "Radiation Pressure Force acting on a Small Particle in a Sound Field," *Soc. Phys. Acoust.*, Vol. 30, No. 4, pp. 280-283, 1984.

Doblhoff_Dier, Gaida, T. Katinger, H., Burger, W., Groschl, M., and Benes, E. "A Novel Ultrasonic Resonance Field Device for the Retention of Animal Cells," *Biotechnol. Prog*, Vol.10, No. 4, pp. 428-432, 1994.

Doinikov, A. A., "Acoustic Radiation Pressure on a Rigid Sphere in a Viscous Fluid Process," R. Soc. London A447, pp. 447-466, 1994.

Embleton, T. F. W., "Mean Force on a Sphere in a Spherical Sound Field. I (Theoretical)," *Acoustical Society of America,* Vol. 26, pp. 40-45, 1954.

Embleton, T. F. W. "The Radiation force on a Spherical Obstacle in a cylindrical Sound Field," *Can. J. Phys.*, Vol. 34, pp. 276-282, 1956.

Erwin Meyer, Ernst-Georg Neumann, *Physical and Applied Acoustic*, An Introduction, Academic Press, 1972.

French, A. P., *Vibrations and Waves*, W. W. Norton and Company Inc. New York, 1971.

Glenn Whitworth and Coakley, W. T., "Particle Column Formation in a Stationary Ultrasonic Field," *Acoustic Society of America*, Vol. 91, No. 1, pp. 79-85, 1991.

Goodman R. R., and Stern, R., "Reflection and Transmission of Sound by Elastic Spherical Shells," *Acoustical Society of America*, Vol. 34, pp. 228-344, 1962.

Gor'kov, L. P., "On the Forces Acting on a Small Particle in an Acoustic Field in an Ideal Fluid," Soviet Phys.-Doklady, Vol. 6, pp. 773-775, 1962.

Gould, Robert K., Coakley, W., Terence and Grundy, Martin A., "Upper Sound Pressure Limits on Particle Concentration in Fields of Ultrasonic Standing-Wave at Megahertz Frequencies," *Ultrasonics*, Vol. 34, No. 4, pp. 239-243, 1991.

Grosch, M., "Ultrasonic Separation of Suspended Particles: 1. Fundamentals," *Acoustica*, Vol. 84, pp. 432-447, 1997.

Gustafson, Karl E., *Partial differential Equation and Hilbert Space Methods*, second edition, John Wiley and Sons, Inc, 1987.

Haar, G., and Wyard, S. J., "Blood Cell Banding in Ultrasonic Standing Wave Fields; a Physical Analysis," *Ultrasound Med. Biol.*, Vol. 4, pp. 111-123, 1978.

Hager, F., Benes, E., "A Summary of all forces acting on Spherical Particles in a Sound Field," Ultrasonics International 91, Conference Proceedings, Le Touquet, France, Butterworth_Heinemann, Oxford, U.K, pp. 283-286, 1991.

Hampton, L. D., "Acoustic Properties of Sediments," *Acoustical Society of America*, Vol. 42, pp. 882-890, 1967.

Hasegawa T., and Watanable,Y., "Acoustic Radiation Pressure on an Absorbing Sphere," *Acoustical Society of America,* Vol. 63, No. 6, pp. 1733-1737, 1978.

Hasegawa, T., " Acoustic Radiation Force on a Sphere in a Quasis_stationary Wave Field –Theory," *Acoustical Society of America*, Vol. 65, No. 1, pp. 32-40, 1979.

Hawkes, J. J., and Coakley, W. T., "A Continuous Flow Ultrasonic Cell-Filtering Method," Enzyme *Microb. Technol.*, Vol. 19, No. 57, 1996.

Hay, A. E., and Burling, R. W., "On Sound Scattering and Attenuation in Suspensions with Marine Applications," *Acoustical Society of America*, Vol. 72, No. 3, pp. 950-957, 1982.

Hertz, H. M., "Standing-wave Acoustic Trap for Nonintrusive Positioning of Microparticles," *J. Appl. Phys.* Vol. 78, No. 8, pp. 4845-4849, 1995.

Higashitani, K., Fukushima, M., and Matsuno, Y., "Migration of Suspended Particles in Plane Stationary Ultrasonic Field," *Chem. Eng. Sci.*, Vol. 36, No. 12, pp. 1977-1888, 1989.

Higashitani, K., Fukushima, M., and Matsuno, Y., "Migration of Suspended Particles in Plane Stationary Ultrasonic Fields," *Chem. Eng. Sci*, Vol. 36, pp. 1187-1192, 1981.

Hughes, D. E., and Nyborg, W. L., "Cell Disruption by Ultrasound," Science 138, pp. 108-114, 1962.

Jerry B. Marion, William F. Hornyak, *Physics for Science and Engineering*, Saunders College Publishing.

Johnson, D. A., Feke, D. L., "Methodology for Fractionation Suspended Particles using Ultrasonic Standing Wave and Divided Flow Fields," *Separation Technology*, Vol. 5, pp. 251-258, 1995.

Junru Wu and Gonghuan Du, "Acoustic Radiation Force on a Small Compressible Sphere in a Focused Beam," *Acoustic Society of America*, Vol. 87, No. 3, pp. 997-1004, 1989.

Kenji Yasuda, Stephan Shuichi Haupt, and Shin-ichiro Umemura, " Using Acoustic Radiation Force as a Concentration Method for Erythrocytes," *Acoustic Society of America*, Vol. 102, No. 1, pp. 642-645, 1997.

Kilburn, D. G., Clarke, D. J., Coakley, W. T., and Bardsley, D. W., "Enhanced Sedimentation of Mammalian Cells Following Acoustic Aggregation," Biotech Bioeng, Vol. 34, pp. 559-562, 1989.

King, V. Louis, Macdonald, F.R.S., "On the Acoustic Radiation Pressure on Spheres," Proc. R. Soc. London Ser. A 147, pp. 212-240, 1934.

Klein D., "Absolute Sound Intensity in Liquids by Spherical Torsion Pendula," *Acoustic Society of America*, Vol. 9, pp. 312-320, 1938.

Kozuka, T., Tuziuti, H., and Fukuda, "One-Dimensional Transportation of Particles using an Ultrasonic Standing Waves," Proc. 6th Int. Sympo. Micro Machine and Human Science, pp. 179-1185, 1996.

Kundt, A., and Lehmann, O., "Longitudinal Vibrations and Acoustic Figures in Cylindrical Columns of Liquids," Annal. Phys. Chem., Vol. 153, No. 1, 1874.

Landau L. D., and Lifshitz E. M., *Fluid Mechanics*, Vol. 6, Pergamon Press, 1959.

Lawrence E. Kinsler, Austin R. Frey, Alan B. Coppens, James V. Sanders, *Fundamentals of Acoustics*, John Wiley and Sons.

Lee C. P., and Wang T. G., "Acoustic Radiation Pressure," *Acoustic Society of America*, Vol. 94, No. 2, pp. 1099-1109, 1993.

Lighthill, J., "Acoustic Streaming," *J. Sound Vib.*, Vol. 61, No. 3, pp. 391-418, 1978.

Mandralis, Z., Bolek, W., Burger, W., Benes, E., and Feke, D. L., "Enhanced Synchronized Ultrasonic and Flow Field Fractionation of Suspensions," *Ultasonics,* Vol. 32, No. 2, pp. 113-121, 1994.

Matula, T., Cordry, S., Roy, R., and Crum, L., "Bjerknes Force and Bubble Levitation under Single-Bubble Sonoluminescence Conditions," *Acoustical Society of America*, Vol. 102, No. 3, pp. 1522-1527, 1997.

McQueen, D. H., "Frequency dependence of ultrasonic cleaning," *Ultrasonic*, 1986.

McSkimin, H. J., " Velocity of Sound in Distilled Water for the Temperature range 20-75° C," *Acoustical Society of America*, Vol. 37, No. 2, pp. 325-328, 1965.

Meegoda N. Jay, Veerawat, K., Perera, Ruvini, Aboobaker, Nazhat, and Zapata, M. Alejandra, "Ultrasound to Decontaminate Dredged Sediments," Proceeding of the 4th. International Symposium on Environmental Geotechnology and Global Sustainable Development, H. I. Inyang Editor, A.A. Balkema Publishers, Danvers, MA. , August 1998

Monura S., and Nakagawa, M., " Heat Transfer Enhancement by Ultrasonic Vibration," Proc. 4th ASME-JSME, Thermal Joint Conf., Vol. 4, pp. 275-282, 1995.

Nomura, Shinfuku, Sasaki, Yuichi, and Murakami, Koichi, " Channel Flow by Applying Ultrasonic Vibration," IEEE Ultrasonics Symposium, pp. 719-722, 1998.

Nyborg, W. L., "Radiation Pressure on a Small Sphere," *Acoustical Society of America,* Vol. 42, pp. 947-952, 1967.

Ohtani, Keisuke, Koike, Yoshikazu, Uheta, Sadayuki, Yokoi, Hiroshi, "Novel Wedge-Shaped Doubly Inclined Chamber for the Flow-through Separation of Suspended Particles," *Ultrasonics,* No. 38, pp. 647-649, 2000.

OSHA Technical Manual, section 3, chapter 5, " Noise Measurement".

Papanu, J. S., Adler, R. J., Gorensek, M. B. and Menon, M. M, "Separation of Fine Particle Dispersions using Periodic Flows in a Spinning Coiled Tube," *AlChE J,* Vol. 32, pp. 798-808, 1986.

Phylis W. S. Pui, Felix Trampler, Stefan A. Sonderhoff, Martin Groeschl, Dougglas G. Kilburn, and James M. Piert, "Batch and Semicontinuous Aggregation and Sedimentation of Hybridoma Cells by Acoustic Resonance Fields," *Biotechnol. Prog.* Vol. 11, No. 2, pp. 146-152, 1995.

Rayleigh, L, *Theory of Sound*, Dover, New York, Vol. 2, 2nd Edition, 1945.

Rhim, W., Chung, S. K., Hyson, M., Trinh, E., Elleman, D., "Large Charged Drop Levitation Against Gravity," *IEEE* Transaction on industry applications, Vol. 1A-23, No. 6, pp. 975-979, 1987.

Richard Holland, *Design of Resonant Piezoelectric Devices*, the Colonial Press Inc., 1969.

Rosenbertg, L. D., *High-Intensity Ultrasonic Fields*, Plenum, New York, 1971.

Rudnick, K., "Measurements of the Acoustic Radiation Pressure on a Sphere in a Standing Wave Field," *Acoustical Society of America*, Vol. 62, pp. 20-22, 1977.

Rudnick, K., "Measurements of the Acoustic Radiation Pressure on a Sphere in a Standing Wave Field," *Acoustical Society of America*, Vol. 70, pp. 1762-1767, 1981.

Schmid, M., Benes, E., Sedlaczek, R., "A Computer-Controlled System for the Measurement of Complete Admittance Spectra of Piezoelectric Resonators," Meas. Sci. Technol., Vol. 1, No. 970, pp. 1976-1984, 1990.

Schram, C. J. and Rendell, M., "Manipulation of Particles in Megahertz Standing Waves," Proceedings Ultrasonics International Conference, pp. 262-267, 1989.

Springston, S. R., Myers, M. N., and Giddings, J. C., "Continuous Particle Fractionation based on Gravitational Sedimentation in Split-Flow thin Cells," Anal. Chem., Vol. 59, pp. 344-350, 1987.

Sollner, K., and Bondy, C., "Mechanism of Coagulation by Ultrasonic Waves," Tran. Faraday Soc., Vol. 32, pp. 616-623, 1936.

Su, Y., Feng, Z., "Numerical Simulation of the Dynamics of Acustically Levitated Drops," *Acoustical Society of America*, Vol. 99, No. 5, pp. 2799-2810, 1996.

Takeda, K., Itoh, Y., Hiraiwa, A., Yasuda, K., and Suda, k., "Separated Detection of Particles and Bubbles in Liquid," Proceedings of the Third International Symposium on Cleaning Technology in Semiconductor Device Manufacturing, Vol. 94, No. 7, pp. 466-473, 1993.

Tolt, T. L., and Feke, D.L., "Separation of Dispersed Phases form Liquids in Acoustically driven Chambers," *Chem Eng Sci*, Vol. 48, pp. 527-540, 1993.

Tolt, T.L. and Feke, D.L.,"Separation Devices Based on Forced Coincidence Response of Fluid-Filed Pipes," *Acoustical Society of America*, Vol. 91, No. 6, pp. 3152-3156, 1992.

Urich, F. J., "The Absorption of Sound in Suspensions of Irregular Particles," *Acoustical Society of America*, Vol. 20, pp. 283-289, 1948.

Weiser M. A. H., and Apfel R. E., "Extension of Acoustic Levitation to include the study of Micron-size Particles in a more Compressible Host Liquid," *Acoustical Society of America*, Vol. 71, pp. 126-131, 1982.

Weiser M. A. H., and Apfel R. E., "Interparticle Forces on Red Cells in a Standing Wave Field," *Acoustica*, Vol. 56, pp. 114-119, 1984.

Westervelt, P. J., "The Theory of Steady Forces caused by Sound Waves," *Acoustical Society of America,* Vol. 23, No. 4, pp. 312-315, 1951.

Whitworth G., Grundy M. A., and Coakley W. T., "Transport and Harvesting of Suspended Particles using Modulated Ultrasound," *Ultrasonic,* Vol. 29, pp. 439-444, 1991.

Whitworth, G., and Coakley, M. A., "Particle Column Formation in a Stationary Ultrasoinc Field," *Acoustical Society of America*, Vol. 91, No. 1, pp. 79- 85, 1992.

Wong S. W., and Chon, W. Y., "Effect of ultrasonic Vibrations on Heat Transfer to Liquids by Natural Convection and by Boiling," *AlChE*, Vol. 15, No. 2, pp. 281-288, 1969.

Woodside, Steven M., Bowen, Bruce D., and Piret, James M., "Measurement of Ultrasonic Forces for Particle-Liquid Separations," *AIChE Journal*, Vol. 43, No., pp. 1727-1736, 1997.

Woodside, Steven M., and Piret, James M., "Acoustic Force Distribution in Resonators for Ultrasonic Particle Separation," *AIChE Journal*, Vol. 44, No. 9, pp. 1976-1984, 1998.

Wright, W. H., Sonek, G. J., Tadir, Y., and Berns, M. W., "Laser Trapping Cell Biology," *IEEEE*, Quantum Electron, Vol. 26, pp. 2148-2157, 1990.

Yasuda, K., and Umemura, S., "Particle Separation using acoustic Radiation Force and Electrostatic Force," *Acoustical Society of America,* Vol. 99, No.4, pp. 1965-1970, 1996.

Yosioka K., and Kawasima Y., "Acoustic Radiation Pressure on a Compressible Sphere," *Acoustics*, Vol. 5, pp. 167-173, 1955.

WWW.crystran.co.uk/qutzdata.htm, Oct 15, 1999, 3:45PM.

Zeill, G. D., *A First Course in Differential Equations with Applications*, PWS Publishers, 1982.

Zenz, F. A., and Othmer, D. F., *Fluidization and Fluid-Particle Systems*, Reinhold, New York, 1960.